

**INVERSE IDENTIFICATION OF ELASTIC MODULI FOR 3D PRINTED PLA, USING  
IMPULSE EXCITATION TECHNIQUE (IET)**

by

Mohsin Afridi,

Bachelor of Engineering, Ryerson University (2007)

A project

presented to Ryerson University

in partial fulfilment of the

requirements for the degree of

Master of Engineering

in the program of

Aerospace Engineering

Toronto, Ontario, Canada, 2019

© Mohsin Afridi 2019

## **AUTHOR'S DECLARATION FOR ELECTRONIC SUBMISSION OF A PROJECT**

I hereby declare that I am the sole author of this project. This is a true copy of the project, including any required final revisions, as accepted by my examiners.

I authorize Ryerson University to lend this project to other institutions or individuals for the purpose of scholarly research.

I further authorize Ryerson University to reproduce this project by photocopying or by other means, in total or in part, at the request of other institutions or individuals for the purpose of scholarly research.

I understand that my project may be made electronically available to the public.

# **INVERSE IDENTIFICATION OF ELASTIC MODULI FOR 3D PRINTED PLA, USING IMPULSE EXCITATION TECHNIQUE (IET)**

Mohsin Afridi

Master of Engineering, Aerospace Engineering, Ryerson University, Toronto (2019)

## **ABSTRACT**

3D Printing has recently undergone extensive development due to its lower cost and flexibility. A number of studies have been carried out to determine 3D printed material properties. This study focuses on the determination of the dynamic properties for PLA. The PLA material is processed through the popular FDM method with three different build orientations. A vibration experiment is conducted to evaluate the first modal frequency and Young's modulus. The results are then compared to the FEM modal analysis and finally the traditional tensile testing results. The anisotropy of the 3D printed components, mainly due to the density changes caused by voids and filament alignment, result in the variation of the Young's modulus which is different than the homogenous bulk material. The calculated Young's moduli values are very slightly higher than the tensile test results which is in conformance with the trend documented by earlier studies on similar printed materials using the same techniques.

## **ACKNOWLEDGEMENTS**

This thesis project would not have been possible without the continuous support, guidance and encouragement of Prof. Seyed M. Hashemi, whose extensive knowledge and experience in the areas of Conventional and Dynamic Finite Elements, and Vibration was instrumental.

I would also like to thank Dr Kazem for his 3D printing knowledge and guidance. Ali Froozanfar for his great support and assistance throughout the design and execution of the experimentation.

I would also like to thank Ryerson University and the Aerospace Engineering Department for the access to the Lab and experimentation equipment.

Finally, very special thanks go out to my parents for their perpetual encouragements and support.

Dedicated to my parents Liaquat Afridi and Khadijah Afridi

## TABLE OF CONTENTS

ABSTRACT.....	iii
ACKNOWLEDGEMENTS .....	iv
TABLE OF CONTENTS.....	vi
LIST OF TABLES .....	viii
LIST OF FIGURES .....	ix
LIST OF APPENDICES.....	x
NOMENCLATURE .....	xi
1. INTRODUCTION .....	1
1.1 Overview .....	1
1.2 Organization of the report.....	5
1.3 Literature survey .....	6
2. EXPERIMENTATION SETUP DESIGN .....	10
3. PRODUCTION OF TEST SPECIMEN .....	15
3.1 Specimen Geometry.....	15
3.2 Specimen Manufacturing .....	18
3.3 Experimentation of Developed Specimens .....	21
4. FEM MODAL ANALYSIS.....	30

5. CONCLUSION AND FUTURE WORK .....	38
5.1 Recommendations For Future Work.....	38
APPENDICES .....	40
APPENDIX A EXPERIMENTATION SETUP AND RESULTS .....	41
Appendix A1 CAD Designed and Printed Laser Sensor Mount.....	42
Appendix A2 3D CAD Experimentation Setup Design .....	43
Appendix A3 Summary of Reported Test Specimens .....	45
APPENDIX B LAB MANUAL.....	47
APPENDIX C EXPERIMENTATION RESULTS .....	74
Appendix C1 IET Results .....	75
Appendix C2 Tensile Testing Results.....	76
APPENDIX D FEM ANALYSIS REPORTS .....	77
REFERENCES .....	175

## LIST OF TABLES

Table 1: 3D printer FDM manufacturing parameters used to produce test specimens.....	19
Table 2: Test Specimen mechanical parameters and results.....	27
Table 3: Young's modulus results from tensile testing for each test specimen.....	29
Table 4: Table of modal frequencies for orientation XYZ .....	33
Table 5: Modal frequencies table for XZY .....	34
Table 6: Modal frequencies table for ZXY .....	35
Table 7: Tensile test results for Young's modulus .....	36
Table 8: Comparison of Young's modulus results from IET and tensile test.....	37

## LIST OF FIGURES

Figure 1: Experimental Setup Schematic.....	10
Figure 2: 3D Catia V5 design for experimental equipment including sensors and test specimen	12
Figure 3: 3D Printed Test Specimen with characteristic lengths illustrated.....	16
Figure 4: XZY build orientation .....	18
Figure 5: 3D printed PLA specimens in three build orientations: .....	20
Figure 6: Screenshot of Piezoelectric impulse hammer force in time domain .....	23
Figure 7: Typical FRF result from laser sensor 1 for XYZ build orientation.....	24
Figure 8: Sample Test run parameters used in DAQ software (CatmanAP) .....	25
Figure 9: Data Analysis screenshot of DAQ software comparing displacement amplitude from two laser sensors and the impact force from the piezoelectric sensor .....	25
Figure 10: FRF of ZXY sample with initial laser 3 position .....	26
Figure 11: FRF of ZXY sample with laser 3 position moved closer to tip.....	26
Figure 12: First mode shape for build orientation XYZ .....	31
Figure 13: First mode shape for build orientation XZY .....	33
Figure 14: First mode shape for build orientation ZXY .....	34

## LIST OF APPENDICES

APPENDICES .....	40
APPENDIX A EXPERIMENTATION SETUP AND RESULTS .....	41
Appendix A1 CAD Designed and Printed Laser Sensor Mount.....	42
Appendix A2 3D CAD Experimentation Setup Design .....	43
Appendix A3 Summary of Reported Test Specimens .....	45
APPENDIX B LAB MANUAL.....	47
APPENDIX C EXPERIMENTATION RESULTS .....	74
Appendix C1 IET Results .....	75
Appendix C2 Tensile Testing Results.....	76
APPENDIX D FEM ANALYSIS REPORTS .....	77

## NOMENCLATURE

$E$  = Young's modulus of elasticity

$A$  = Cross-sectional area of beam

$\rho$  = density

$l$  = Free vibration length

$I$  = Second area moment of Inertia of the beam

$L$  = length of the beam

$\omega$  = natural frequency

$\lambda$  = non-dimensional natural frequency

$X, Y, Z$  = rectangular Cartesian coordinate system

# **1. INTRODUCTION**

## **1.1 OVERVIEW**

Beams are considered as fundamental components of intricate system models and complex structures. Any structure when subjected to dynamic loads transmits vibration that can result in fatigue or even catastrophic failure through the resonance phenomena. In aerospace design, the aircraft wing, for example, can experience aerodynamic loads and vibrations that can result in phenomena such as flutter or buffeting that can damage or even compromise the structure. Every structure has at least one natural frequency that can be analyzed and help determine the modal parameters of the structure. Since dynamic characteristics of a system are determined by mass, stiffness, damping and the boundary conditions, any change to these can affect the modal frequency. The dynamic response of the structure excited by any stimulus can help determine the modal parameters and therefore inherent elastic properties of the beam material.

Weight is a major factor in aerospace design and results in a constant shift towards lighter materials that can be cheaply and readily manufactured. Forming and Subtractive manufacturing have traditionally been the processes of choice for the industry but additive manufacturing has now become the focus of development and research due to its capacity to revolutionize manufacturing with its flexibility and efficiency. Several technologies and manufacturing approaches have resulted from this push towards 3D printing, the most popular of which is the Fused Deposition Method (FDM) that can deploy a range of plastic materials.

Due to the rise in environmental concerns, the sustainable materials requirement has resulted in an industry wide drive to develop and adopt biodegradable materials to replace the use of oil based polymers and plastics. Poly Lactic acid (PLA) is a bioactive thermoplastic, aliphatic

polyester derived from renewable natural resources such as cornstarch in North America and other natural starch sources, e.g. sugarcane, readily available around the world. PLA, a 100% biopolymer and biodegradable material, has already found many uses in the biomedical and pharmaceutical application due to its biocompatible properties. Other application scope is in the automotive and aerospace industries where research is underway to tailor and improve the thermo-physical and mechanical properties as multifunctional polymeric composites. PLA therefore was an early candidate for the 3D printing FDM process.

The FDM method for 3D printing is the most widely used and involves heating the material and a printer base plate after which a bottom up, sequential layered approach is used to place the material filament is carried out, through a numerically controlled nozzle. The heated material solidifies as soon as it comes out of the nozzle (Wenzheng Wu, 2017).

Unlike its constituent homogeneous material, the 3D printed components display anisotropy due to the filament alignment in certain directions, inter-layer and inter-filament voids (also known as inter-bead, intra-bead and interfacial bead) (Haque., 2018, ) to name a few, somewhat similar to fibres in a composite material matrix. Recent research through traditional tensile tests (Y. Song, (2017) ) (ASTM International , 2015) show an elasto-plastic, orthotropic mechanical response with a strong asymmetry between both tension and compression. A large effort by recent available research literature has been to understand manufacturing parameters and other external factors to improve the mechanical properties of 3D printed polymers. The results of literature review section briefly delves in some of the different properties and reasoning behind their deviation from the bulk material. This project is focused on the determination of the resulting dynamic properties that are characteristic of the 3D printed PLA components.

Free vibration analysis has been used to determine a range of material properties, such as elastic constants (Young's modulus and Shear modulus), damping coefficient, etc. The method, also known by names such as Impulse/Impact excitation, resonance, vibration, eigenfrequency, and ping test, is a non-destructive (ND) material characterization technique in which elastic solid is lightly struck with a hammer or projectile, giving it energy to vibrate at its natural frequency (D. Ridley-Ellis, 2018).

Most experiments reported in the open literature are specific to an application where the determination of certain properties can help evaluate the material better than others are. For example, a material such as a polymer to be considered for damping purposes focuses on the time-dependent amplitude decay that can be extracted from a mechanical vibration as a result of a suitable impulse. Such experimentation to determine the Q factor and damping ratio is independent of dimensions therefore no specific test specimen form is required as long as the required frequency is obtained from the component. A number of other experiments have also been applied to determine various properties, such as storage modulus, loss modulus (Wei Sun, (2018) ) etc. These properties can also be determined through both the traditional mechanical static methods such as tensile testing, four point bending and nanoindentation (N.B. Podymova, 2013) and dynamic methods such resonant ultrasound spectroscopy (Davide S. Paolino, 2017) and Impulse Excitation Test (IET). The IET technique, easy to perform and efficient, provide an attractive methodology to obtain the intended parameters. Extensive successful corroborating work has already been performed using the methodology referenced in the literature review section.

This methodology requires picking up the vibrational signals, analyzing the vibrational signals and determining the resonant frequency. The simple geometries used such as rectangular beams have been extensively used with formulas available in literature. These researches have

focused on temperature and geometrical variations based on simple rectangular beams and rods. Since no studies have evaluated the dynamic properties of the PLA 3D printed parts through a vibration analysis, there is a requirement to carry out experimental investigation using IET. FEM simulations and traditional mechanical axial testing results are used for verification of the IET results for this project. Based on the literature review in Section 1.2, this experimentation study has selected the determination of the first fundamental frequency of 3D printed PLA beams and the Young's modulus as the objective for this dynamic investigation. The Young's modulus is extensively used in engineering and science applications to determine the dynamic response of the material to external forces and can be used to compare material quality as presented in the literature review section.

In a homogeneous, isotropic material, the longitudinal loaded tensile test results for the elastic modulus are the same as those obtained through IET based. Both testing methodologies follow the Hook's law. It is also well known that due to the flexing, the surface is placed under more stress than the test specimen center. If due to a stiffness gradient present in the thickness, for example in this case the voids (beads and micro-cracks) close to the surface, then the results of the IET in flexural mode are different and more precise. Due to this reasoning IET is very suitable for porous and brittle materials such as ceramics and 3D printed polymers. As also stated by earlier publications (HEYLIGER, 2001) (CHO, 2007).

IET is also versatile since the amount of deformation involved is minute because of the small elastic strains imparted by the impulse excitation, which allows repeatability of experimentation in relatively quick and simple tests. IET works well with the simplified assumptions on which simple beam theory such as the Euler-Bernoulli is based on. IET can be conducted over a wide range of temperature and provide insight on the microstructure along with

the already mentioned mechanical properties. The IET is widely used in the ceramic, wood and aluminum, industry due to its simple non-destructive testing nature and applicability in quality control, apart from research. The literature review section discusses some of the recent studies that were conducted to expand the scope of the quality control aspect of IET.

Various types of sensors have been used in recent studies including traditional contact sensors such as accelerometers and piezoelectric sensors or non-contact sensors including microphone and laser sensors, to determine the Young's modulus using an IET setup. This project has implemented the available laser displacement sensors as part of the non-contact and non-destructive experimentation process.

## **1.2 ORGANIZATION OF THE REPORT**

Followed by the Chapter 1 section 1.1 introduction, this section 1.2 explains the arrangement of this project report. Section 1.3 presents a broad literature review that briefly compiles and lists the recent research studies conducted for a number of topics affecting this project. The topics include material characteristic research of 3D printed materials including PLA, the applicable theories and methodologies that can be used for verification of the experimental results. The literature review section emphasizes the specific dynamic analysis methodologies and techniques that have been used for various materials characterizations.

Chapter 2 specifies the equipment setup designed for the experimentation process. Schematics and Illustrations are provided for better understanding of the equipment, technique and the process of experimentation to be carried out for the project.

Chapter 3 further discusses the manufacturing of the test specimens and the FDM process parameters used. The test specimen physical and dimensional characteristics are also presented in this section.

The Chapter 4 explains the FEM modal analysis method employed using the ANSYS software to generate the natural frequencies and the mode shapes generated.

Chapter 5 presents the conclusion of the report, followed by suggested areas of future research. The report ends with the appendices.

### **1.3 LITERATURE SURVEY**

The aim of this section is to survey the theoretical, experimental and finite element backgrounds of this research project in respect of the vibrational analysis of the 3D printed PLA rectangular beam samples.

The bending vibration of beams characterized by Euler-Bernoulli model of a slender (i.e., thin, engineering, long, etc.) beam, can be considered as a special case of the Timoshenko beam theory, obtained by neglecting the shear and rotary inertia effects, have been well studied and documented. The mathematical modeling of beam dynamics using the simple linear Euler-Bernoulli theory has been selected for this project due to its simplicity, conventional use and availability of formulas that can provide good results considering the assumptions of deflections in a transversely loaded beam with little or negligible shear deformations etc. (S.M. Hashemi, 1987) (Gang Wang) (Ewen., 2007).

This literature review is focused on the latest developments in experimental vibration analysis of 3D printed components. The objective was to get a better insight into the existing approaches and select the one that would suit our research in the vibration analysis of 3D printed PLA components.

A literature review of the recent developments in mechanical characterization of the 3D printed materials was conducted by (John Ryan C. Dizon, (2018) , p. 45), who have listed several works from the extensive fields of application for the printed materials such as construction, apparel, dentistry, medicine, electronics, automotive, robotics, military, oceanography, aerospace, and satellites. The “3D printing industry amounted to 13 billion dollars in 2016. The automotive industry applications amounted to over 3.9 billion and ~2.4 from aerospace. Considerable higher revenues are reported from the medical and dental applications for 2016. With an annual growth rate forecast of 22.3% for next few years and ~29 billion of revenues expected in 2020”.

A number of works have limited the scope of their mechanical characterization studies to polymer materials. The polymer materials, though much lower in strength than metals, are much lighter with lower densities and have higher strains at failure. In some cases, plastics have demonstrated higher strength per unit weight than metals (Y. Song, (2017) ).

Another more specific study on measurements of mechanical response of unidirectional 3D-printed PLA was carried out that characterized the elasto-plastic materials as orthotropic with a strong asymmetry and toughness in the extrusion direction as transverse direction. The results claim toughness increase for the 3D printed parts when compared to the homogeneous injection-moulded PLA (Y. Song, (2017) ).

The Impulse Excitation Test (IET) technique selected for the experimentation project has been successfully employed in numerous research works for a variety of non-isotropic materials. In one of the recent publications (Wenlei Song, (2017) ), the IET was applied to identify the mechanical parameters of laminated composites, in comparison with the results obtained from FEM analysis. With acceptable variation of under 4%, the methodology served as a reference for this project (Wenlei Song, (2017) ). Another recent study that used IET in comparison with tensile test results to attain Young's modulus value, recorded a 10% mean standard deviation between the two methods (Lotfi Toubal, 2018).

IET was used to determine the residual Young's modulus for damaged composite laminates in a recent study (Davide S. Paolino, 2017). When compared with standard tensile tests, the study proved IET to be a rapid and effective method for measuring longitudinal Young's modulus. IET results were not affected by local inhomogeneity in thick composite laminates, as it was categorized as a global technique that was better suited to determine the overall Young's modulus of damaged composites. Another useful conclusion made in reference (Davide S. Paolino, 2017), was that the Young's modulus evaluated through IET are on average slightly higher than those obtained from the standard tensile tests are.

A diagnostic study was conducted earlier by (P Chiariotti, 2013) to exploit the IET determination of Young's modulus for detection of brake pad assemblies. The study proved the Young's modulus determination robust enough to identify the damage and concluded that additional properties such as the damping ratio or Q factor (used as a basis for diagnostic methods) does not increase the robustness of the employed methodology. The results recorded 40% decrease of effective Young's modulus in damaged pads.

Other similar recent IET applications include the efforts to determine small changes in elastic moduli and damping in wood (D. Ridley-Ellis, 2018) (Guan, (2016) ) (Walunj Prashant S, (2015) )

The major sources of error for the IET experimentation have been evaluated by (M.F. Slim and A. Alhussein, 2017) as the test specimen thickness followed by density. In conclusion, the IET has proven to be an excellent method to determine the Young's modulus for a wide variety of materials including metals, composites, ceramics, coatings etc. (D. Ridley-Ellis, 2018) (N.B. Podymova, 2013) (Davide S. Paolino, 2017) (HEYLIGER, 2001) (Gang Wang) (Guan, (2016) ) (M.F. Slim and A. Alhussein, 2017) (Wei Sun, (2018) ) (Lotfi Toubal, 2018) (Monti., (2017) ) (Ramesh., 2015) (Somen K. Bhudolia, (2017) ).

## 2. EXPERIMENTATION SETUP DESIGN

This section explains the methodology adopted to perform the dynamic investigation on the 3D printed material samples. The experimental test set up design and the modal analysis was carried out in compliance to the ASTM E1876-15 (ASTM International , 2015) and E756 – 05 (ASTM International, 2017) standards. The basic setup schematic block diagram is illustrated in Figure 1. The 3D representation of the final physical equipment design setup is illustrated in Figure 2. The test specimen dimensions are discussed in detail in Chapter 3.

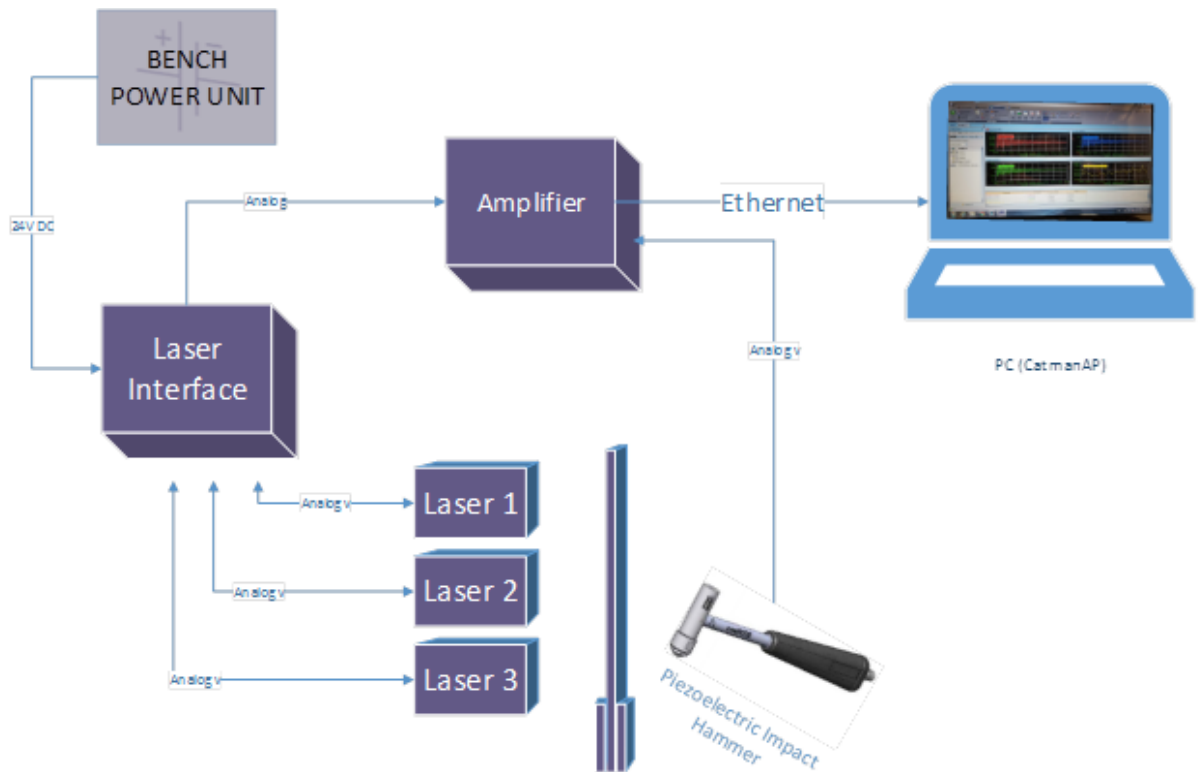


*Figure 1: Experimental Setup Schematic*

A simple yet modular experimental setup is devised which includes a rigid horizontal extrusion attached to a metal table. Another rigid vertical extrusion is fixed onto the center rail using brackets that house three Laser displacement sensors (Mitak 3). The heavy steel table provides an isolated platform for the sensors and modular measurement equipment. The rest of the experiment test equipment including the PC, Amplifier unit (HBM X400A), Laser Interface (Durham Instruments) and the Bench Power Supply (BK Precision 673) were all setup on a separate lab desk.

The sensor base or ‘mounts’ were designed using 3D CAD (Catia V5), per sensors external dimensions and then converted to STL (Stereo lithography format) for 3D printing to hold the sensors firmly. This configuration provided easy adjustment of the sensor height along the specimen and could accommodate for different test specimen lengths. The Sensor mount design is illustrated in Appendix A1.

The distance between the laser sensors to the test specimen was set to an optimal value of 50mm, as per manufacturer specs for exploiting the complete range of vibration-triggered displacements of the test specimen. The bracket facing the sensors was fixed to maintain the set distance while the rear bracket was tightly clamped through a C-Clamp after aligning the test specimen centre line along the incident laser sensor beams and clamp limit as illustrated in Figure 2: 3D Catia V5 design for experimental equipment including sensors and test specimen and Appendix A2. Appendix B contain the lab manual developed for the efficient use of the test equipment in future with the objective of reducing the setup time, through systematic documentation for the conduction of IET experimental hardware and the Data Acquisition (DAQ) CatmanAP software.

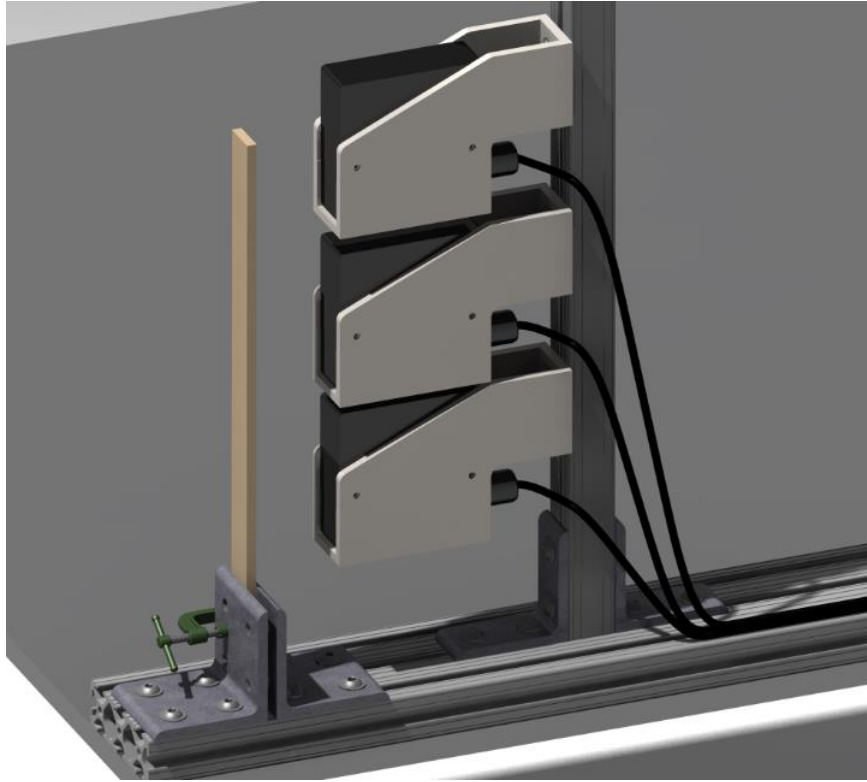


*Figure 2: 3D Catia V5 design for experimental equipment including sensors and test specimen*

There are a number of boundary conditions that can be used for vibration analysis of a beam as discussed in the literature review section. The cantilever boundary conditions (which is considered to be the most demanding case for practical applications) (Ewen., 2007) is selected for this experimentation. In case of the cantilever, it is important to note that the node position of the mode shape is defined by the fixed boundary condition. Well-established formulas in conjunction with, the specimen dimensions that provide a good aspect ratio can be used to determine anisotropic material properties (D. Ridley-Ellis, 2018).

The IET method selected can provide very good approximation results with the use of Euler-Bernoulli model of a cantilever beam. With the use of non-destructive laser sensors along

with the DAQ capable of measuring at very high frequencies and nanoscale displacement measurements, a simple piezoelectric impulse hammer can be used to force induce very light impulses that can accurately determine the Frequency Response Functions (FRFs) for the first resonant frequency.

The clamping force in the fixed boundary conditions (BC) can have an effect on the stiffness of the test specimen and can result in slight variation of frequency results. To acquire a better understanding of the frequency variation experienced during multiple test setup and test-runs for the same sample, the clamping force was considered. Confined by the in-availability of a torque measuring setup in the lab, a methodology based on rough estimates was also developed to simulate partially clamped and fully clamped conditions based on the number of turns applied to tighten the C-clamp placed over the brackets.

Result readings were measured with the different simulated clamping conditions and the variation in results was recorded. The variability in the frequency results due to the clamping conditions was calculated to be 2%. This variation was acceptable as it ensured the factor for the boundary condition would not have a major impact on the experimental results. The detailed analysis of the data leading to this result is beyond the scope of this report.

Different clamping lengths as marked on Figure 3: 3D Printed Test Specimen with characteristic lengths illustrated were used to generate results with two sets of clamping areas. This allowed the beam to simulate two sets of free vibration lengths, which would result in different resonant frequencies for the same test specimen. Using non-dimensionalized equation (1) shown below, the results were compared for each set of values to determine the variation in the resonant frequency results for the same sample.

The sensor setup was designed to capture measurements along the centre line of the test specimen in an attempt to isolate and capture the first modal frequency for the test specimen. The redundant sensors are used to ensure that only the targeted flexural mode frequencies are detected by all sensors.

To trigger the vibration, a Piezoelectric Impact hammer (Dytran Dynapulse 5800B4) was used with a soft silicone tip, to gently tap the test specimen. The impacts location was kept close to the fixed end about approximately 20mm above the clamped boundary, as this ensured enough amplitude for the specimen free edge to be recorded by the sensors range and minimized double tap impulses. The impulse hammer taps were restricted to the test specimen's centre line to induce a pure bending resonant frequency to mitigate as much as possible any bending-torsion coupled frequencies. For future research it is pertinent to mention here that similar setups such as suggested in (Lotfi Toubal, 2018) and (ASTM International , 2015) can also be used to measure shear values.

The bench power unit step-down voltage set to 24V-DC powers the Laser sensors through a Laser Interface. The Analog output voltage from the Laser Interface is delivered to the HBM X400A Amplifier that delivers the measurements to the PC based DAQ software. A Piezoelectric Impact hammer is used to induce the forced vibrations. Finally, the time domain and frequency domain results of the test specimen beams are obtained using the HBM CatmanAP software. Figure 7: Typical FRF result from laser sensor 1 for XYZ build orientation shows a typical output received from the CatmanAP DAQ system by conducting IET experimentation.

### **3. PRODUCTION OF TEST SPECIMEN**

#### **3.1 SPECIMEN GEOMETRY**

The Section 8 of the ASTM E1876-15 standard specifies a minimum ratio value of at least 5 between the length and the thickness of the IET test specimen beam. For ease in calculation, the standard does state preference for a ratio of 20 to 25. As mentioned earlier this project has focused on the simple relationship based on the Euler-Bernoulli beam theory. As a result, the minimum criteria associated with a slender beam to be considered an Euler-Bernoulli beam is a ratio of 10 between the length and the thickness and studies have been conducted to a ratio of 100 to extract better results. A brief literature survey of the similar IET experimental tests published was conducted to document the breadth of dimensional ranges used for the test specimen (Davide S. Paolino, 2017) (Wenlei Song, (2017) ) (Guan, (2016) ). Based on the type of the material the relevant ranges of the test specimen lengths were determined to be 200 to 500mm, width of 10 to 50mm and thickness ranging from 2 to 5mm. The literature survey table is presented in Appendix A3. More information can be found in the references and further reporting on the data has been omitted here for the sake of brevity.

The laser sensors stacked vertically across the test specimen centerline along with the designed mounts required a minimum test specimen length of 260mm for the designed setup, if all three are used to provide redundant resonant frequency measurements. Finally, the 3D printing equipment limitations were also considered before selecting the dimensions some of which are illustrated in Figure 3, which are discussed in detail in the Section 3.2. One of the build orientation due to the printer hardware limitation could only be printed to a maximum length of 245mm. This is illustrated Figure 3b. The other two build orientations as per Figure 3a were printed to a length

of 270mm. These provide a length to thickness ration of 70 and 77, which meet the Euler-Bernoulli beam criteria. The designed width was selected as 20mm and a thickness of 3.5mm was selected for all build orientations.

Other than the length of the specimen, the clamped area boundary and centerline are also marked on the specimen in Figure 3 that are used to ensure proper alignment of all specimens in the rigid test fixture (Somen K. Bhudolia, (2017) ).

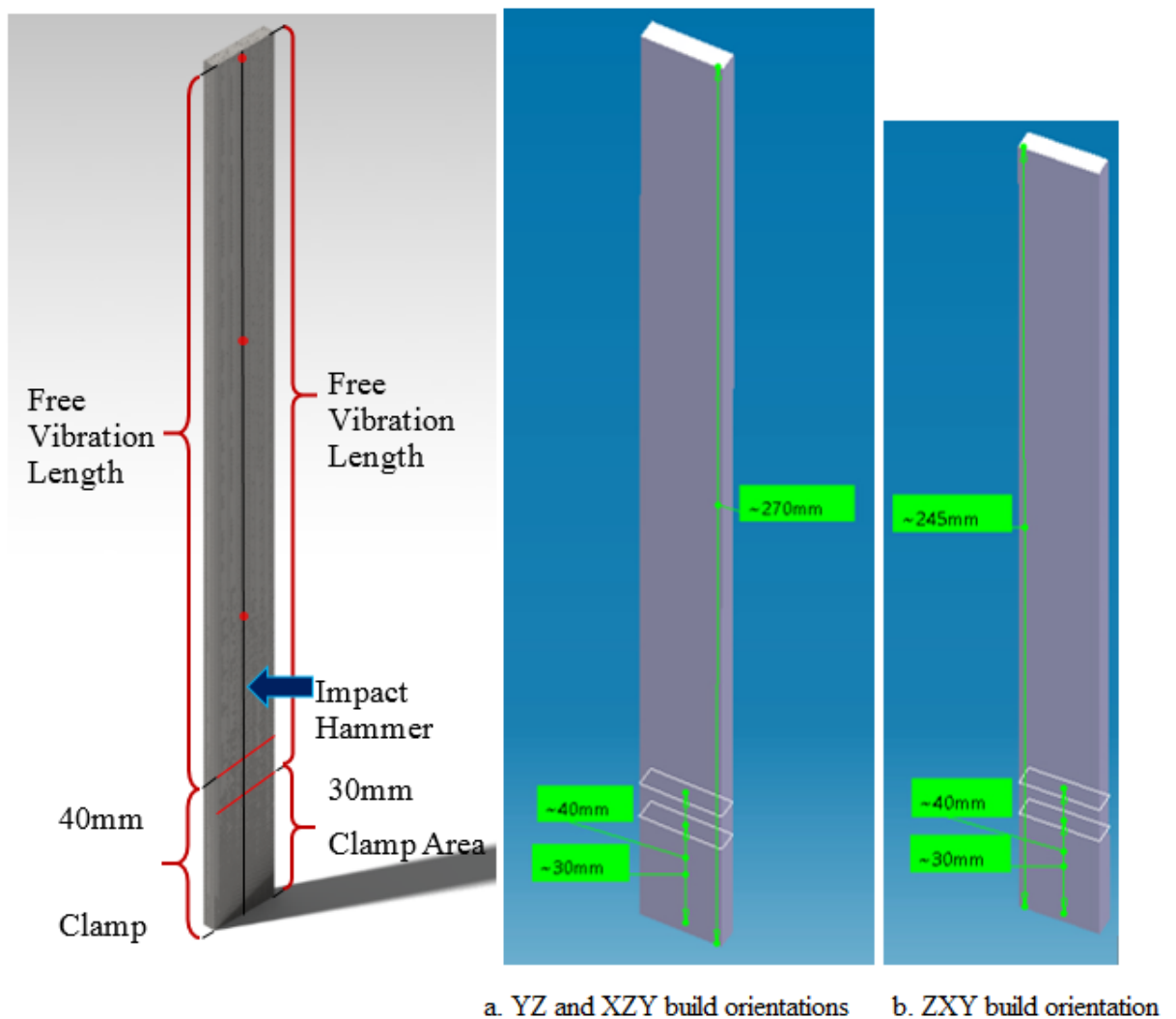


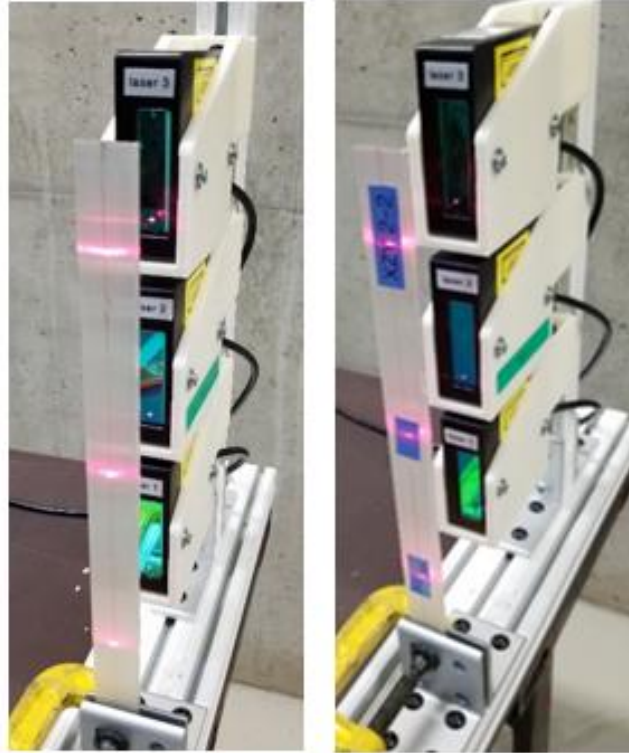
**Figure 3: 3D Printed Test Specimen with characteristic lengths illustrated**

It is important to note that two sets of clamped lengths for the sample were used for this experimentation as discussed in Chapter 2 above.

The test specimen dimensions were measured using a Vernier caliper and a micrometer was used to measure the thickness of the samples. A number of measurements were taken for each sample and averaged to help factor in the variability of each sample 3D printed using layers of the PLA filament. Based on the specimens' weight, lengths, and dimensions of the cross-sectional areas the densities were calculated. These densities are then used in the formulas listed in Section 3.3 to determine the Young's modulus.

A few recent studies that examined the transparent PLA specimens with others containing pigmentation resulting in a variation of properties and material finish concluded the transparent PLA without pigmentation to be stronger and more precise dimensionally (Valerga. A. , (2017) ) (Juliana Breda Soares, (2018) ).

Since the PLA test specimen used were transparent for this experimentation, it did provide an unforeseen result for test specimen of orientation XZY. All test specimen of the XZY build orientation failed to register any reading through the laser sensors. Through a number of test iterations other causes for the failure of the sensors to register readings were ruled out. It was observed that the incident laser beam underwent diffraction which could probably be attributed to the FDM filament pattern on the XZY samples (without pigmentation). A number of work around were tested to enable the acquisition of readings for XZY samples, these included using markers and lead pencils on the beam incident points as well as using small stickers shown below in Figure 4.



a. Laser diffraction

b. Workaround using stickers

*Figure 4: XYZ build orientation*

### 3.2 SPECIMEN MANUFACTURING

A total of 11 test specimen were 3D printed using Prusa i3 MK2S printer. The manufacturing process and design parameters are presented in Table 1.

*Table 1: 3D printer FDM manufacturing parameters used to produce test specimens*

<b>Manufacturing / design Parameter</b>	<b>Value</b>	<b>Manufacturing / design Parameter</b>	<b>Value</b>
Material	PLA	Bed temperature	60 °C
Print direction	XYZ/XZY/ZXY	Layer height	0.14 mm
Raster angle	0°	Printing speed	2400 mm/min
Filament diameter	2.85 mm	Cooling	No fan cooling
Nozzle diameter	0.4 mm	infill	100%
Nozzle temperature	205 °C		

Figure 5 below illustrates the build orientation of 3D printed PLA specimens printed flat (XYZ), on-edge (XZY), and upright (ZXY). All manufactured specimens are tested using the apparatus described in section 2 and results are presented in Section 3.

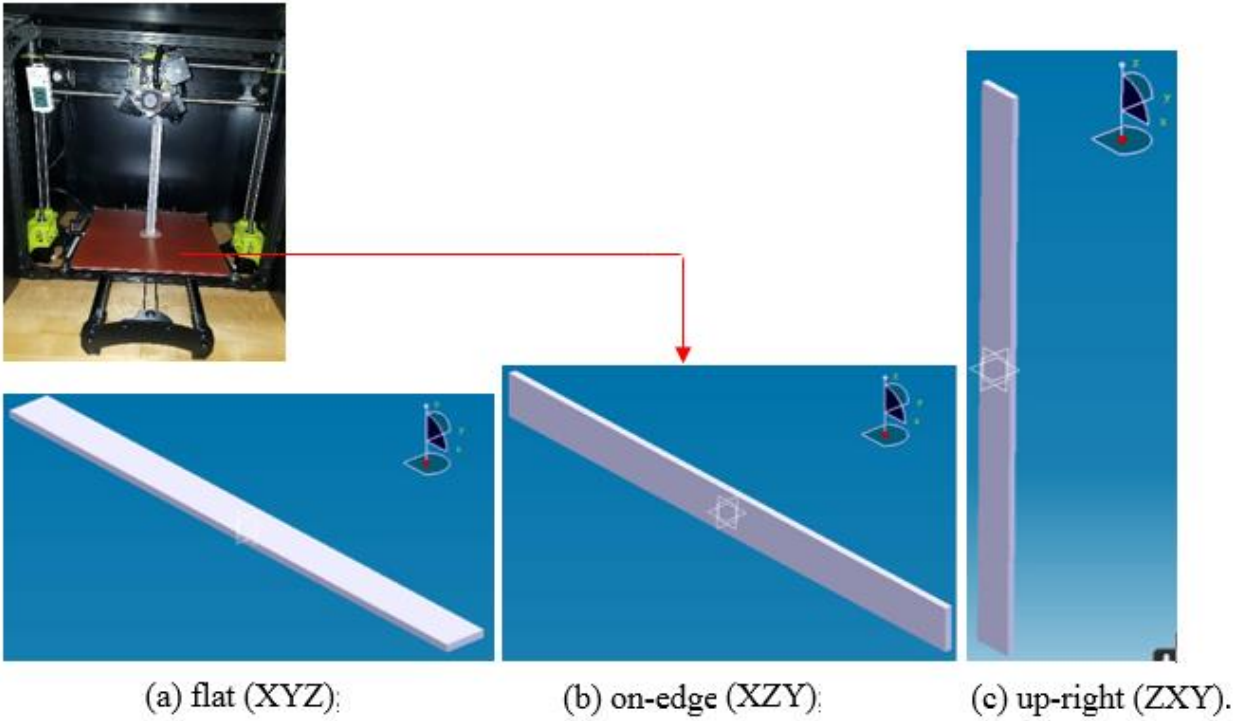


***Figure 5: 3D printed PLA specimens in three build orientations:***

Tensile testing per ASTM D638 was performed to evaluate the Young's modulus along the specimen length. Test specimen are 3D printed per ASTM D638-14 type I. All manufacturing and design parameters for dynamic samples were also used for these tensile specimens 3D printing. This way, Young's modulus of dynamic samples can be obtained accurately using tensile testing and there is no need to rely on data sheet information from the filament provider. To ensure material uniformity the same batch of the filament was used in the printing of all specimens. No surface treatment or finishing of any sort was applied (Davide S. Paolino, 2017) to the test specimen.

### 3.3 EXPERIMENTATION OF DEVELOPED SPECIMENS

Using the setup discussed in previous sections along with the manufactured test specimens, the experimentation was carried out systematically as per the instruction manual documented and attached in Appendix C. The Frequency Response Functions (FRFs) were recorded along with the specimen mechanical and dimensional parameters to determine factors such as density and beam moment of Inertia.

To reduce the impact of the sensors' mass on the structural dynamic characteristics, laser sensors are adopted to realize a non-contact test. In addition, to ensure that the resonance frequencies can be excited as much as possible in the considered frequency range, the excitation point was kept close to the clamped end to avoid double taps and enable an elastic impulse to be imparted to the specimen. The picking vibration points were chosen carefully (Wei Sun, (2018) ) as illustrated in Figure 3 to ensure that the same resonant frequency is detected by redundant sensors. After recording consistent results, the sensor positioning was altered by shifting all the laser sensors by 20mm to see if any variation in sensor results could be detected. With all sensors at the new positions, as expected, the setup provided the same resonant frequency values with a difference in amplitudes. This consistency with the change in sensor positioning is illustrated through FRF plots in Figure 8 and Figure 11.

Using the placement of the sensors at multiple locations the modal shapes could also be graphed. For such applications, a continuous scanning Laser Vibrometry equipment would be a better choice. Similarly, the damping characteristics could also be calculated from the scope results generated during the IET. The focus of this experimentation though remains limited to the determination of the fundamental first natural frequency of the 3D printed PLA beam specimen in

order to generate the Young's modulus. Once the experimentation results for all specimens are determined then the next step is to model the beams in ANSYS using actual specimen dimensions and carry out Modal Analysis on all build orientations illustrated in Figure 5. These results are compared to the experimentation results attained through the following steps in the next chapter and finally the traditional tensile test results.

Similar to the fact that restricting the number of moving parts in a machinery can raise dramatically the reliability of the machinery, this experimentation procedure is selected to harness the non-contact property of lasers for measuring the minute displacements introduced through measured, forced impact hammer induced pulses.

By limiting any changes to the test specimen's mass or any other characteristic property by attaching an accelerometer or any other sensor etc. the probability of better test results is improved. A simple setup as described in Sections 2 and 3 requires a cantilever beam with one end rigidly fixed and the other vibrating freely.

To determine the frequency response function (FRF) of the specimen, the impact hammer test is performed using the DAQ acquisition software (CatmanAP) as illustrated in the experimentation manual in Appendix C. A typical output is illustrated in Figure 6. The three laser sensors aligned along the centerline provide redundant FRF results with varying amplitudes to confirm the modal frequency acquired from the test. A centerline and clamping limits were marked as illustrated earlier in Figure 3 to align the laser incidence points along the same line in order to isolate the first modal frequency. Care was also taken to induce a forced impulse transversely through the impact hammer on the same centerline in order eliminate any force causing the test specimen to twist laterally resulting in an incorrect modal frequency. The impulse force was

recorded and varieties of force values were used to measure the amplitude and resulting frequency. Figure 6 shows the screenshot result from the piezoelectric impulse hammer using the DAQ software.

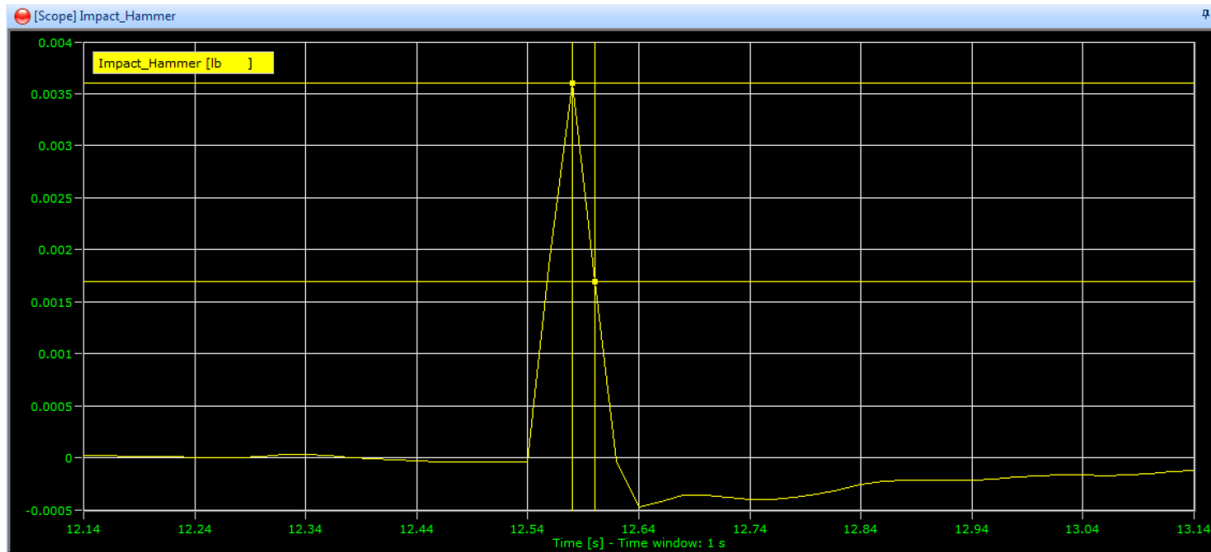


*Figure 6: Screenshot of Piezoelectric impulse hammer force in time domain*

An effort was made to conduct all the initial sets of tests with the focus on analyzing real time live FRFs and scope results for all channels (three laser sensors and the impact hammer) rather than waiting for the final large amount of data gathered from multiple test runs. This provided the opportunity to process real-time results on the spot and change or tweak any factor that had an adverse impact on the results. Following the same methodology of closely monitoring each aspect of the experiment, a number of factors were analyzed and improved e.g. the Clamping force and the impact impulse force induced. These factors along with the selected test parameters illustrated in Figure 8, were tweaked to produce clear, optimized and replicate-able results.

Through trial and error an optimum impulse excitation force was determined to enable acquisition of clear frequency results for all build orientations. The data analysis option in the DAQ software provides the user with the means to add any amount of required test runs data in a single analysis window to compare all the results on the timeline. The user can control a cursor back and forth on the timeline and analyze all resulting graphical peak values from all channels simultaneously. Figure 9 presents an example of a data analysis screenshot from the DAQ illustrating the impact force peaks on the timeline along with the maximum values for each channel, i.e., all three lasers and the impact hammer. It was observed that slight changes in the free lengths (as low as 1mm) could result in small deviations of natural frequency, e.g., 0.19 Hz, in this case.

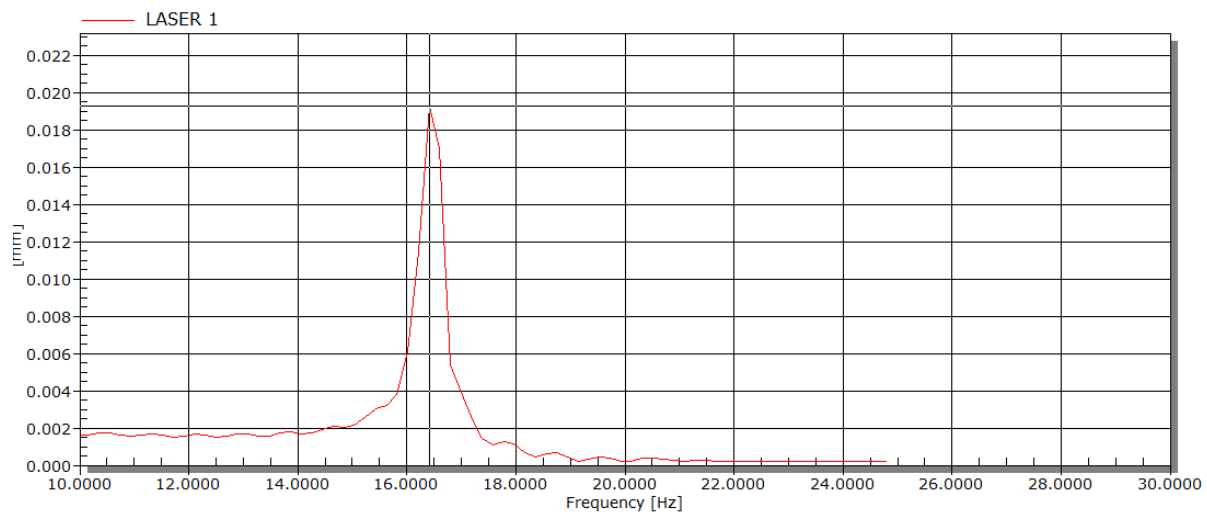


***Figure 7: Typical FRF result from laser sensor 1 for XYZ build orientation***

Default sample rate = 50 Hz  
 Slow sample rate = 20 Hz  
 Fast sample rate = 2400 Hz  
 Number of samples default sample rate = 442  
 Number of samples slow sample rate = 0  
 Number of samples fast sample rate = 0  
 Start mode = Manual  
 Start time = 15/12/2018 11:37:43 PM  
 Stop mode = Manual  
 Stop time = 15/12/2018 11:37:52 PM  
 catmanEasy/AP version = 3.3.5.58  
 Numerical precision = 8 Byte Float

**Figure 8: Sample Test run parameters used in DAQ software (CatmanAP)**

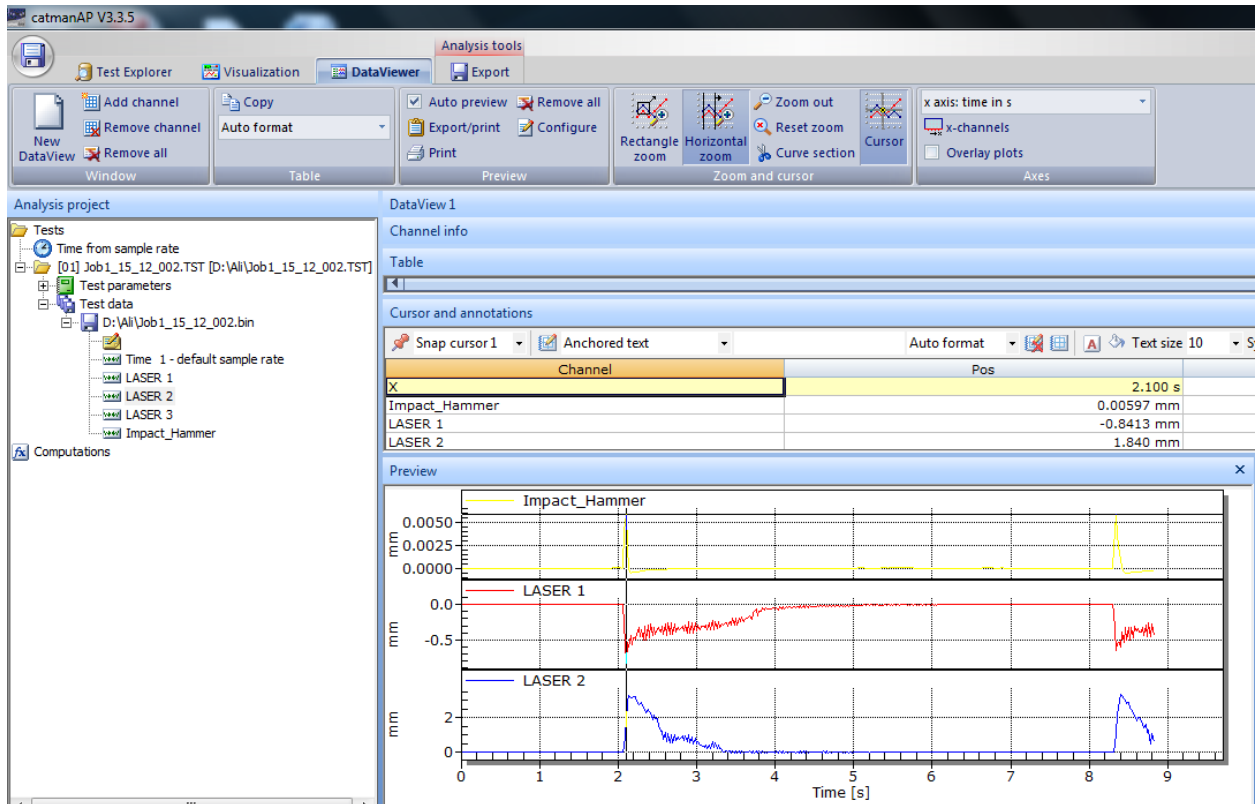


**Figure 9: Data Analysis screenshot of DAQ software comparing displacement amplitude from two laser sensors and the impact force from the piezoelectric sensor**

To demonstrate the consistency and repeatability of the results, a ZXY build orientation sample with an FRF value is illustrated in Figure 8 below. The same sample when tested again with the laser sensor moved closer to the free end tip of the test specimen beam can be seen to provide the same result with an increased maximum displacement (see Figure 9).

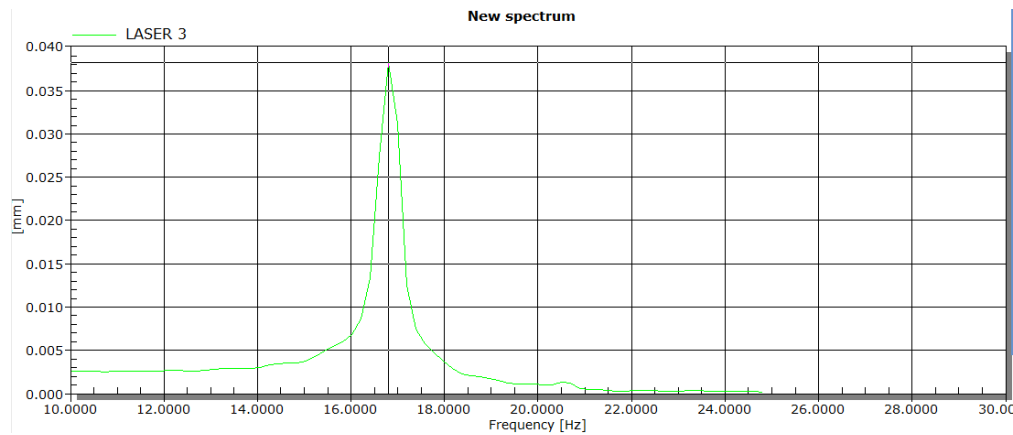


***Figure 10: FRF of ZXY sample with initial laser 3 position***

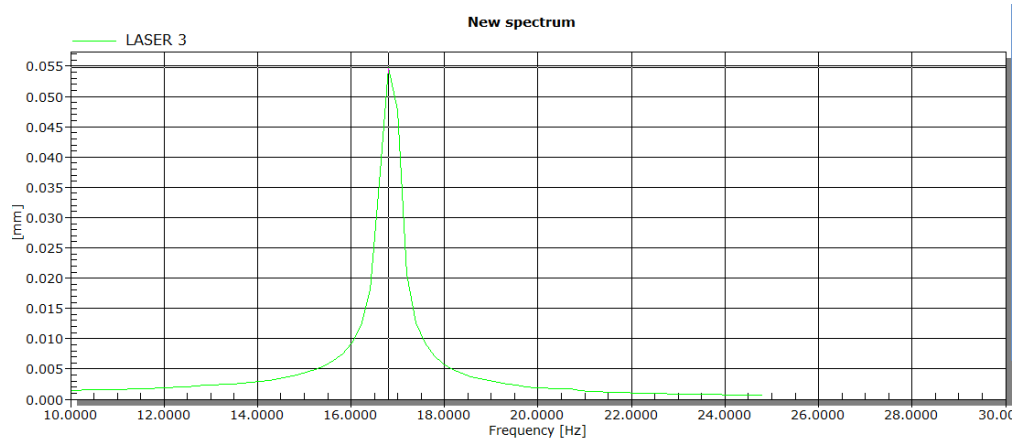


***Figure 11: FRF of ZXY sample with laser 3 position moved closer to tip***

As mentioned earlier, the 3D printed test specimen dimensions were measured at five equidistant spots along the length of the sample and results were averaged. Similarly, the mass was

measured as listed in Table 2 below, along with the corresponding resultant first modal frequencies obtained through the IET experimentation.

*Table 2: Test Specimen mechanical parameters and results*

<b>SPECIMEN</b>	<b>H (mm)</b>	<b>B (mm)</b>	<b>L (mm)</b>	<b>Mass (g)</b>	<b>Frequency (Hz)</b>
1-0 XYZ	3.462	20.262	271	23.3	16.41
1-1 XYZ	3.397	20.378	271	22.8	15.63
1-2 XYZ	3.511	20.148	271	23.33	16.41
1-3 XYZ	3.476	20.152	271	23.24	16.41
1-4 XYZ	3.443	20.238	271	23.16	16.21
2-1XZY	3.706	19.896	271	23.47	16.8
2-2XZY	3.650	19.996	271	23.47	16.6
2-3XZY	3.720	20.112	271	23.73	16.8
3-1 ZXY	3.900	20.085	245	22.3	20.31
3-2 ZXY	3.879	20.09	245	22.01	20.31
3-3 ZXY	3.957	20.09	245	22.38	20.9

As discussed earlier, the Young's modulus is a fundamental property and a key parameter in mechanical engineering design to predict material behavior under forced deformation. The reason for selecting the Young's modulus as the main objective of this experimental study, as opposed to the resonance frequencies is due to the proven robustness of elastic modulus as an indicator of the material quality. Studies where factors such as temperature and moisture content have been considered, show little changes in resonance frequencies but can result in marked

changes in the systems' Young's modulus (Lotfi Toubal, 2018). These factors have little change on the resonance frequency but marked effect on the Young's modulus

The first modal frequencies for the 3D printed specimens, as presented in Table 2 above, are then used to calculate E values for each specimen using the following relationship between the non-dimensional frequency (1) as reported in reference (S.M. Hashemi, 1987);

$$\lambda^2 = \frac{\rho A l^4}{EI} \omega^2 \quad (1)$$

with

$$\lambda_1 = 3.5160$$

$$\lambda_2 = 22.0345$$

$$\lambda_3 = 61.6972$$

$$\lambda_4 = 120.902$$

where  $I = \frac{bh^3}{12}$ .

The first nondimensional frequencies listed above are compared to the right hand side of the Equation (1), where  $\rho$  is the test specimen density, A is the cross-sectional,  $l$  is the free

vibrating length,  $\omega$  is the measured natural frequency, and E is the Young's Modulus. Equation (1) is used with the dimensional and other test specimen parameters to determine Young's moduli.

***Table 3: Young's modulus results from tensile testing for each test specimen***

<b>Test Specimen</b>	<b>E (Pa)</b>
1-0 XYZ	3.402E+09
1-1 XYZ	3.417E+09
1-2 XYZ	3.154E+09
1-3 XYZ	3.382E+09
1-4 XYZ	3.397E+09
2-1XZY	3.009E+09
2-2XZY	3.089E+09
2-3XZY	3.074E+09
3-1 ZXY	2.549E+09
3-2 ZXY	2.835E+09
3-3 ZXY	3.018E+09

The results presented in Table 3 above are the Young's modulus evaluated through the IET experiment for each 3D printed test specimen.

#### **4. FEM MODAL ANALYSIS**

The FEM analysis is the fastest tool to determine the modal frequencies of the 3D printed PLA beams since it only requires modeling of the beams using test specimen design dimensional data and input of other available mechanical material properties. Even if all the required properties are not accurately input, the FEM method can still be used with the available bulk material data available to determine the modal frequencies. Although not very accurate, the FEM provides useful results to validate the preliminary IET experimental frequencies.

The 3D test specimen build orientation illustrated in Figure 1 Figure 5 above, were modeled in ANSYS using the design data selected for the 3D printed PLA beams. Modal Analysis was then conducted for all three build orientations.

With the printing of all IET test specimen completed and dimensions carefully recorded, the average dimensional values for all three build orientations were then used to update the ANSYS models. Material's mechanical properties determined through tensile tests were also used as input to further develop simulation test specimen as close to the actual IET test specimen as possible. A list of all the measurements and properties used to define the ANSYS models are provided in the ANSYS report presented in Appendix D. In what follows, the final ANSYS modal analysis results for the three build orientations are presented.

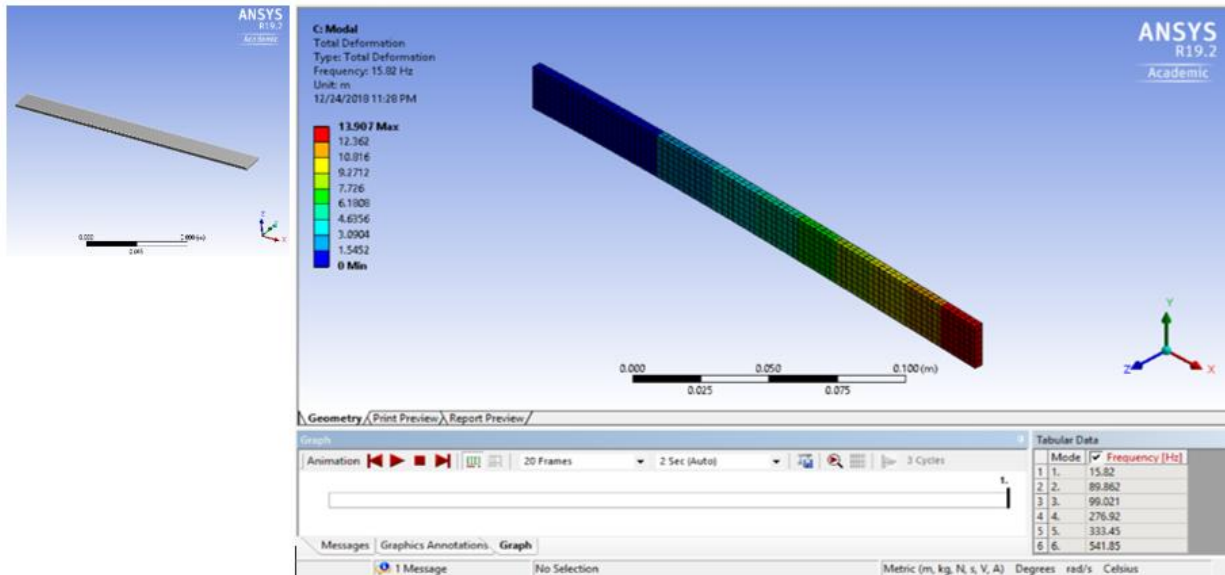


**Figure 12: First mode shape for build orientation XYZ**

The FEM results conducted in Ansys can also readily generate the mode shapes for visual validation of results. Since the software can easily determine a range of modal frequencies and shapes, the user can then select and isolate the results for the first modal frequency that does not display any twist or torsion. The bending mode shape associated with the fundamental frequency for the XYZ orientation, only contains bending and (no twist), as can be seen in Figure 12.

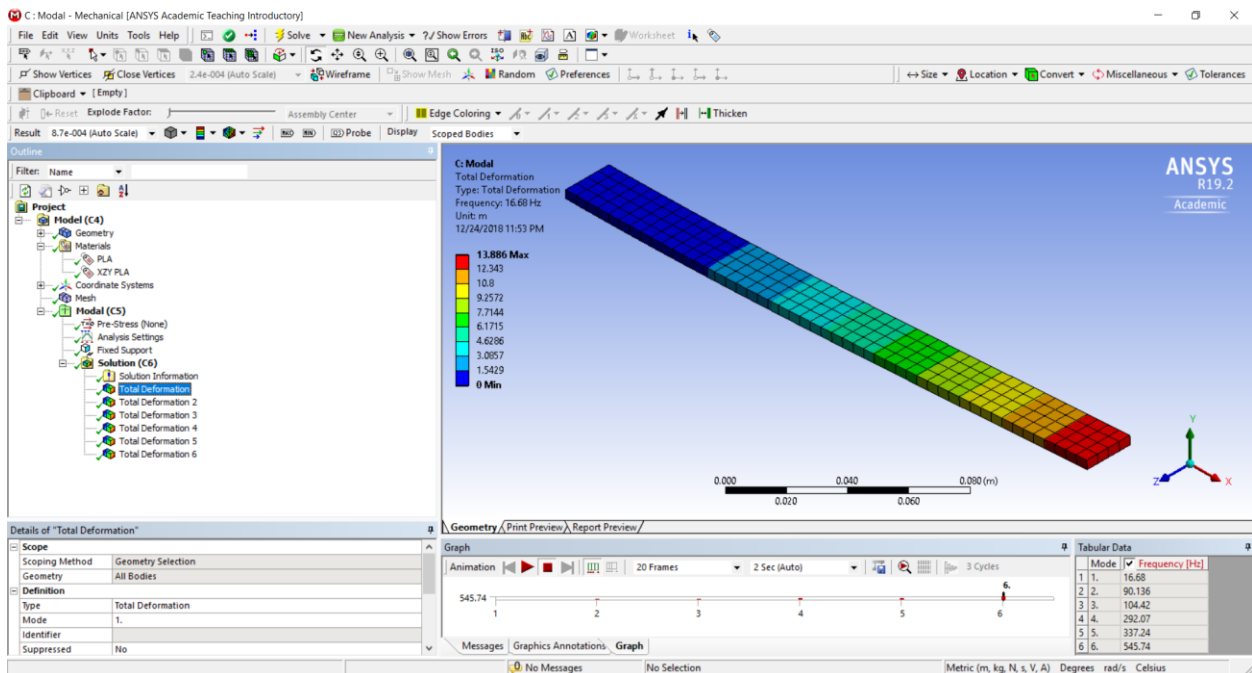
The FEM analysis was conducted for all build orientations, with actual 3D printed test specimen dimensions, modeled and simulated for the final modal frequency analysis presented in Table 4,

Table 5 and Table 6, and Figure 12 Figure 13 and Figure 14.

**Table 4: Table of modal frequencies for orientation XYZ**

Mode	Frequency [Hz]
1.	15.82
2.	89.862
3.	99.021
4.	276.92
5.	333.45
6.	541.85

The second sample was modelled with build orientation of XZY.



**Figure 13: First mode shape for build orientation XZY**

**Table 5: Modal frequencies table for XZY**

Mode	Frequency [Hz]
1.	16.68
2.	90.136
3.	104.42
4.	292.07
5.	337.24
6.	545.74

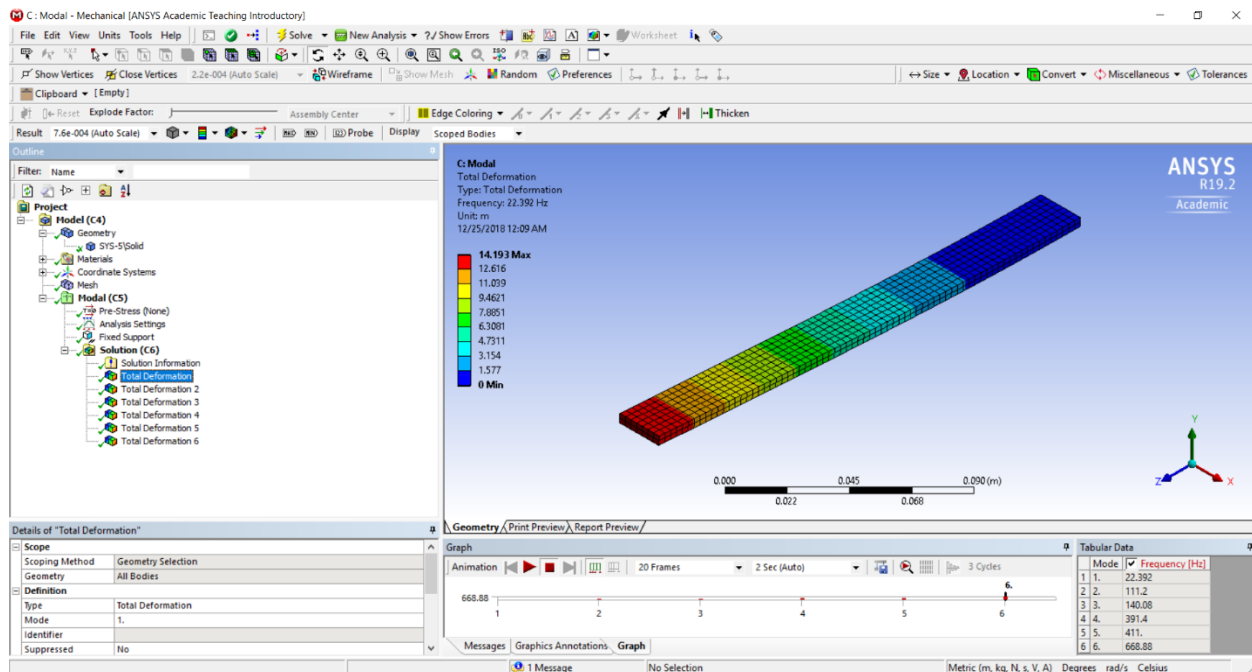


**Figure 14: First mode shape for build orientation ZXY**

***Table 6: Modal frequencies table for ZXY***

<b>Mode</b>	<b>Frequency [Hz]</b>
1.	22.392
2.	111.2
3.	140.08
4.	391.4
5.	411.
6.	668.88

The Young's modulus results obtained from the traditional tensile test are presented in Table 7. The tensile test results are used as a benchmark for comparison with the IET experimental results. The FEM analysis is also based on the results of the tensile test, as mentioned earlier.

*Table 7: Tensile test results for Young's modulus*

<b>Build Orientation</b>	<b>Max force (lbf)</b>	<b>Failure Stress (psi)</b>	<b>Strength (MPa)</b>	<b>E (GPa)</b>
XYZ	633.576	8767.719	60.4513	3.108
XYZ	581.239	8045.874	55.474	3.026
XYZ	543.048	7584.888	52.295	3.295
XYZ	596.226	8354.298	57.600	3.110
XYZ	615.650	8613.430	59.387	3.212
		Average	57	3.15
		Standard Deviation	3.26	0.1
		CV	5.70%	3.30%
ZXY	512.349	6831.565	47.102	2.994
ZXY	485.754	6044.210	41.673	2.866
ZXY	511.049	6390.210	44.058	2.835
ZXY	501.742	6709.263	46.258	2.972
		Average	44.8	2.92
		Standard Deviation	2.43	0.08
		CV	5.40%	2.70%
XZY	674.218	9194.757	63.395	3.115
XZY	672.535	9188.890	63.355	3.148
XZY	666.527	9097.895	62.727	3.090
XZY	667.800	9047.839	62.382	3.145
XZY	668.076	9047.410	62.379	3.091
		Average	62.800	3.120
		Standard Deviation	0.5	0.03
		CV	0.80%	0.90%

The IET Young's modulus results from Table 4 are averaged for each build orientation (first two results have been omitted for the two extra test specimens printed i.e. 1-0 XYZ and 1-1 XYZ, for better accuracy and consistency of samples), and are compared to the average Young's modulus results from Table 7 obtained through the tensile tests (please refer to Table 8.)

***Table 8: Comparison of Young's modulus results from IET and tensile test***

<b>Build Orientation</b>	<b>E (GPa) IET</b>	<b>E (GPa) Tensile</b>	<b>Deviation %</b>
XYZ	3.31	3.15	5.1
XZY	3.06	3.12	2.0
ZXY	2.80	2.92	4.1

As can be seen from Table 8, the comparison provides a very good agreement of results with the most deviation recorded as 5.1% in the XYZ build orientations.

## **5. CONCLUSION AND FUTURE WORK**

The IET experimentation carried out was found to be a rapid, global, result oriented technique for accurately finding the Young's modulus for 3D printed PLA Euler-Bernoulli beams. Compared to the traditional tensile tests, IET provided unlimited repetitive results due to the non-destructive nature of the experimentation. In corroboration of previous IET works, the experimentation for this project provided excellent results.

The tests and numerical modeling were carried out for 3D printed PLA, with three build orientations namely, XYZ, XZY and ZXY. The build orientation XZY proved challenging in generating results through the use of the laser sensor. This could be associated with the laser beam diffraction observed in printed material. This issue was addressed by adding small stickers to the beam incidence point. The results from the IET experimentation, the tensile tests and the FEM Modal analysis were found to be in close agreement with each other with a maximum error of 5.1%.

### **5.1 RECOMMENDATIONS FOR FUTURE WORK**

The IET as discussed in the project can be used to evaluate various elastic properties for a wide variety of materials included 3D printed. This can include thin films and coatings that can be produced much cheaply and still provide results readily. Other factors such as temperature and moisture, already the focus of some research, can also be tested without relying on manufacturer specs for the bulk material. Apart from elastic properties damping characteristics can be evaluated with applications for passive damping materials in aircraft interior components and fittings to structural design for specific components marked for weight saving initiatives. As

indicated earlier, in this report the same data for this project can also be used to calculate the damping properties of the 3D printed PLA beams.

Another applicable area can be testing of MEMs components, using the same equipment sensors, by measuring displacement on a nano-scale; the DAQ can capture frequencies up to 20 kHz.

Research can also focus on comparison between different boundary conditions, and other variations of the experimentation methodology, to develop a better understanding of the technique's applicability.

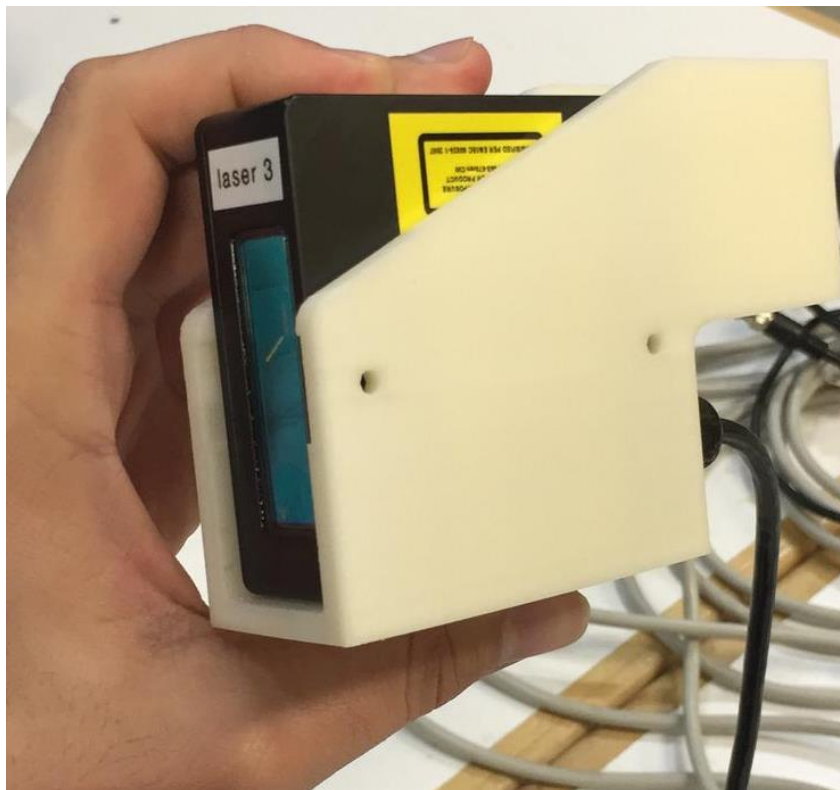
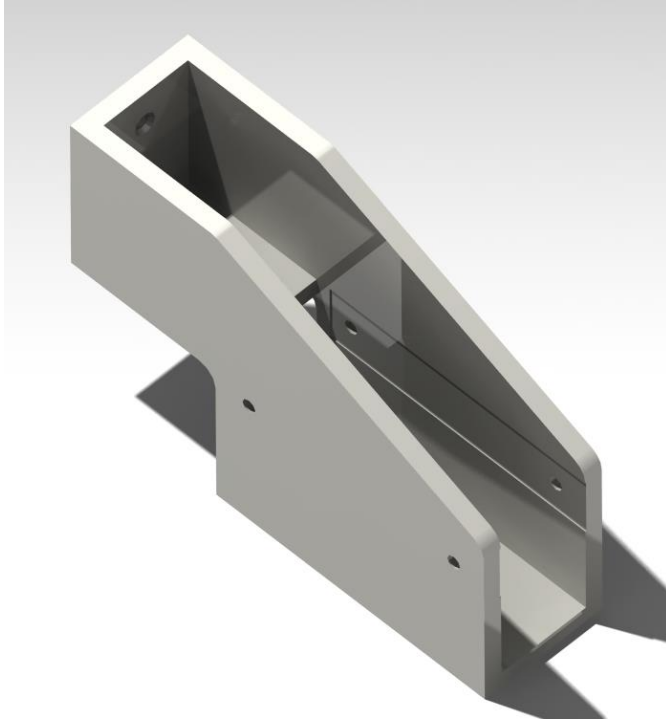
The IET's health diagnostic capabilities can be exploited for performing model-based damage detection using the current experimental setup along with DAQ.

## **APPENDICES**

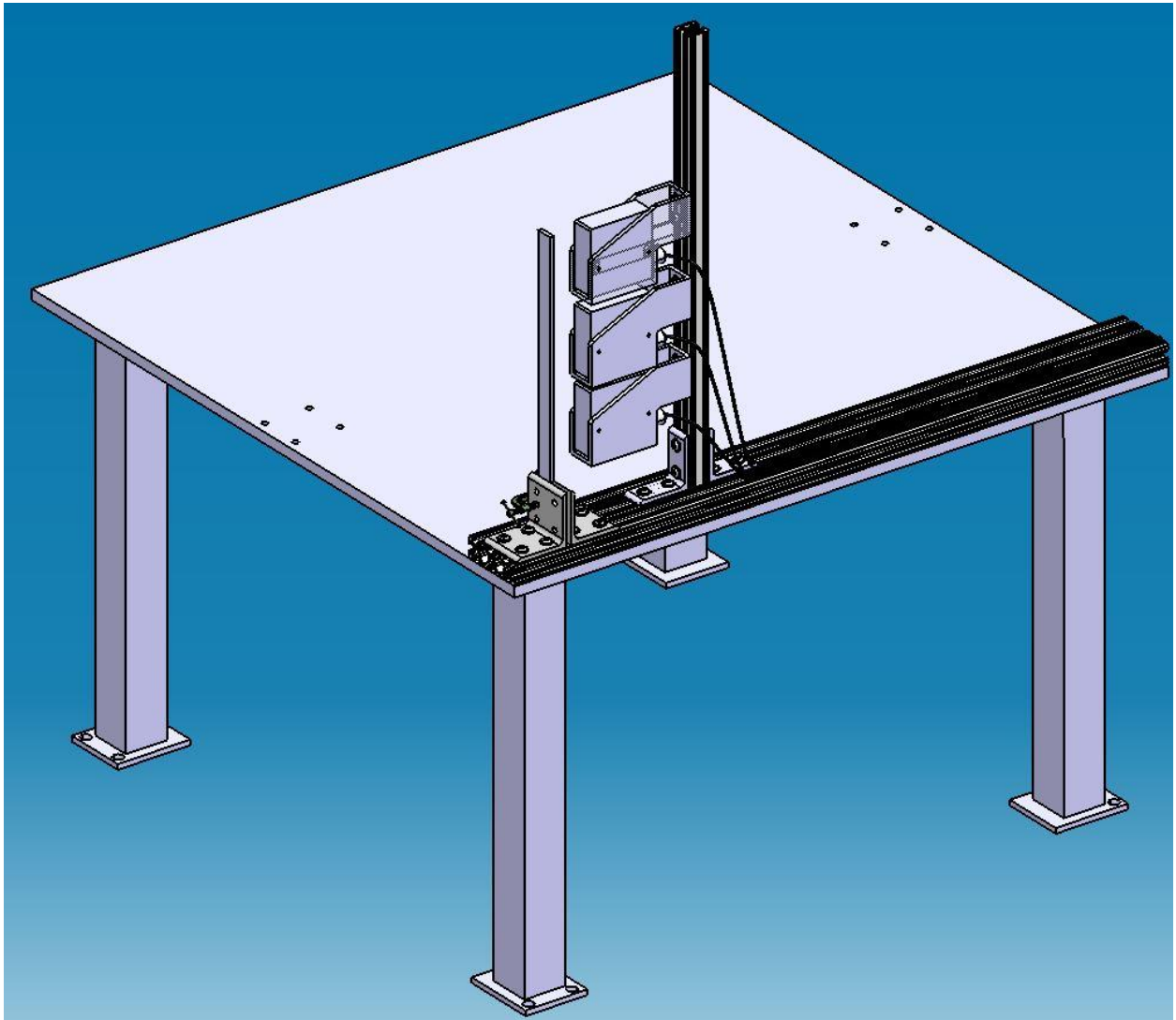
## **APPENDIX A EXPERIMENTATION SETUP AND RESULTS**

## APPENDIX A1 CAD DESIGNED AND PRINTED LASER SENSOR MOUNT

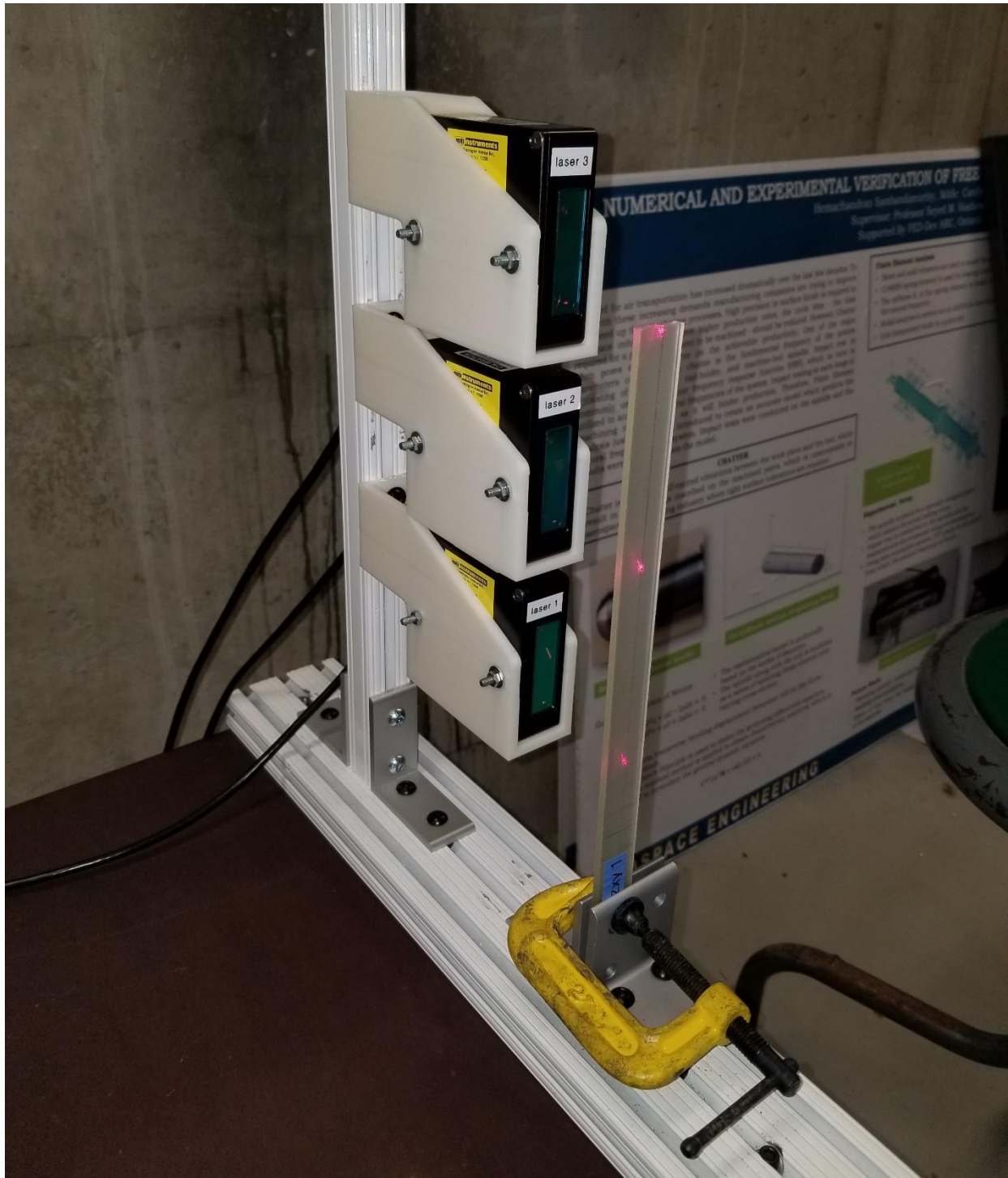
3D model for laser sensor mount in Catia V5 and 3D printed result



## APPENDIX A2 3D CAD EXPERIMENTATION SETUP DESIGN



Actual test setup with the specimen clamped in front of the sensors

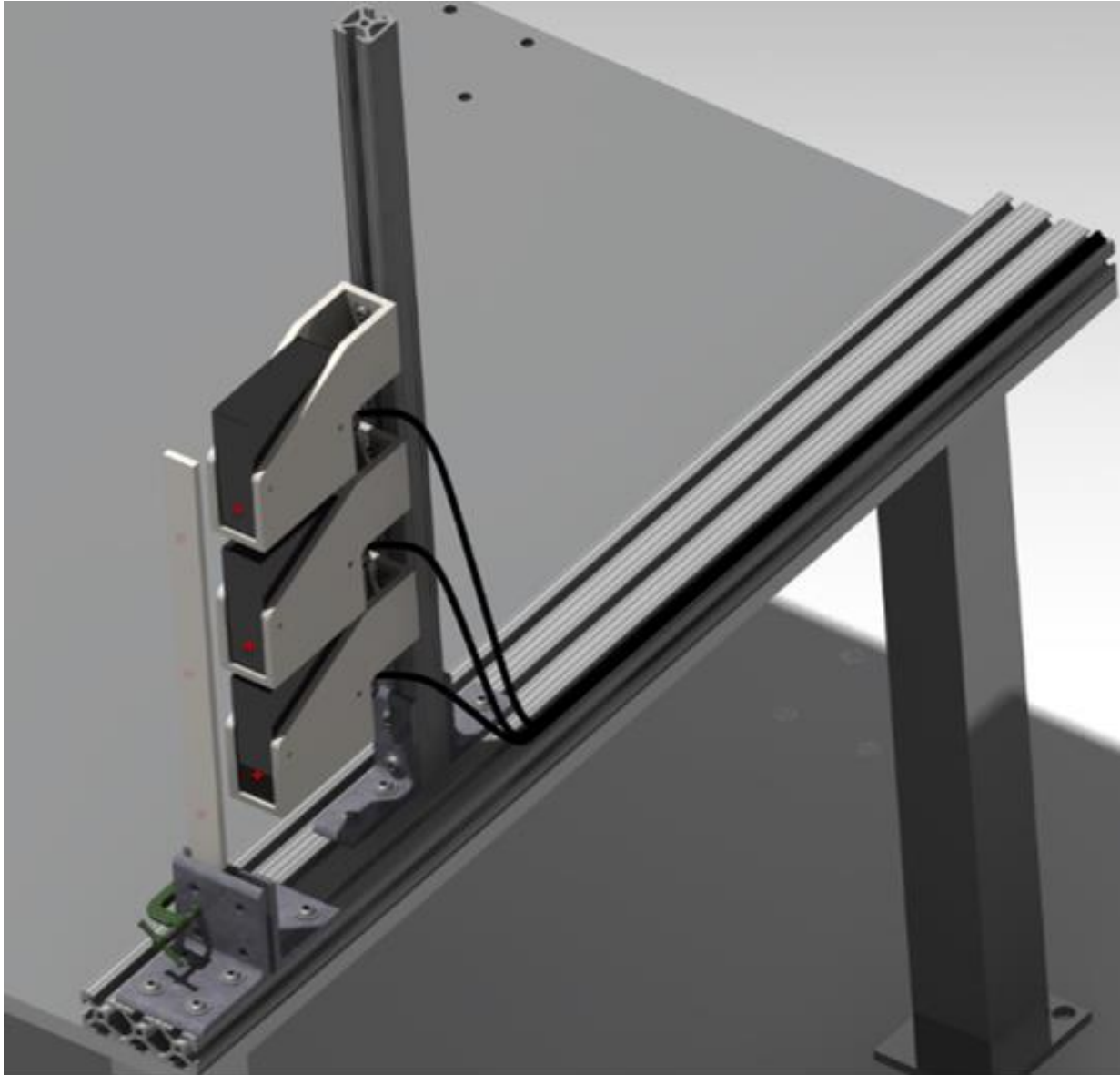


## APPENDIX A3 SUMMARY OF REPORTED TEST SPECIMENS

L (mm)	W (mm)	T (mm)	MATERIAL	BC	Env	NAME	YR	ADDITIONAL INFO
230 or 340	50	2,2.6, 3, 3.7,4. 5,5	wood comp	Clamped	Relative Humidity of 03+- 5% and Temp of 20+-2 degree Centigra de	Determining shear modulus of thin wood composite materials using a cantilever beam vibration method, Cheng Guan, Houjiang Zhang, John F.Hunt, Haicheng Yan.	2015	To minimize Vibrational shear effects, the ratio of free length to thickness of specimen should be greater than 14.5,
400	40	30	Carbon fiber	Clamped 50		Study of free vibration charachteristics of carbon epoxy based composite beams, R.Ramesh 2015		
350	25	25	Styrofoam	Supporte d at mid- lent, free-free		45easurement young modulus and shear modulus of polystyrene foam by longitudinal and flexural vibratio, Hiroshi Yoshihara 2018		
160	25	2.9-3	Carbon fiber / liquid MMA resin, Carbon / Epoxy	Clamped 30		Enhanced Vibration damping and dynamic mechanical charachteristics of composites with novel pseudo- thermoset matrix system, Somen K. Bhudolia, 2017		impact hammer position at 15% of free beam , ASTM E756-05

L (mm)	W (mm)	T (mm)	MATERIAL	BC	Env	NAME	YR	ADDITIONAL INFO
210,220, 280	10	1.96, 2.01, 3.86	Glare, 2024-T3	Clamped		Charactrization of the elastic and damping propersties of traditional FML and FML based on a self reinforced polypropylene, J. Iriondo, 2015		ASTM E756-05,
250	25	4	Jute / Epoxy	Clamped				ASTM E756-05,
200	60	3	Aluminum	Clamped to Iron Mass of 30kg No reasonin g		Measurement of vibrational modal parameters using laser pulse excitation techniques, P. Castellini, 2003	2004	Impact Hammer 23g
300	40	2	Steel	Clamped		Feasibility Analysis of using piezoceramic transducers for cantilever beam modal testing, Bor-Tsuen Wang, 1996	1997	
550	25	10	Mild Steel & Aluminum	Clamped		Investigation on modal parameers of rectangular cantilever beam using Experimental modal analysis, Walunj Prashant S., 2015	2015	

## **APPENDIX B LAB MANUAL**



## **Dynamic Investigation through Laser sensors**

### LAB MANUAL

Mohsin Afridi | MEng Project | 5-12-18

## **Important Information**

The Ryerson University FRAMES Lab is equipped with various structural and material analysis sensors, equipment, hardware and software. The focus of this manual is on Dynamic Investigation through use of Laser sensors.

This how-to document is a complete systematic process of setting up a dynamic Investigation using the available equipment Ryerson FRAMES Lab.

Since the experimental setup involves a number of equipment from different vendors and each vendor provides a setup or functional manual going through each one and then determining issues such as compatibility etc. can be a tedious process.

The setup sequence for ease of setup:

1. Sensor and Hardware setup
2. Software setup
3. Sensor placement and Equipment Integration

## **Sensor & hardware setup**

The Hardware equipment involved in the setup include the following:

- Laser sensors (Mti Instruments Microtrak III Laser Sensors)
- Piezoelectric sensor (Dytran Dynapulse 5800B4)
- Laser Sensor Interface (Duram Instruments)

- Data Amplifier Unit (HBM X400A)
- Bench Power Supply and
- PC/ Laptop

## Sensors

The Laser sensor has the following effective range and proposed orientation for reliable results.

Students should refer to the detailed specification provided by the manufacturer for a better understanding of the limitations and range and other factors affecting the performance of the sensor.

Following are specs and setup orientation illustrations from the Manufacturers Brochure:



Figure 2: Laser displacement sensor

Product Info		Technical Specifications										
P/N	Model	Measurement Range	Accuracy	Min. Range	Stand-Off	Resolution	Noise	Spot Size	Interface	Type	Frequency Response	Request Info
8000-6473	LTS-050-10	10mm (0.39")	0.03% FSO	43.75mm (1.71")	50mm (1.95")	0.191 $\mu$ m	1.625 $\mu$ m RMS	36 $\mu$ m	RS485 to USB	RED Laser, 3R Laser Class	20kHz	Request Info

Table 1: Laser Sensor Manufacturer's specification

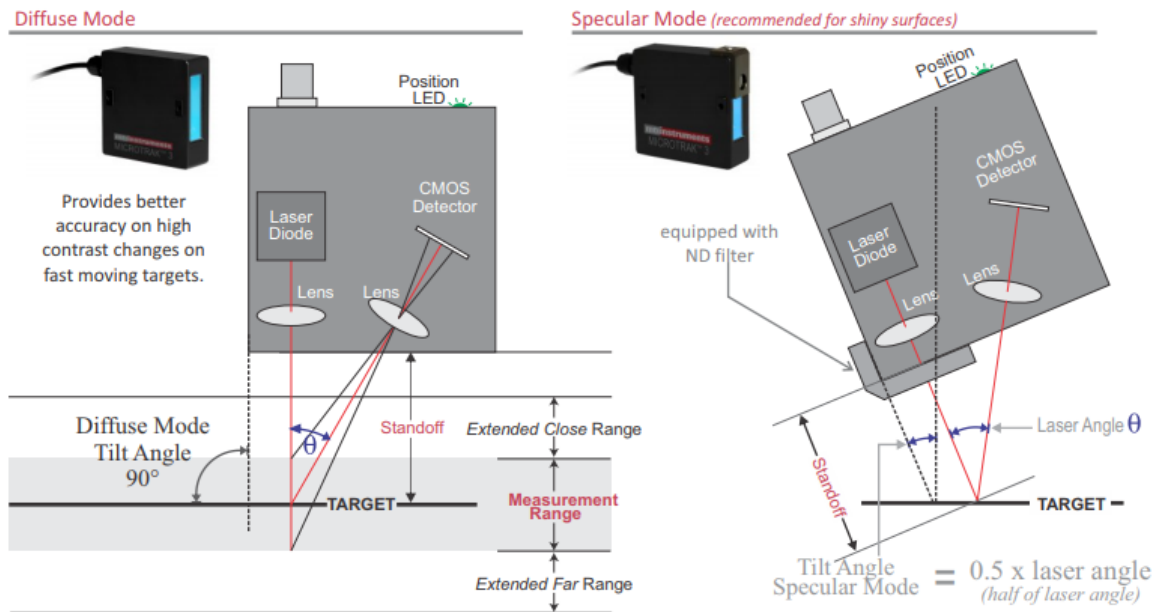


Figure 3: Laser displacement sensor mode of operation and range schematic

## Piezoelectric sensor

The Dytran Dynapulse 5800B4 contains a piezoelectric sensor that can be directly connected to the Amplifier channel for DAQ. Below is an image of the Impulse hammer with integrated sensor.

NOTE: A soft, silicone tip is recommended for elastic impulses at low frequencies.



## Sensor Interface

The Laser sensor Interface from Durham Instruments connects directly to the Laser sensors and the Data Acquisition Unit.

As per the illustrations below, the connection for both Laser sensors and the Data Acquisition Unit, have labels on each side with each connector individually labelled for quick tracing of individual sensors.

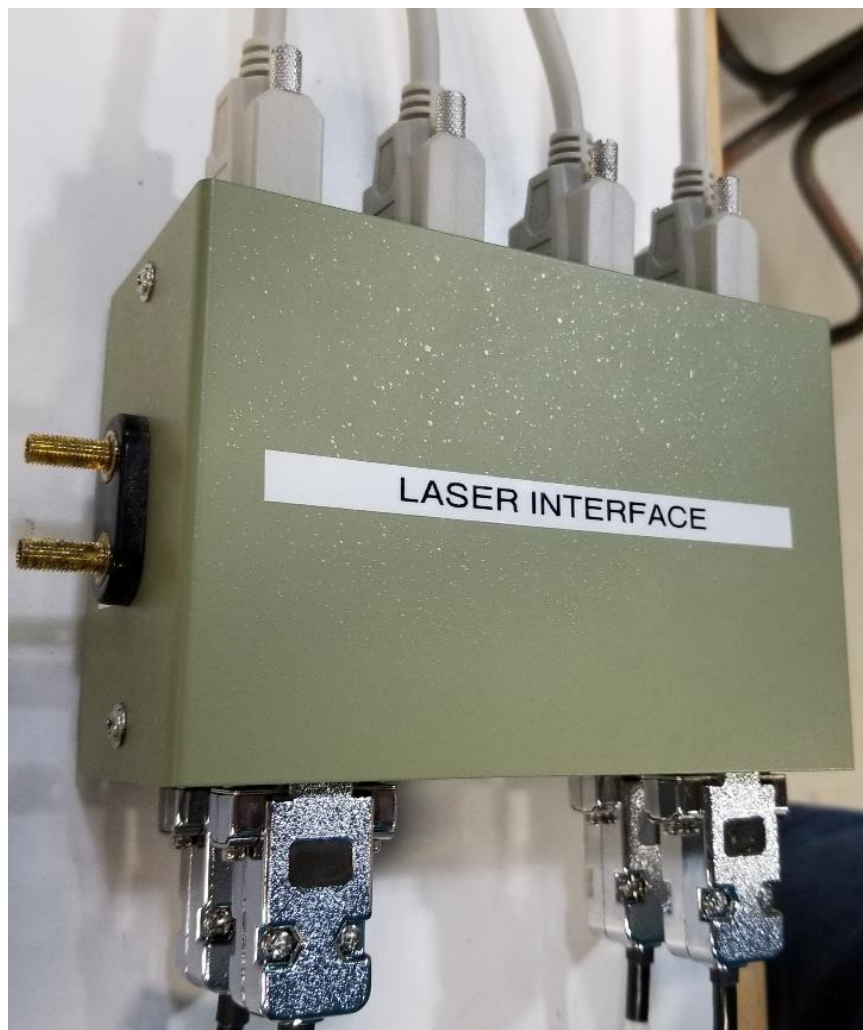


Figure 4: Laser Interface top-iso view illustrating sensor and amplifier connections

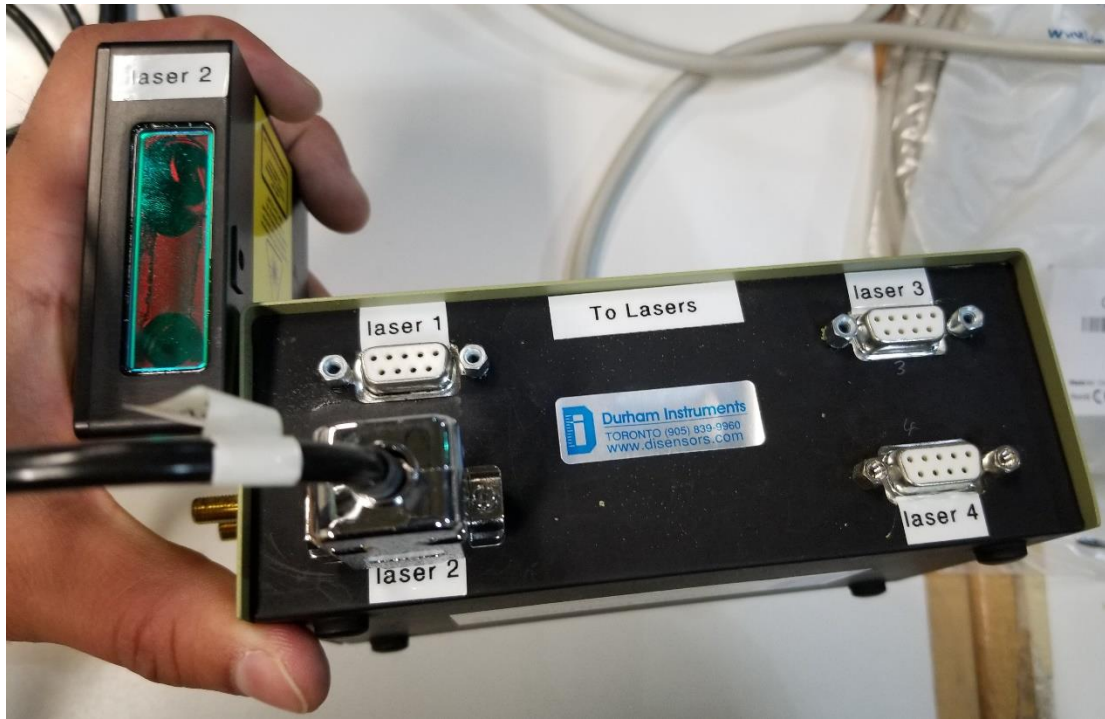


Figure 5: Laser Interface illustrating sensor connections labelled for each sensor



Figure 6: Laser Interface illustrating the power input terminals on the left side

NOTE: Please note the Orientation of the Bench Power Source terminals connected on the side of the Interface unit. Wrong terminals will not power up the laser sensors properly.



Figure 7: Bench Power Unit

The Laser sensors also derive their power from the Bench power supply connection. As per the laser requirements, the Bench voltage is set to nominal 24 Volt as per manufacturer specs.

Amplifier Unit

The Amplifier unit is an HBM X400A model that has four input channels for four sensors. The unit has its own separate power connection. Once the HBM DAQ software is installed, the user can control the blinking of these LEDs to test the connection status and location of each sensor connection.



Figure 8: HBM X400A in DAQ setup

The Amplifier Unit is connected to the PC through an Ethernet Cable. For more details the link to manufacturer specification brochure is provided in the hyperlink on image below

## **QUANTUM<sup>X</sup>** **MX440A**

Universal amplifier

### **Special features**

- 4 individually configurable inputs (electrically isolated)
- Connection of more than 12 transducers technologies
- Data rate: up to 19,200 Hz
- 24-bit A/D converter per channel for synchronous, parallel measurements
- Active low pass filter
- TEDS support
- Supply voltage (DC): 10 V ... 30 V
- Supply voltage for active transducers (DC): 5 V ... 24 V



Figure 9: HBM X400A four channel amplifier unit.

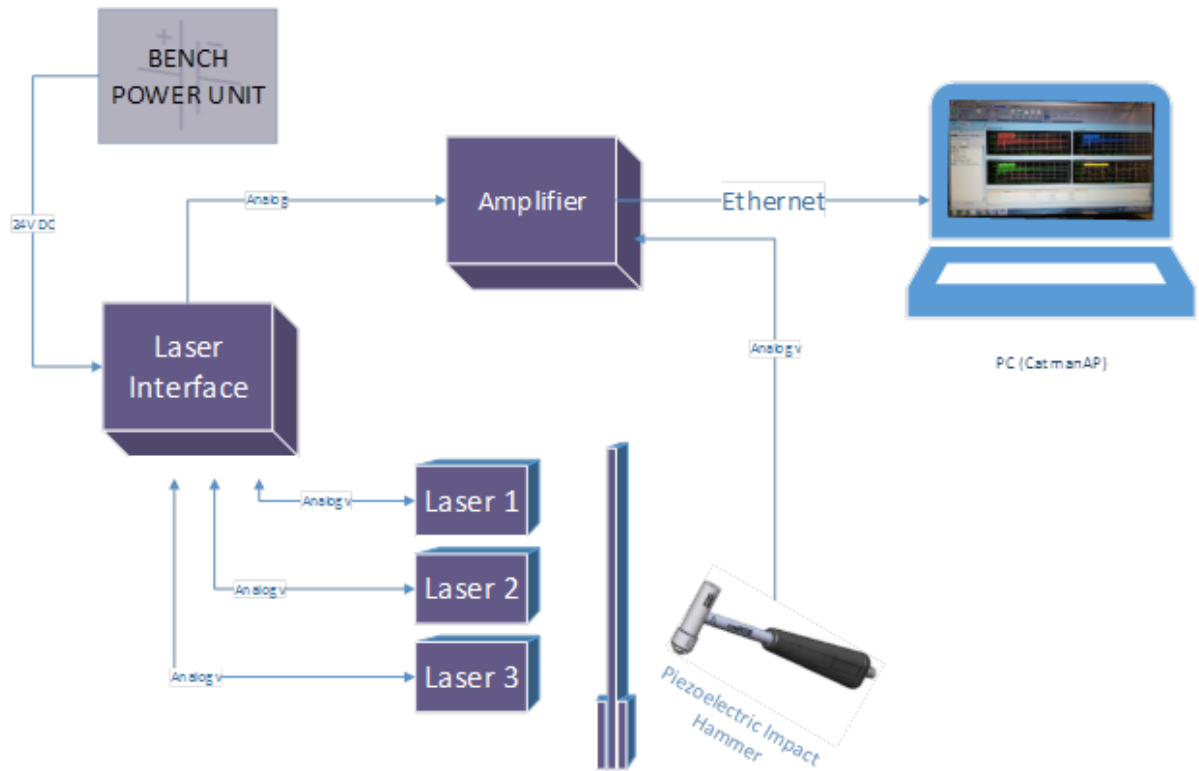
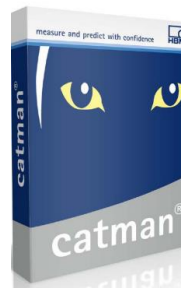


Figure 10: Experimental Layout Schematic

After connecting, the sensors through the interface to the acquisition unit the user shall install the CatmanAP, Data Acquisition software.

## Software setup



### catman

Data Acquisition and Analysis software

#### Special features

- Visualization of measurement data
- Online analysis through powerful math library
- Store and export data in various formats
- Analysis of data
- Reporting

HBM produces the Data Acquisition Unit X400A. It has developed the CatmanAP Software for Data Acquisition and Analysis. The lab carries on CD drive a copy of the software version 3.3 with the required License for use.

NOTE: Higher versions for the same software are available online with added features and functionality but do require a newer License. Therefore, user shall install the same version available in the lab until the newer version is available.

Software installation steps are very straight forward as shown below:

- Insert CD
- Run executable file to install the software
- Once the software has been completely installed, the user shall be prompted for the License.
- The product license is provided with the CD. Enter the License as shown below:

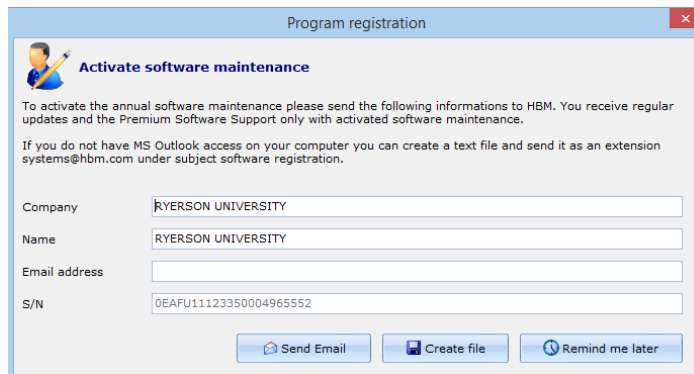
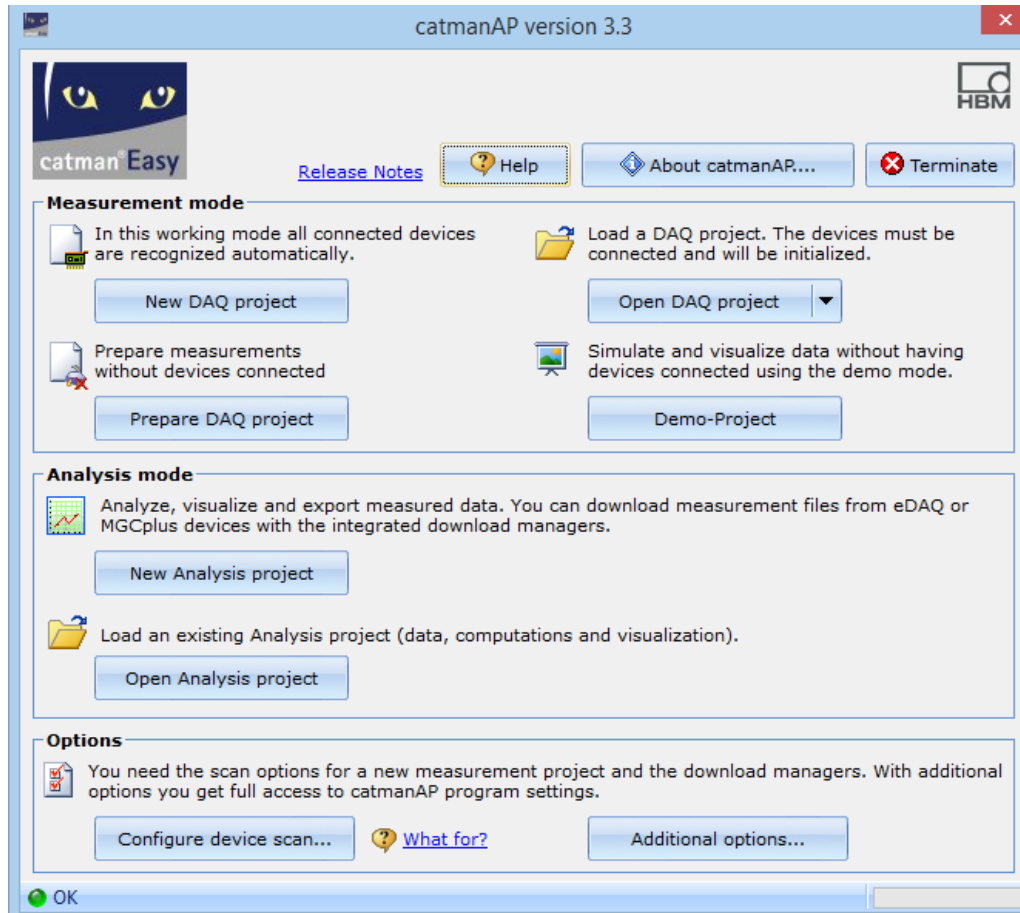
A screenshot of a 'Program registration' window. The window has a title bar with 'Program registration' and a close button. Inside, there's a section titled 'Activate software maintenance' with a small icon of a person with a pencil. Below this, there's text explaining that to activate annual software maintenance, users need to send information to HBM. It also mentions that if users don't have MS Outlook access, they can create a text file and send it to systems@hbm.com. There are four input fields: 'Company' (filled with 'RYERSON UNIVERSITY'), 'Name' (filled with 'RYERSON UNIVERSITY'), 'Email address' (empty), and 'S/N' (filled with '0EAFU11123350004965552'). At the bottom, there are three buttons: 'Send Email', 'Create file', and 'Remind me later'.

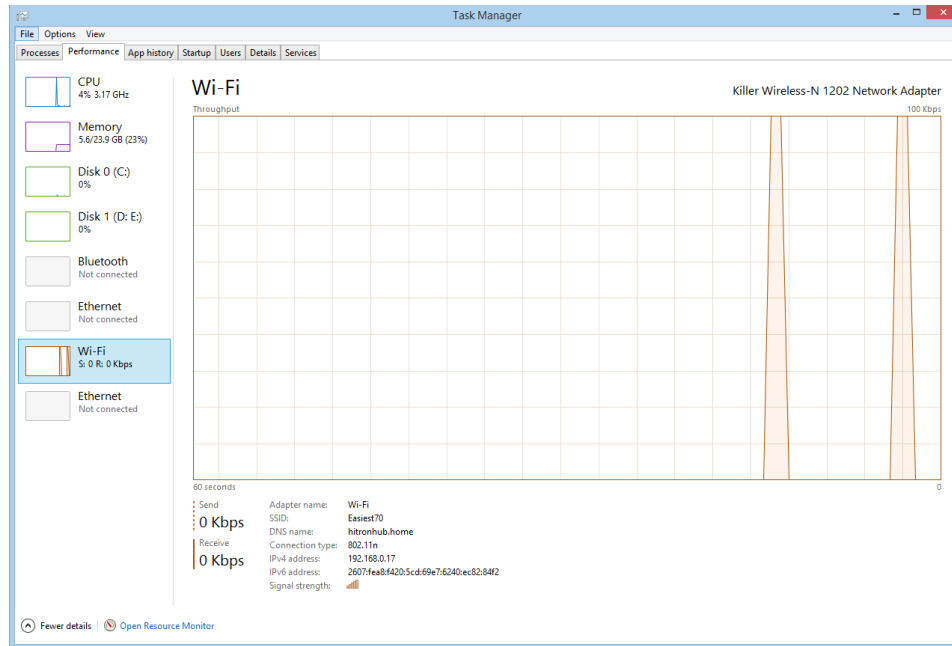
Figure 11: Enter License in the bottom field (Only field required)

Launching the CatmanAP software opens the following Main User Interface :

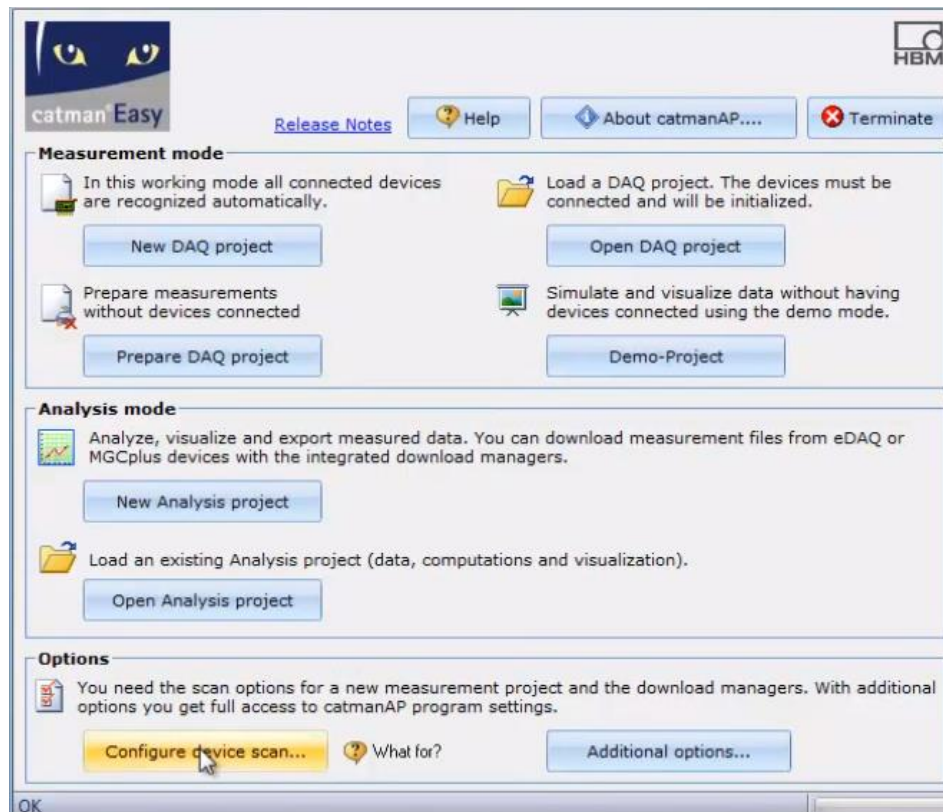


The first important step to configure and ensure connectivity with the X400A DAQ is to select the “Configure device scan” under Options section.

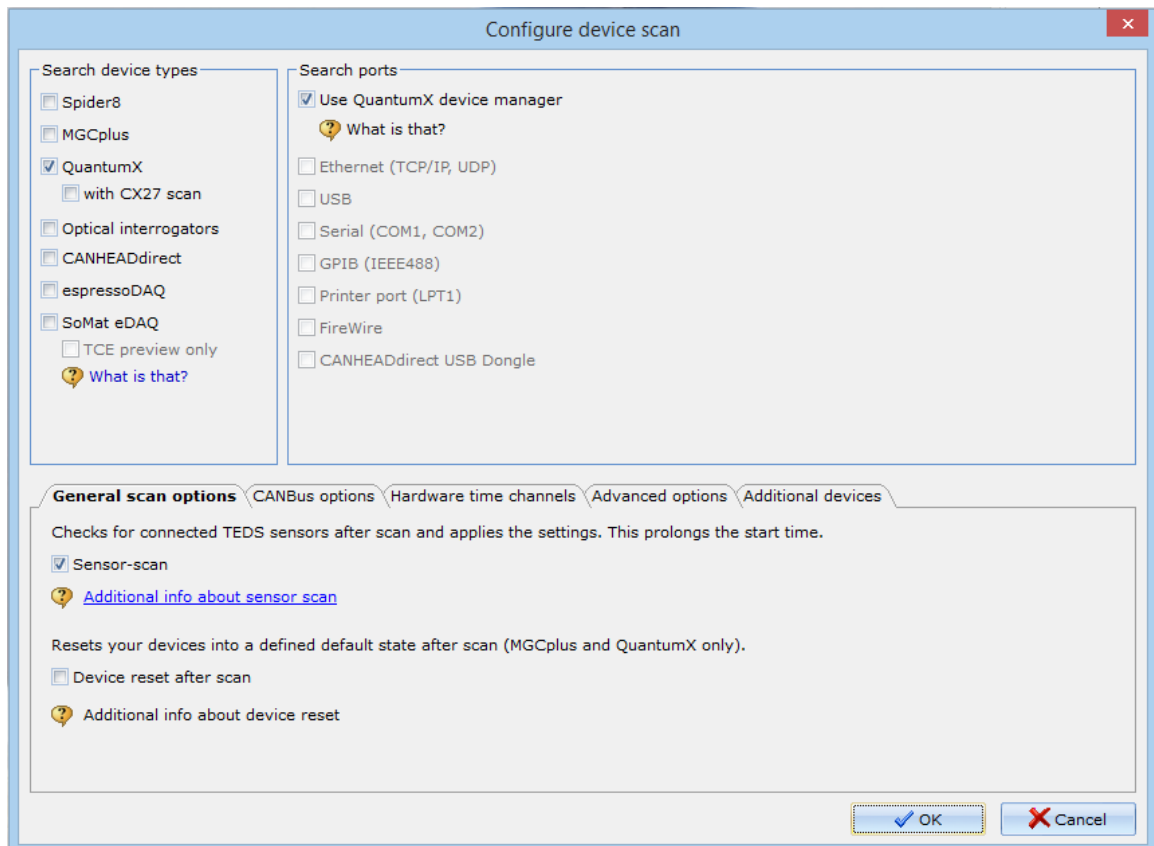
NOTE: User shall enter the PC’s IP Address for the Ethernet connection. There are many simple ways to find the address. One such method is to use Ctrl+Alt+Del to enter the Task Manager and select the Ethernet tab on the left as illustrated below



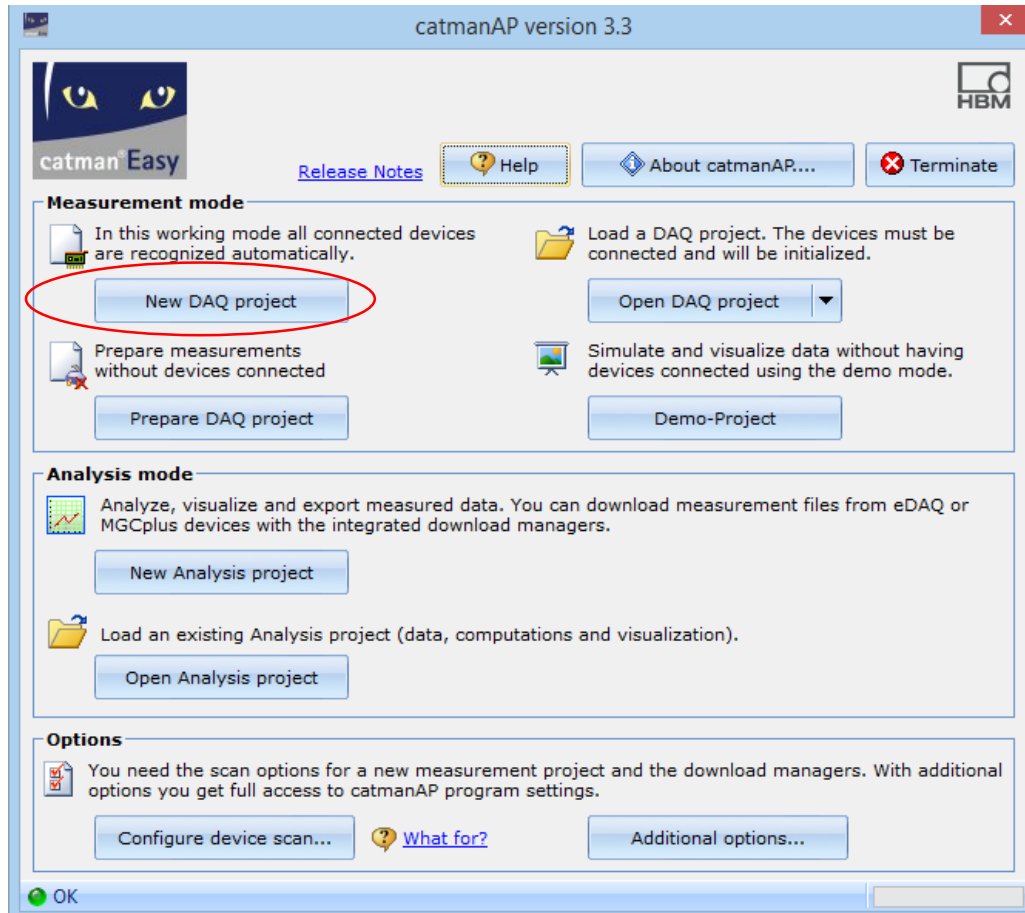
Select the Configure Device scan as shown below:



Select the “QuantumX” option under Search devices types and “Use QuantumX device manager” under Search Ports section. Also, check the “Sensor-scan” option under the “General scan options”.



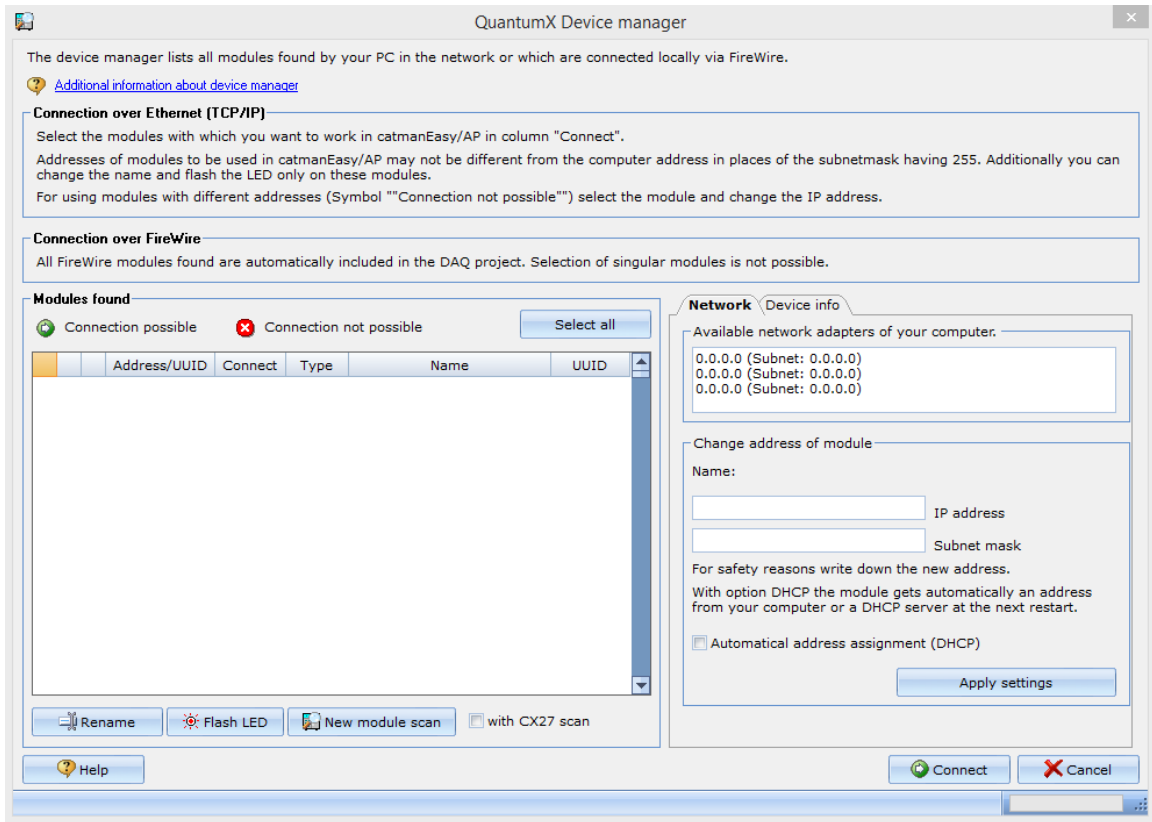
Upon selecting the “New DAQ Project” as shown below, the software shall automatically search for the DAQ unit connection.



Note: Ethernet connection has to be established between the PC and DAQ.

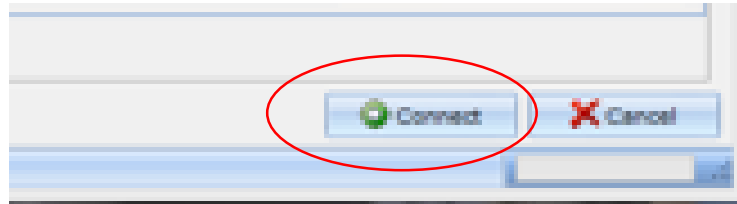
The Software Searches for the DAQ Module using the network address

The IPv4 address can be readily acquired through the Ctrl+Alt+Del option under the “Ethernet” Connection

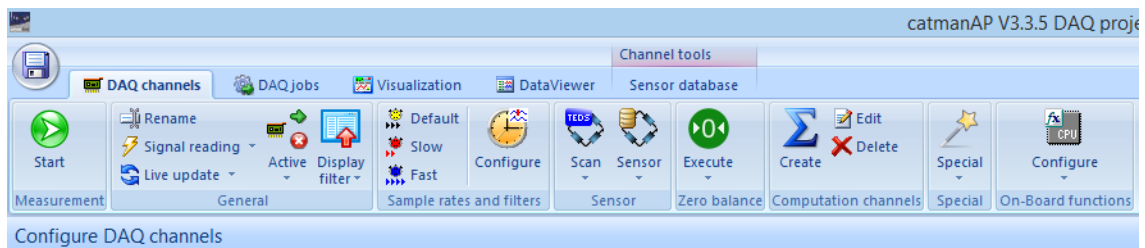


The 'Modules found' field is empty if no available connection is established to the DAQ unit. The user can set the IP address of the module as shown above to enable the connection to DAQ unit.

Select “Connect” or enter once the Module is automatically detected upon Launch.



Once module is detected the software home screen appears as follows

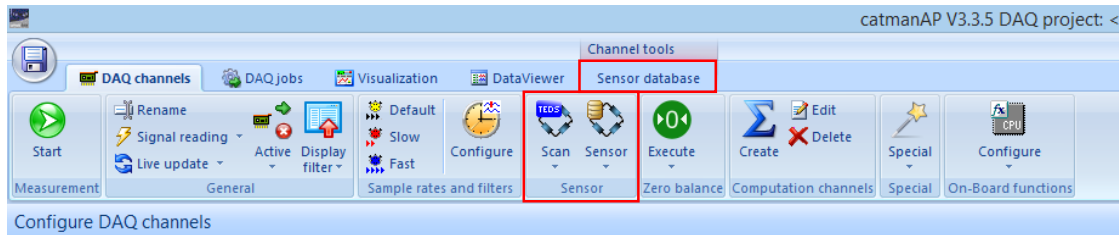


Sensor Selection using software is important. Normal sensors from vendor can be ordered with TED’s support that are readily recognized by the software.

In the absence of the TEDS support, the user shall specify the sensor from the list of sensors provided.

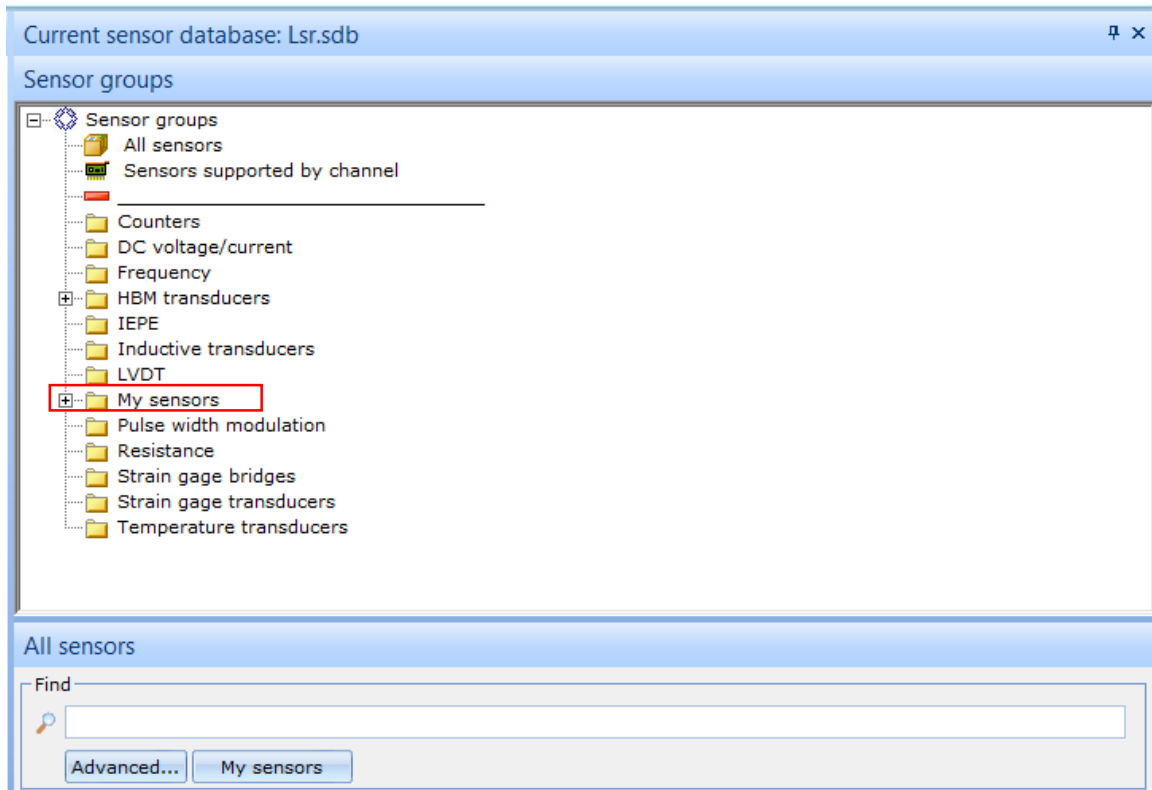
A number of [tutorials](#) are available [online](#) for different ways sensors can be configured using the acquisition software.

Note: User shall go over the sensor specs in detail to properly configure the software settings for optimal result generation from experiments.

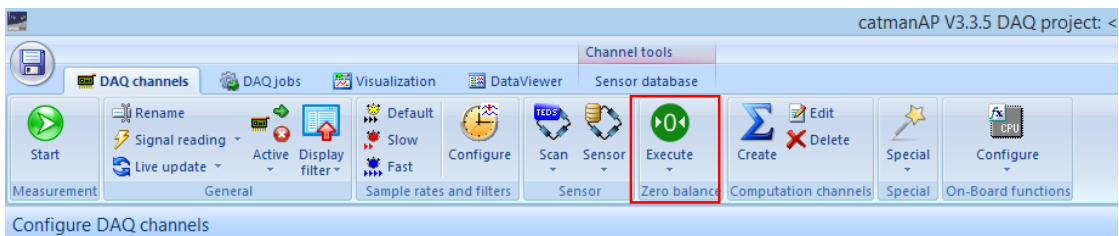


The current sensors on channels from the module are listed and status is shown

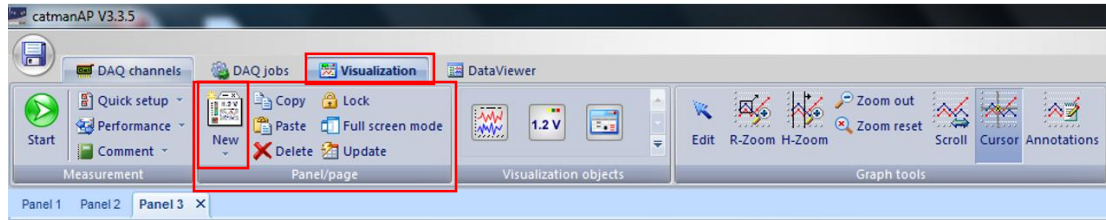
Select the “my sensors” tab under the sensors group to select the following customized sensor as per the manufacture specifications:



Once sensors are specified, select the “Execute” green button to initialize the sensors for the new set of readings.

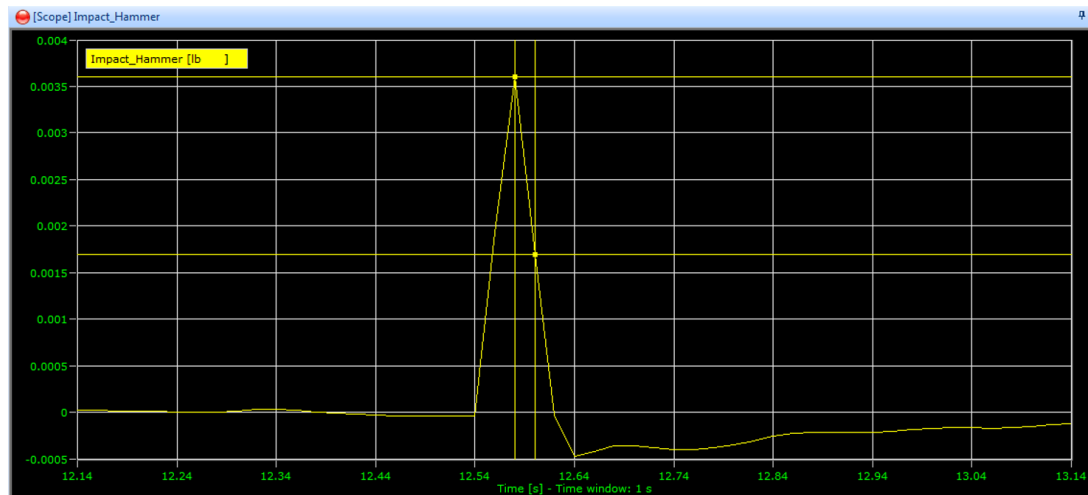


To view sensor reading in a graphical interface the “Visualization” tab should be selected.



Using the “New” Drop down menu on the Visualization Tab various Panels can be created and each can be customized with the different graph options from the visualization objects

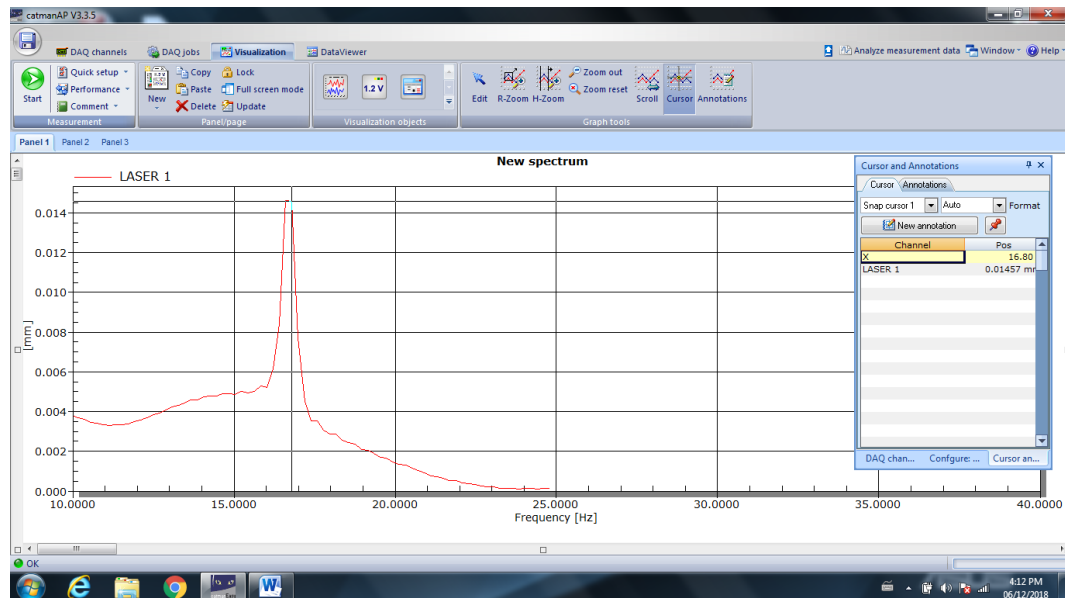
Following real time scope graphs for each sensor Channel can be observed below:



User can select multiple Channel representations on the same scope or create a different one for each. The above screenshot represents an Impulse from a Piezoelectric Impact Hammer sensor.

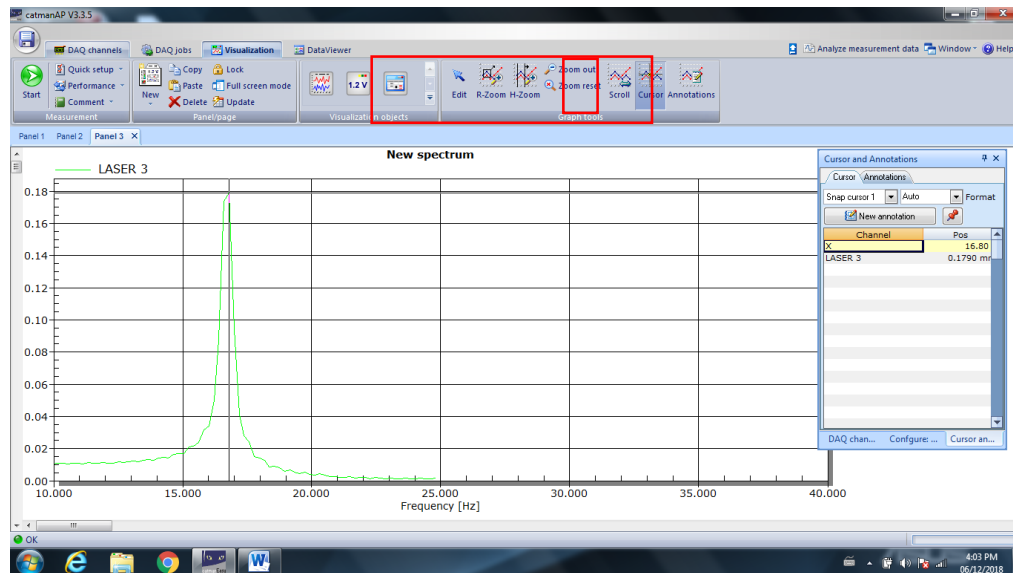
As explained earlier the Panels can be customized with various Visualization objects such as different Graphs and Charts and even real time digital value output fields etc.

Each Tab can be customized for one or many of these objects.

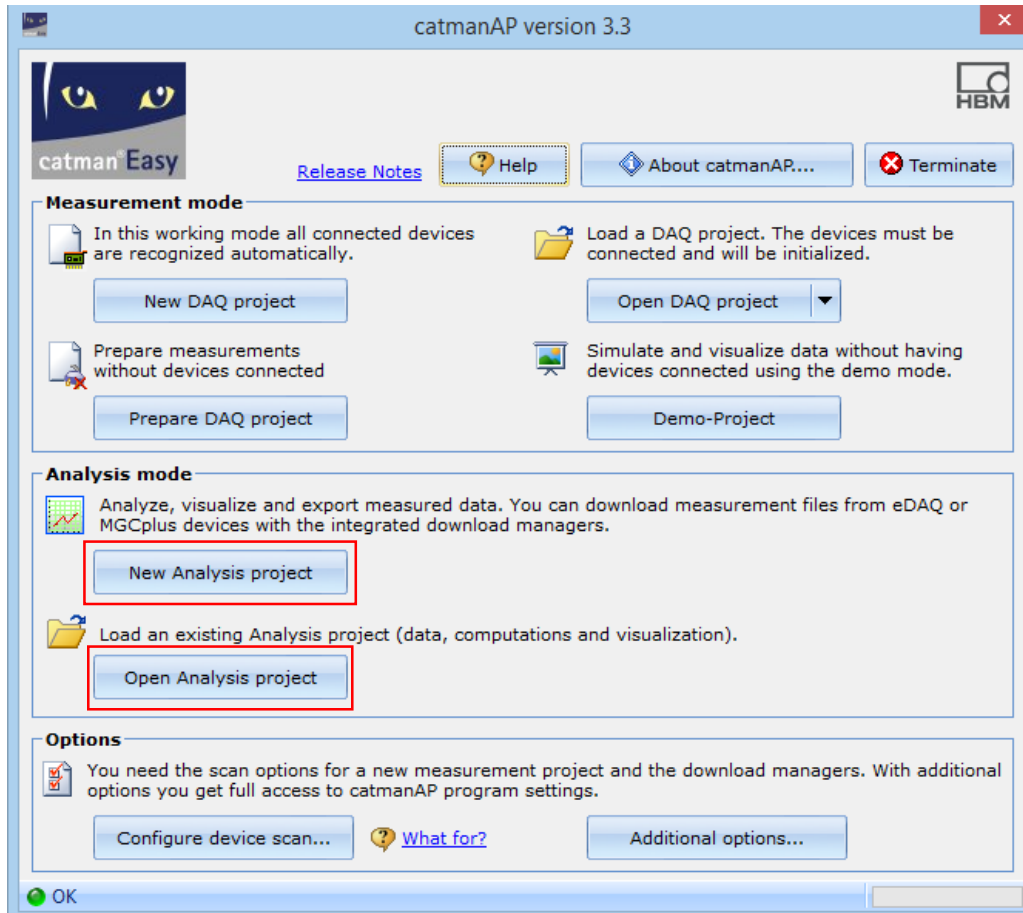


In the screenshots each separate Panel contains one sensor graph as illustrated.

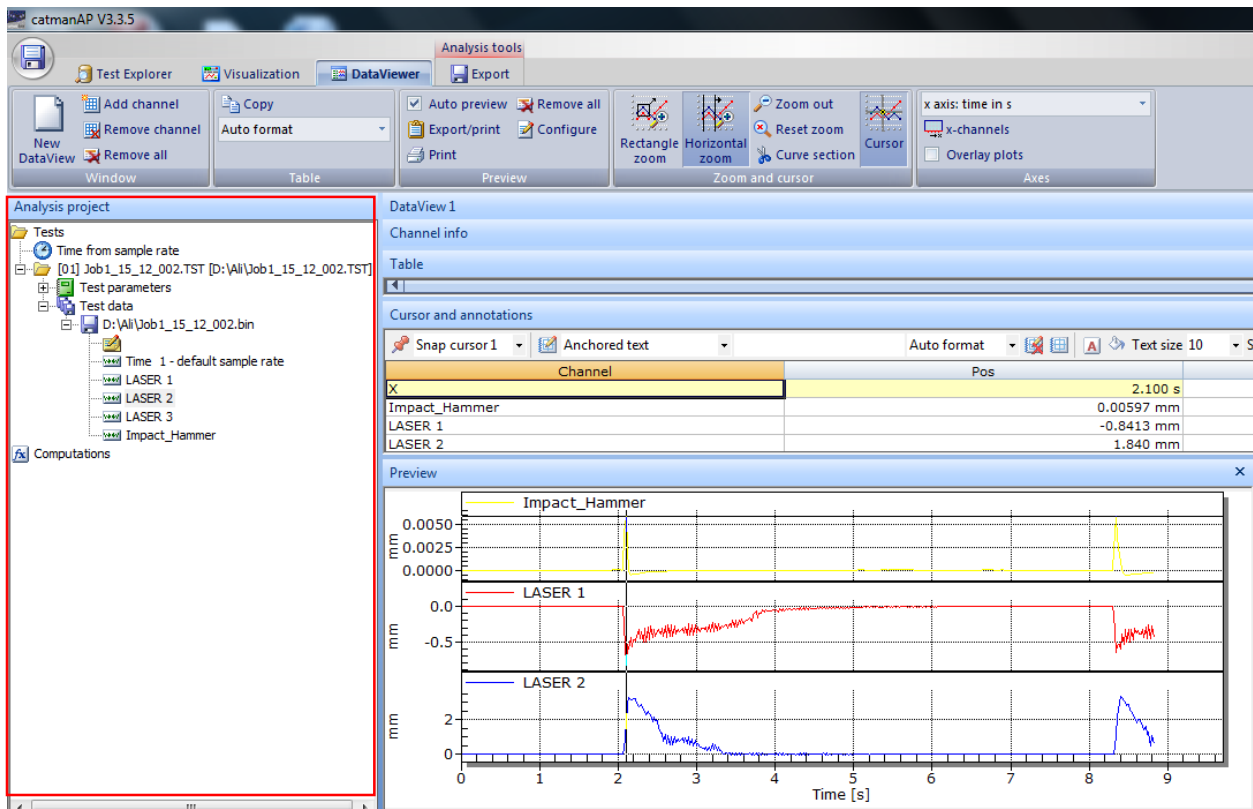
The Zoom options and Cursor can be used to traverse any point on the graph. Normally this is to determine the readings on Peak values or any other point of concern the user deems important.



For Analysis at any time after the Project jobs (Test runs) are saved. They can be accessed directly from the startup interface by loading an already saved analysis project or by creating a new one

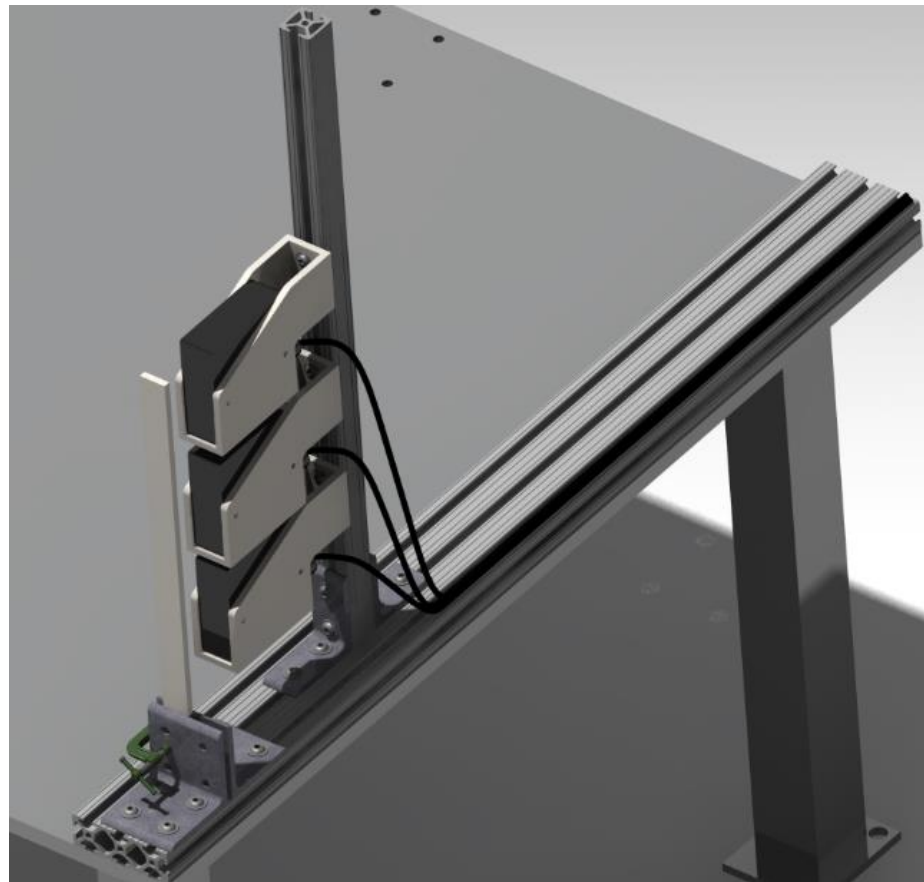
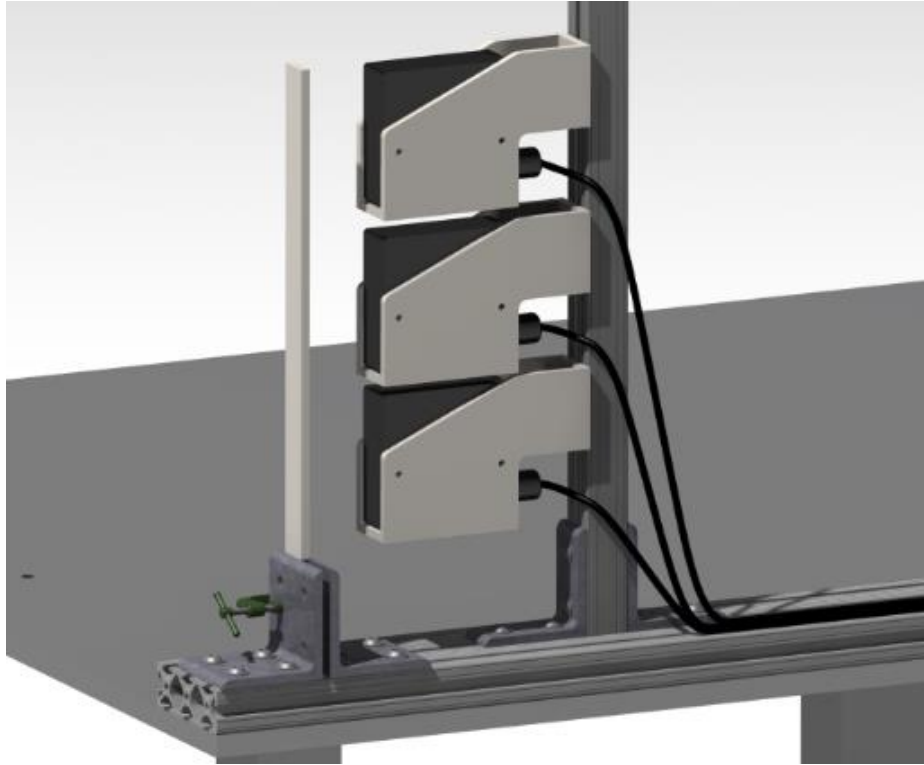


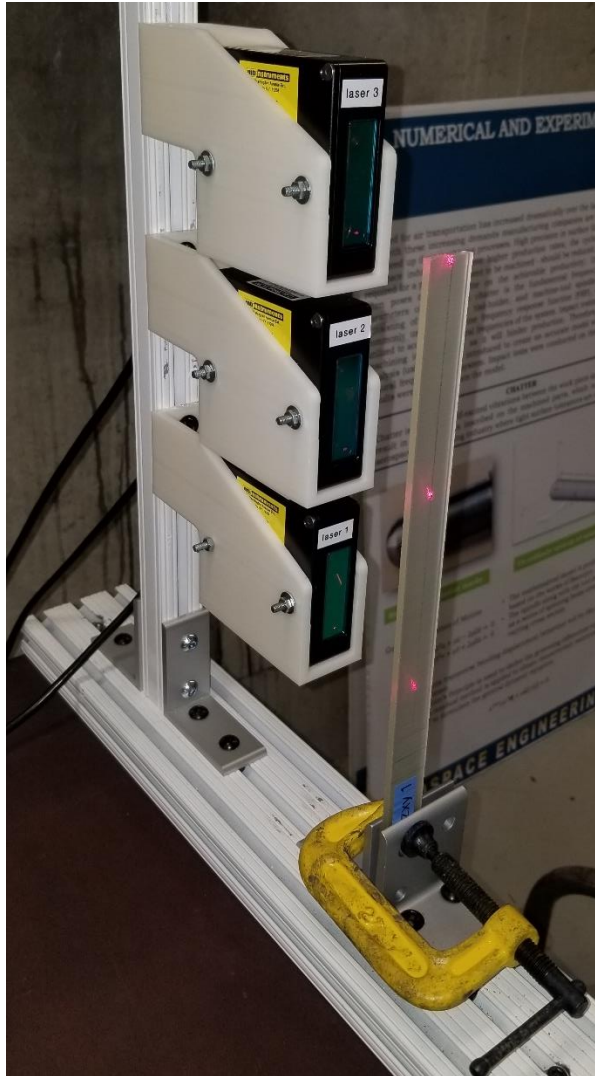
The Analysis Interface is illustrated below.



User can add any jobs (Test runs) from the project visible in the Analysis Project window on the left by simple “drag and drop” feature.

Once Analysis or experimentation is completed. The software offers a number of formats to store information including ones used in Excel, Matlab, csv etc.





## USEFUL LINKS

- [ONLINE TUTORIAL ON HOW TO CONFIGURE SENSORS](#)
- [CatmanAP DAQ Software Brochure](#)
- [Manufacturer's Specification for the CatmanAP Software](#)

## **APPENDIX C EXPERIMENTATION RESULTS**

## APPENDIX C1 IET RESULTS

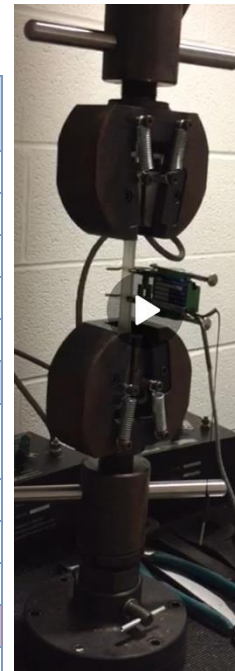
Results from the IET Experiment and calculated E values based on specimen Parameters

$\rho$	Cross-sectional Area	$\omega - (\text{rad/sec})^2$	Length <sup>4</sup>	Non-dimensional <sup>2</sup>	I	E (Pa)	#
1225.673	7.116E-05	10631.068	0.0033177	12.362	7.314E-11	3.402E+09	0-1 XYZ
1215.19	6.855E-05	9880.3582	0.0033177	12.362	6.464E-11	3.417E+09	1-1 XYZ
1216.699	7.321E-05	10631.068	0.0033177	12.362	8.057E-11	3.154E+09	1-2 XYZ
1223.982	7.093E-05	10631.068	0.0033177	12.362	7.324E-11	3.382E+09	1-3 XYZ
1226.412	7.115E-05	10631.068	0.0033177	12.362	7.330E-11	3.397E+09	1-4 XYZ
1174.275	7.445E-05	11142.388	0.0033177	12.362	8.687E-11	3.009E+09	2-1 XZY
1186.286	7.334E-05	10878.672	0.0033177	12.362	8.223E-11	3.089E+09	2-2 XZY
1170.223	7.433E-05	11142.388	0.0033177	12.362	8.461E-11	3.074E+09	2-3 XZY
1161.99	7.881E-05	16284.693	0.0021367	12.362	1.011E-10	2.549E+09	3-1 ZXY
1152.801	7.445E-05	16284.693	0.0021367	12.362	8.521E-11	2.835E+09	3-2 ZXY
1148.842	7.413E-05	17244.567	0.0021367	12.362	8.411E-11	3.018E+09	3-3 ZXY

## APPENDIX C2 TENSILE TESTING RESULTS

Following are the tensile test E results for the three build orientations:

Max force (lbf)	Failure stress (psi)	Strength (MPa)	Young's Modulus (GPa)
633.5769653	8767.719745	60.45132339	3.1084
581.2393799	8045.87483	55.47437595	3.026
543.0488892	7584.888821	52.29598805	3.2958
596.2262573	8354.298192	57.600881	3.1104
615.6503906	8613.430871	59.38760754	3.2124
	Average	57.0	3.15
	Standard Deviation	3.26	0.10
	CV	5.7%	3.3%
512.3497314	6831.565139	47.10200205	2.994
306.6999817	4017.571362	27.70019033	3.107
485.7545166	6044.210674	41.67338199	2.8667
511.0496826	6390.210615	44.05896854	2.8356
501.7422485	6709.263612	46.25876238	2.9724
	Average	44.8	2.92
	Standard Deviation	2.43	0.08
	CV	5.4%	2.7%
674.2185669	9194.757768	63.39564807	3.115
672.5359497	9188.890053	63.35519158	3.1483
666.5275269	9097.895233	62.72780414	3.0903
667.800293	9047.839964	62.38268507	3.1451
668.0767822	9047.41046	62.37972374	3.091
	Average	62.8	3.12
	Standard Deviation	0.50	0.03
	CV	0.8%	0.9%



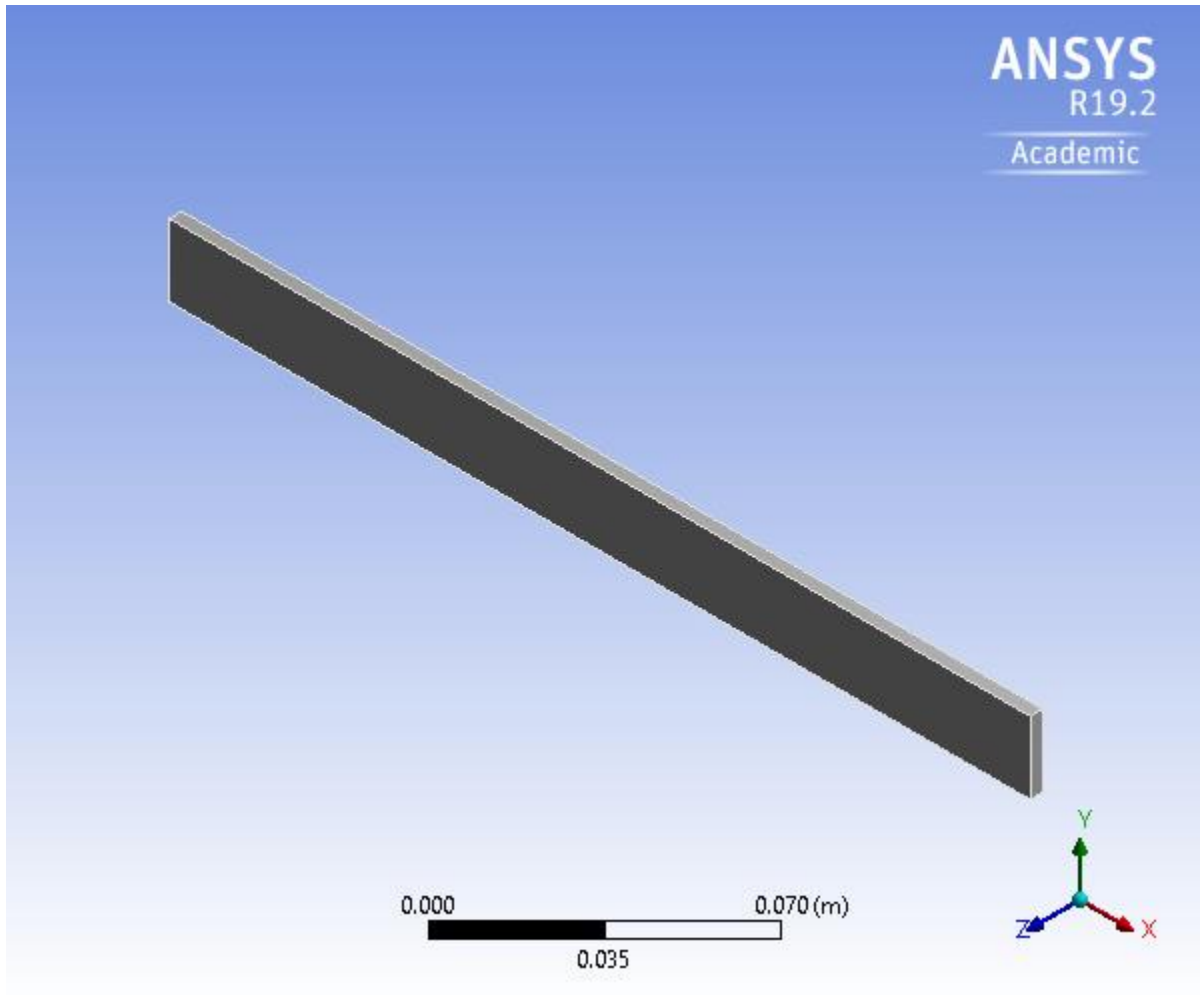
NOTE: The value in pink is off due to specimen defect that was discovered and was not considered in comparison with the IET result values.

## **APPENDIX D FEM ANALYSIS REPORTS**



#### Appendix D1 Build orientation XYZ

First Saved	Monday, December 24, 2018
Last Saved	Monday, December 24, 2018
Product Version	19.2 Release
Save Project Before Solution	No
Save Project After Solution	No



## Contents

- Units
- Model (C4)
  - Geometry
    - SYS\Solid
  - Materials
    - XZY PLA
    - ZXY PLA
    - PLA
    - New Folder

- XYZ PLA
- Coordinate Systems
- Mesh
- Modal (C5)
  - Pre-Stress (None)
  - Analysis Settings
  - Fixed Support
  - Solution (C6)
    - Solution Information
    - Results
- Material Data
  - XYZ PLA

Units

**TABLE 1**

Unit System	Metric (m, kg, N, s, V, A) Degrees rad/s Celsius
Angle	Degrees
Rotational Velocity	rad/s
Temperature	Celsius

Model (C4)

Geometry

**TABLE 2**  
**Model (C4) > Geometry**

Object Name	Geometry
State	Fully Defined
Definition	
Source	C:\Users\asus\AppData\Local\Temp\WB_DESKTOP-N3USIQU_asus_7184_2\unsaved_project_files\dp0\SYS\DM\SYS.scdoc
Type	SpaceClaim
Length Unit	Meters
Element Control	Program Controlled
Display Style	Body Color
Bounding Box	
Length X	0.241 m
Length Y	2.0148e-002 m

Length Z	3.5118e-003 m
Properties	
Volume	1.7052e-005 m <sup>3</sup>
Mass	2.0747e-002 kg
Scale Factor Value	1.
Statistics	
Bodies	1
Active Bodies	1
Nodes	6946
Elements	1134
Mesh Metric	None
Update Options	

Assign Default Material	No
Basic Geometry Options	
Solid Bodies	Yes
Surface Bodies	Yes
Line Bodies	Yes
Parameters	Independent
Parameter Key	
Attributes	Yes
Attribute Key	
Named Selections	Yes

Named Selection Key	
Material Properties	Yes
Advanced Geometry Options	
Use Associativity	Yes
Coordinate Systems	Yes
Coordinate System Key	
Reader Mode Saves Updated File	No
Use Instances	Yes
Smart CAD Update	Yes

Compare Parts On Update	No
Analysis Type	3-D
Mixed Import Resolution	None
Clean Bodies On Import	No
Stitch Surfaces On Import	No
Decompose Disjoint Geometry	Yes
Enclosure and Symmetry Processing	Yes

**TABLE 3**  
**Model (C4) > Geometry > Parts**

Object Name	SYS\Solid
-------------	-----------

State	Meshed
Graphics Properties	
Visible	Yes
Transparency	1
Definition	
Suppressed	No
Stiffness Behavior	Flexible
Coordinate System	Default Coordinate System
Reference Temperature	By Environment
Behavior	None
Material	
Assignment	XYZ PLA
Nonlinear Effects	Yes
Thermal Strain Effects	Yes
Bounding Box	

Length X	0.241 m
Length Y	2.0148e-002 m
Length Z	3.5118e-003 m
Properties	
Volume	1.7052e-005 m <sup>3</sup>
Mass	2.0747e-002 kg
Centroid X	0.1205 m
Centroid Y	-2.074e-003 m
Centroid Z	2.2441e-003 m
Moment of Inertia Ip1	7.2317e-007 kg·m <sup>2</sup>
Moment of Inertia Ip2	1.0044e-004 kg·m <sup>2</sup>
Moment of Inertia Ip3	1.0112e-004 kg·m <sup>2</sup>
Statistics	
Nodes	6946
Elements	1134

Mesh Metric	None
CAD Attributes	
PartTolerance:	0.00000001
Color:143.175.143	

New Folder

Coordinate Systems

**TABLE 4**  
**Model (C4) > Coordinate Systems > Coordinate System**

Object Name	Global Coordinate System
State	Fully Defined
Definition	
Type	Cartesian
Coordinate System ID	0.
Origin	
Origin X	0. m
Origin Y	0. m

Origin Z	0. m
Directional Vectors	
X Axis Data	[ 1. 0. 0. ]
Y Axis Data	[ 0. 1. 0. ]
Z Axis Data	[ 0. 0. 1. ]

Mesh

**TABLE 5**  
**Model (C4) > Mesh**

Object Name	Mesh
State	Solved
Display	
Display Style	Maximum Corner Angle
Defaults	
Physics Preference	Mechanical

Element Order	Program Controlled
Element Size	3.e-003 m
Sizing	
Use Adaptive Sizing	Yes
Resolution	Default (2)
Mesh Defeaturing	Yes
Defeature Size	Default
Transition	Fast
Span Angle Center	Coarse
Initial Size Seed	Assembly
Bounding Box Diagonal	0.24187 m
Average Surface Area	1.9243e-003 m <sup>2</sup>
Minimum Edge Length	3.5118e-003 m
Quality	
Check Mesh Quality	Yes, Errors

Error Limits	Standard Mechanical
Target Quality	Default (0.050000)
Smoothing	Medium
Mesh Metric	None
Inflation	
Use Automatic Inflation	None
Inflation Option	Smooth Transition
Transition Ratio	0.272
Maximum Layers	5
Growth Rate	1.2
Inflation Algorithm	Pre
View Advanced Options	No
Advanced	
Number of CPUs for Parallel Part Meshing	Program Controlled
Straight Sided Elements	No

Number of Retries	Default (4)
Rigid Body Behavior	Dimensionally Reduced
Triangle Surface Mesher	Program Controlled
Topology Checking	Yes
Pinch Tolerance	Please Define
Generate Pinch on Refresh	No
Statistics	
Nodes	6946
Elements	1134

Modal (C5)

**TABLE 6**  
**Model (C4) > Analysis**

Object Name	Modal (C5)
State	Solved
Definition	
Physics Type	Structural
Analysis Type	Modal
Solver Target	Mechanical APDL
Options	
Environment Temperature	22. °C
Generate Input Only	No

**TABLE 7**  
**Model (C4) > Modal (C5) > Initial Condition**

Object Name	Pre-Stress (None)
State	Fully Defined
Definition	
Pre-Stress Environment	None Available

**TABLE 8**  
**Model (C4) > Modal (C5) > Analysis Settings**

Object Name	Analysis Settings
State	Fully Defined
Options	
Max Modes to Find	6
Limit Search to Range	No
Solver Controls	
Damped	No
Solver Type	Program Controlled
Rotordynamics Controls	
Coriolis Effect	Off
Campbell Diagram	Off
Output Controls	

Stress	No
Strain	No
Nodal Forces	No
Calculate Reactions	No
General Miscellaneous	No
Analysis Data Management	
Solver Files Directory	C:\Users\asus\AppData\Local\Temp\WB_DESKTOP-N3USIQU_asus_7184_2\unsaved_project_files\dp0\SYS-1\MECH\
Future Analysis	None
Scratch Solver Files Directory	
Save MAPDL db	No

Contact Summary	Program Controlled
Delete Unneeded Files	Yes
Solver Units	Active System
Solver Unit System	mks

**TABLE 9**  
**Model (C4) > Modal (C5) > Loads**

Object Name	Fixed Support
State	Fully Defined
Scope	
Scoping Method	Geometry Selection
Geometry	1 Face
Definition	
Type	Fixed Support
Suppressed	No

## Solution (C6)

**TABLE 10**  
**Model (C4) > Modal (C5) > Solution**

Object Name	Solution (C6)
State	Solved
Adaptive Mesh Refinement	
Max Refinement Loops	1.
Refinement Depth	2.
Information	
Status	Done
MAPDL Elapsed Time	4. s
MAPDL Memory Used	360. MB
MAPDL Result File Size	2.1875 MB
Post Processing	
Beam Section Results	No

The following bar chart indicates the frequency at each calculated mode.

**FIGURE 1**  
**Model (C4) > Modal (C5) > Solution (C6)**

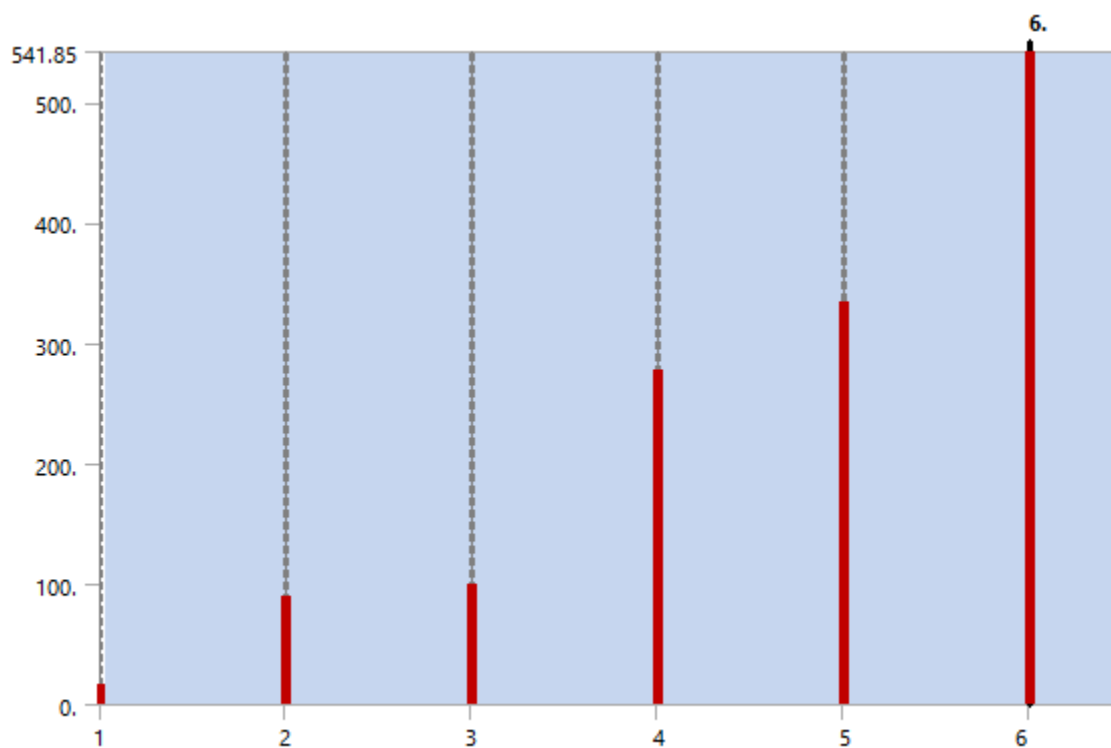


**TABLE 11**  
**Model (C4) > Modal (C5) > Solution (C6)**

Mode	Frequency [Hz]
1.	15.82
2.	89.862
3.	99.021
4.	276.92
5.	333.45
6.	541.85

**TABLE 12**  
**Model (C4) > Modal (C5) > Solution (C6) > Solution Information**

Object Name	Solution Information
State	Solved
Solution Information	
Solution Output	Solver Output
Newton-Raphson Residuals	0
Identify Element Violations	0
Update Interval	2.5 s
Display Points	All
FE Connection Visibility	
Activate Visibility	Yes
Display	All FE Connectors
Draw Connections Attached To	All Nodes
Line Color	Connection Type
Visible on Results	No

Line Thickness	Single
Display Type	Lines

**TABLE 13**  
**Model (C4) > Modal (C5) > Solution (C6) > Results**

Object Name	Order	Modal Deflection 1	Modal Deflection 2	Modal Deflection 3	Modal Deflection 4	Modal Deflection 5	Modal Deflection 6	Modal Deflection 7	Modal Deflection 8	Modal Deflection 9	Modal Deflection 10	Modal Deflection 11
	Deflection 1	Deflection 2	Deflection 3	Deflection 4	Deflection 5	Deflection 6	Deflection 7	Deflection 8	Deflection 9	Deflection 10	Deflection 11	
	n 1	n 2	n 3	n 4	n 5	n 6	n 7	n 8	n 9	n 10	n 11	
Status	Solved											
Scope												
Scoping Method	Geometry Selection											
Geometry	All Bodies											

Definition												
type	T	Total Deformation										
code	M	.	.	.	.	.	.	.	.	.	.	
identifier	I											
suppressed	S	No										
Results												
minimum	M	0. m										
maximum	M	3.907 m	3.869 m	3.904 m	3.909 m	7.19 m	3.922 m	3.907 m	3.869 m	3.904 m	3.909 m	7.19 m

Average	.4419 m	.4656 m	.9698 m	.0902 m	.0775 m	.1659 m	.4419 m	.4656 m	.9698 m	.0902 m	.0775 m
Minimum Occurs On	SYS\Solid										
Maximum Occurs On	SYS\Solid										
Information											
Frequency	5.82 Hz	9.862 Hz	9.021 Hz	76.92 Hz	33.45 Hz	41.85 Hz	5.82 Hz	9.862 Hz	9.021 Hz	76.92 Hz	33.45 Hz

**TABLE 14**  
**Model (C4) > Modal (C5) > Solution (C6) > Total Deformation**

Mode	Frequency [Hz]
1.	15.82

2.	89.862
3.	99.021
4.	276.92
5.	333.45
6.	541.85

**TABLE 15**  
**Model (C4) > Modal (C5) > Solution (C6) > Total Deformation 2**

Mode	Frequency [Hz]
1.	15.82
2.	89.862
3.	99.021
4.	276.92
5.	333.45
6.	541.85

**TABLE 16**  
**Model (C4) > Modal (C5) > Solution (C6) > Total Deformation 3**

Mode	Frequency [Hz]
------	----------------

1.	15.82
2.	89.862
3.	99.021
4.	276.92
5.	333.45
6.	541.85

**TABLE 17**  
**Model (C4) > Modal (C5) > Solution (C6) > Total Deformation 4**

Mode	Frequency [Hz]
1.	15.82
2.	89.862
3.	99.021
4.	276.92
5.	333.45
6.	541.85

**TABLE 18**  
**Model (C4) > Modal (C5) > Solution (C6) > Total Deformation 5**

Mode	Frequency [Hz]
1.	15.82
2.	89.862
3.	99.021
4.	276.92
5.	333.45
6.	541.85

**TABLE 19**  
**Model (C4) > Modal (C5) > Solution (C6) > Total Deformation 6**

Mode	Frequency [Hz]
1.	15.82
2.	89.862
3.	99.021
4.	276.92
5.	333.45
6.	541.85

**TABLE 20**  
**Model (C4) > Modal (C5) > Solution (C6) > Total Deformation 7**

Mode	Frequency [Hz]
1.	15.82
2.	89.862
3.	99.021
4.	276.92
5.	333.45
6.	541.85

**TABLE 21**  
**Model (C4) > Modal (C5) > Solution (C6) > Total Deformation 8**

Mode	Frequency [Hz]
1.	15.82
2.	89.862
3.	99.021

4.	276.92
5.	333.45
6.	541.85

**TABLE 22**  
**Model (C4) > Modal (C5) > Solution (C6) > Total Deformation 9**

Mode	Frequency [Hz]
1.	15.82
2.	89.862
3.	99.021
4.	276.92
5.	333.45
6.	541.85

**TABLE 23**  
**Model (C4) > Modal (C5) > Solution (C6) > Total Deformation 10**

Mode	Frequency [Hz]
1.	15.82
2.	89.862

3.	99.021
4.	276.92
5.	333.45
6.	541.85

**TABLE 24**  
**Model (C4) > Modal (C5) > Solution (C6) > Total Deformation 11**

Mode	Frequency [Hz]
1.	15.82
2.	89.862
3.	99.021
4.	276.92
5.	333.45
6.	541.85

**TABLE 25**  
**Model (C4) > Modal (C5) > Solution (C6) > Results**

Object Name	Total Deformation 12
State	Solved

Scope	
Scoping Method	Geometry Selection
Geometry	All Bodies
Definition	
Type	Total Deformation
Mode	6.
Identifier	
Suppressed	No
Results	
Minimum	0. m
Maximum	13.922 m
Average	6.1659 m
Minimum Occurs On	SYS\Solid
Maximum Occurs On	SYS\Solid
Information	

Frequency	541.85 Hz
-----------	-----------

**TABLE 26**  
**Model (C4) > Modal (C5) > Solution (C6) > Total Deformation 12**

Mode	Frequency [Hz]
1.	15.82
2.	89.862
3.	99.021
4.	276.92
5.	333.45
6.	541.85

Material Data

XYZ PLA

**TABLE 27**  
**XYZ PLA > Constants**

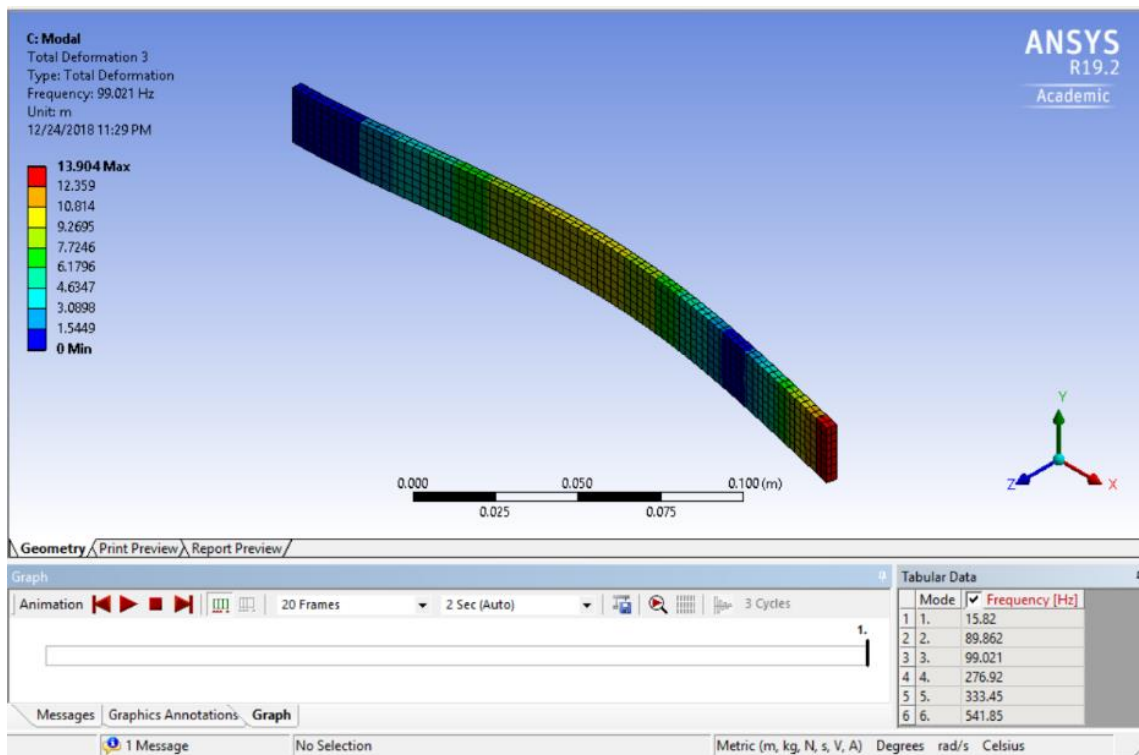
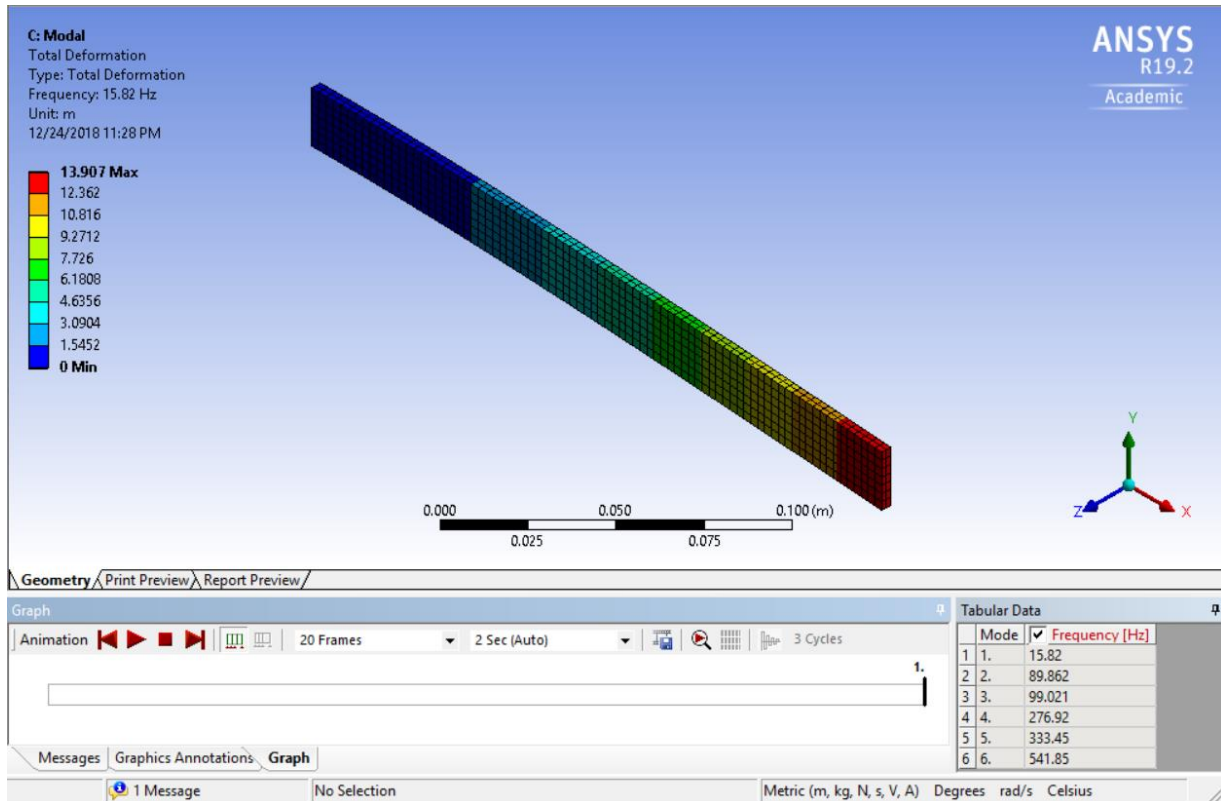
Density	1216.7 kg m <sup>-3</sup>
---------	---------------------------

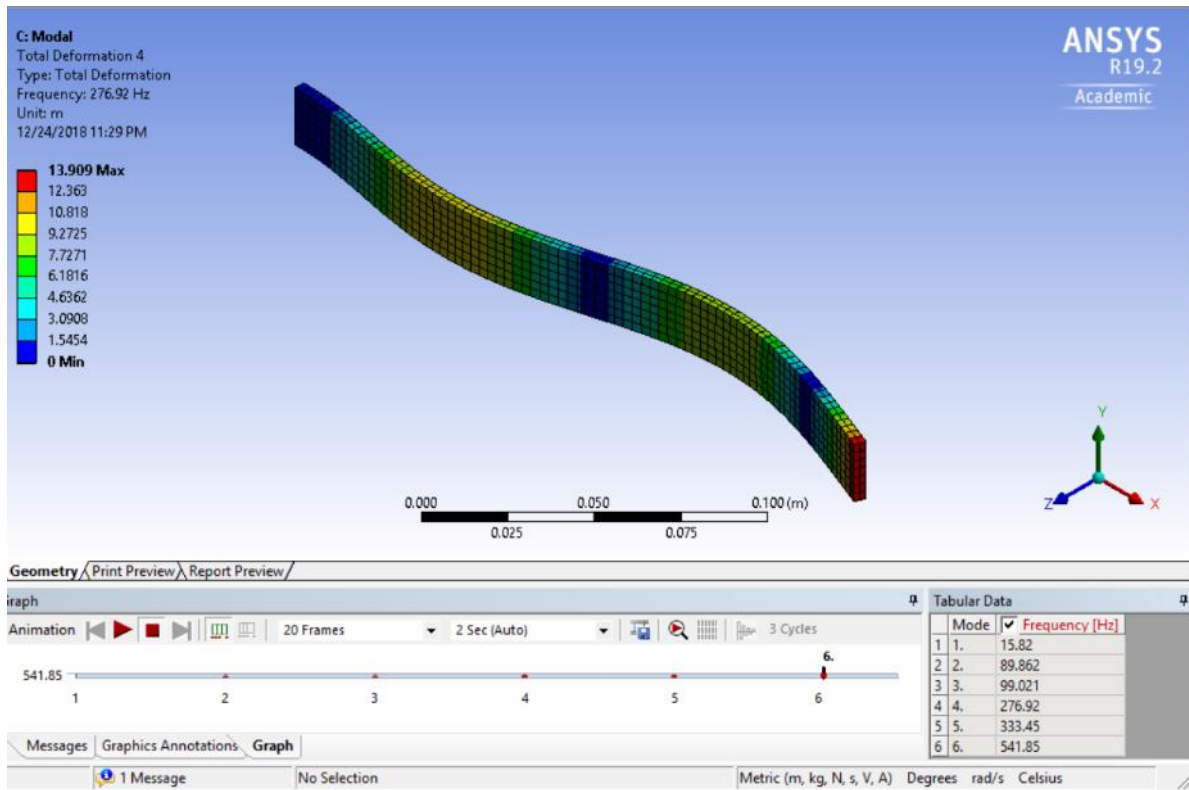
**TABLE 28**  
**XYZ PLA > Color**

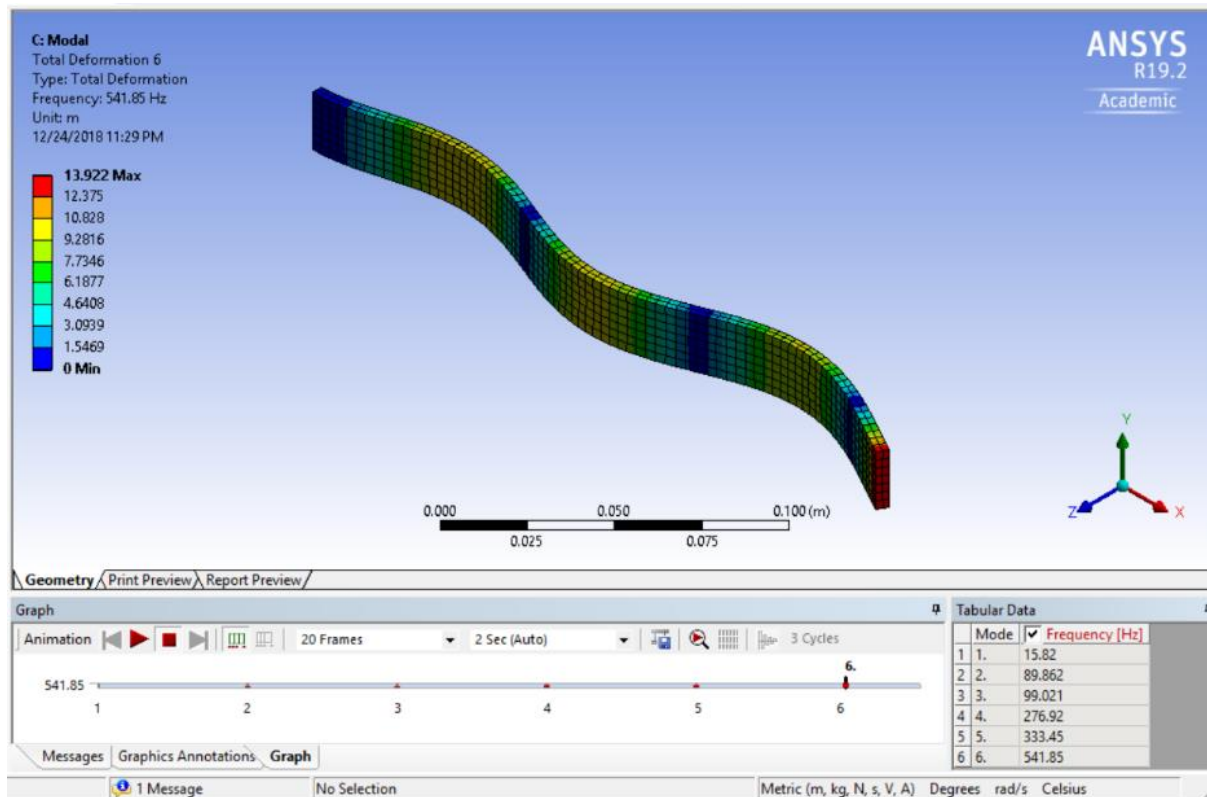
Red	Green	Blue
181	194	156

**TABLE 29**  
**XYZ PLA > Orthotropic Elasticity**

Young's Modulus in X direction Pa	Young's Modulus in Y direction Pa	Young's Modulus in Z direction Pa	Poisson's Ratio XY	Poisson's Ratio YZ	Poisson's Ratio XZ	Shear Modulus in XY Pa	Shear Modulus in YZ Pa	Shear Modulus in XZ Pa	Temperature C
3.15e+009	3.12e+009	2.92e+009	.35	.35	.35	1.159e+009	1.07e+009	1.029e+009	





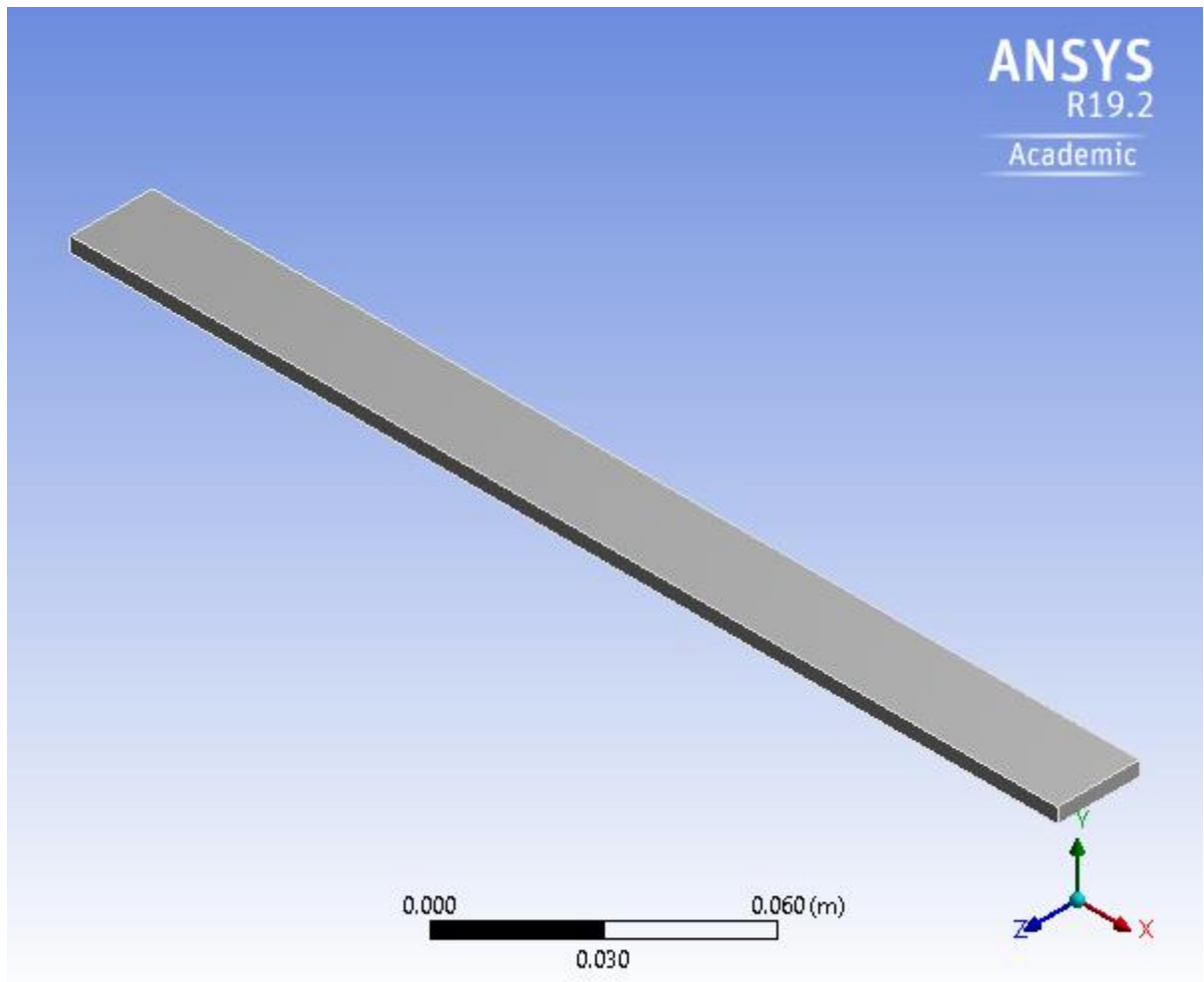


## Appendix D2 Build orientation XZY

First Saved	Monday, December 24, 2018
Last Saved	Monday, December 24, 2018
Product Version	19.2 Release
Save Project Before Solution	No

Save Project After Solution

No



## Contents

- [Units](#)
- [Model \(C4\)](#)
  - [Geometry](#)
    - [SYS-2\Solid](#)

- [Materials](#)
  - [PLA](#)
  - [XYZY PLA](#)
- [Coordinate Systems](#)
- [Mesh](#)
- [Modal \(C5\)](#)
  - [Pre-Stress \(None\)](#)
  - [Analysis Settings](#)
  - [Fixed Support](#)
  - [Solution \(C6\)](#)
    - [Solution Information](#)
    - [Results](#)
- [Material Data](#)
  - [XYZY PLA](#)

Units

TABLE 1

Unit System	Metric (m, kg, N, s, V, A) Degrees rad/s Celsius
Angle	Degrees
Rotational Velocity	rad/s
Temperature	Celsius

Model (C4)

Geometry

Model (C4) &gt; Geometry

Object Name	Geometry
State	Fully Defined
Definition	
Source	C:\Users\asus\AppData\Local\Temp\WB_DESKTOP-N3USIQU_asus_7184_2\unsaved_project_files\dp0\SYS-2\DM\SYS-2.scdoc
Type	SpaceClaim
Length Unit	Meters
Element Control	Program Controlled
Display Style	Body Color
Bounding Box	
Length X	0.241 m
Length Y	3.65e-003 m

Length Z	1.996e-002 m
Properties	
Volume	1.7558e-005 m <sup>3</sup>
Mass	2.0829e-002 kg
Scale Factor Value	1.
Statistics	
Bodies	1
Active Bodies	1
Nodes	1640
Elements	196
Mesh Metric	None
Update Options	
Assign Default Material	No

Basic Geometry Options	
Solid Bodies	Yes
Surface Bodies	Yes
Line Bodies	Yes
Parameters	Independent
Parameter Key	
Attributes	Yes
Attribute Key	
Named Selections	Yes
Named Selection Key	
Material Properties	Yes
Advanced Geometry Options	

Use Associativity	Yes
Coordinate Systems	Yes
Coordinate System Key	
Reader Mode Saves Updated File	No
Use Instances	Yes
Smart CAD Update	Yes
Compare Parts On Update	No
Analysis Type	3-D
Mixed Import Resolution	None

Clean Bodies On Import	No
Stitch Surfaces On Import	No
Decompose Disjoint Geometry	Yes
Enclosure and Symmetry Processing	Yes

TABLE

3

Model (C4) > Geometry > Parts

Object Name	SYS-2\Solid
State	Meshed
Graphics Properties	
Visible	Yes
Transparency	1
Definition	
Suppressed	No

Stiffness Behavior	Flexible
Coordinate System	Default Coordinate System
Reference Temperature	By Environment
Behavior	None
Material	
Assignment	XZY PLA
Nonlinear Effects	Yes
Thermal Strain Effects	Yes
Bounding Box	
Length X	0.241 m
Length Y	3.65e-003 m
Length Z	1.996e-002 m
Properties	
Volume	1.7558e-005 m <sup>3</sup>
Mass	2.0829e-002 kg

Centroid X	0.1205 m
Centroid Y	1.75e-004 m
Centroid Z	1.98e-003 m
Moment of Inertia Ip1	7.1464e-007 kg·m <sup>2</sup>
Moment of Inertia Ip2	1.015e-004 kg·m <sup>2</sup>
Moment of Inertia Ip3	1.0084e-004 kg·m <sup>2</sup>
Statistics	
Nodes	1640
Elements	196
Mesh Metric	None
CAD Attributes	
PartTolerance:	0.00000001
Color:143.175.143	

Coordinate Systems

Model (C4) > Coordinate Systems > Coordinate System

Object Name	Global Coordinate System
State	Fully Defined
Definition	
Type	Cartesian
Coordinate System ID	0.
Origin	
Origin X	0. m
Origin Y	0. m
Origin Z	0. m
Directional Vectors	
X Axis Data	[ 1. 0. 0. ]
Y Axis Data	[ 0. 1. 0. ]
Z Axis Data	[ 0. 0. 1. ]

Mesh

Model (C4) &gt; Mesh

Object Name	Mesh
State	Solved
Display	
Display Style	Maximum Corner Angle
Defaults	
Physics Preference	Mechanical
Element Order	Program Controlled
Element Size	5.e-003 m
Sizing	
Use Adaptive Sizing	Yes
Resolution	Default (2)
Mesh Defeaturing	Yes
Defeature Size	Default

Transition	Fast
Span Angle Center	Coarse
Initial Size Seed	Assembly
Bounding Box Diagonal	0.24185 m
Average Surface Area	1.921e-003 m <sup>2</sup>
Minimum Edge Length	3.65e-003 m
Quality	
Check Mesh Quality	Yes, Errors
Error Limits	Standard Mechanical
Target Quality	Default (0.050000)
Smoothing	Medium
Mesh Metric	None
Inflation	
Use Automatic Inflation	None
Inflation Option	Smooth Transition

Transition Ratio	0.272
Maximum Layers	5
Growth Rate	1.2
Inflation Algorithm	Pre
View Advanced Options	No
Advanced	
Number of CPUs for Parallel Part Meshing	Program Controlled
Straight Sided Elements	No
Number of Retries	Default (4)
Rigid Body Behavior	Dimensionally Reduced
Triangle Surface Mesher	Program Controlled
Topology Checking	Yes
Pinch Tolerance	Please Define
Generate Pinch on Refresh	No
Statistics	

Nodes	1640
Elements	196

Modal (C5)

TABLE

6

Model (C4) > Analysis

Object Name	Modal (C5)
State	Solved
Definition	
Physics Type	Structural
Analysis Type	Modal
Solver Target	Mechanical APDL
Options	
Environment Temperature	22. °C
Generate Input Only	No

TABLE

7

Model (C4) > Modal (C5) > Initial Condition

Object Name	Pre-Stress (None)
State	Fully Defined
Definition	
Pre-Stress Environment	None Available

TABLE

8

Model (C4) > Modal (C5) > Analysis Settings

Object Name	Analysis Settings
State	Fully Defined
Options	
Max Modes to Find	6
Limit Search to Range	No
Solver Controls	
Damped	No

Solver Type	Program Controlled
Rotordynamics Controls	
Coriolis Effect	Off
Campbell Diagram	Off
Output Controls	
Stress	No
Strain	No
Nodal Forces	No
Calculate Reactions	No
General Miscellaneous	No
Analysis Data Management	

Solver Files Directory	C:\Users\asus\AppData\Local\Temp\WB_DESKTOP- N3USIQU_asus_7184_2\unsaved_project_files\dp0\SYS-3\MECH\
Future Analysis	None
Scratch Solver Files Directory	
Save MAPDL db	No
Contact Summary	Program Controlled
Delete Unneeded Files	Yes
Solver Units	Active System
Solver Unit System	mks

TABLE

9

Model (C4) > Modal (C5) > Loads

Object Name	Fixed Support
State	Fully Defined
Scope	
Scoping Method	Geometry Selection
Geometry	1 Face
Definition	
Type	Fixed Support
Suppressed	No

Solution (C6)

TABLE

10

Model (C4) > Modal (C5) > Solution

Object Name	Solution (C6)
State	Solved
Adaptive Mesh Refinement	
Max Refinement Loops	1.

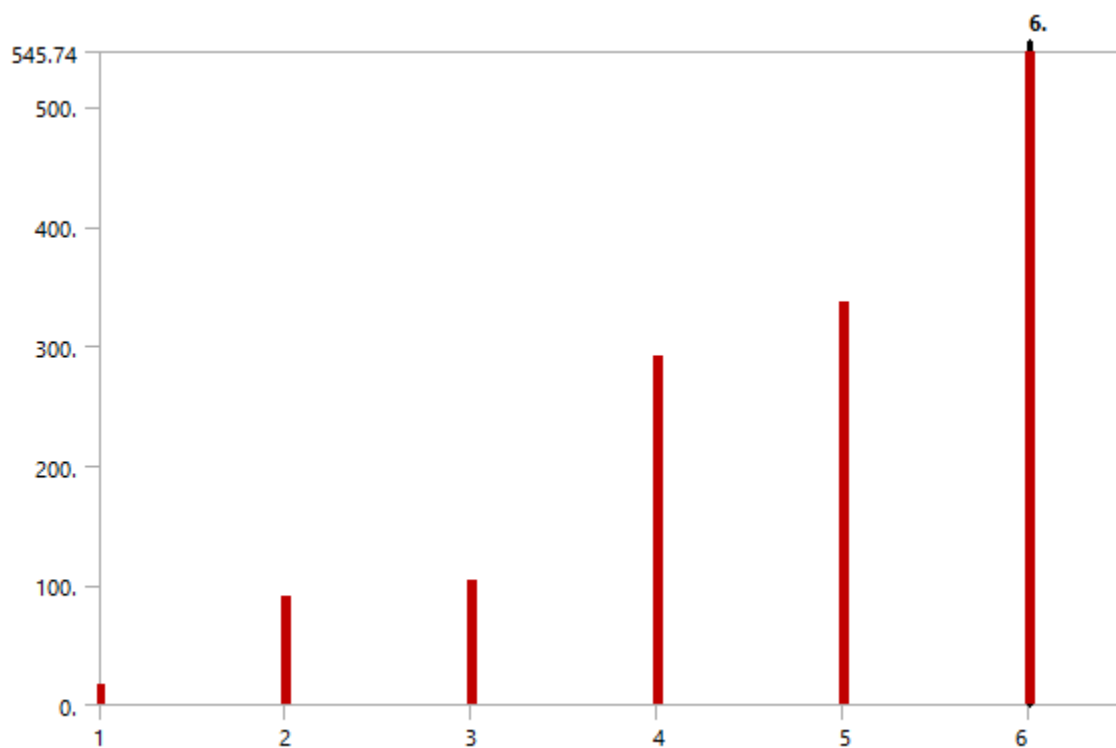
Refinement Depth	2.
Information	
Status	Done
MAPDL Elapsed Time	3. s
MAPDL Memory Used	94. MB
MAPDL Result File Size	768. KB
Post Processing	
Beam Section Results	No

The following bar chart indicates the frequency at each calculated mode.

FIGURE

1

Model (C4) > Modal (C5) > Solution (C6)



TABLE

11

Model (C4) > Modal (C5) > Solution (C6)

Mode	Frequency [Hz]
1.	16.68
2.	90.136
3.	104.42
4.	292.07
5.	337.24

6.	545.74
----	--------

TABLE

12

Model (C4) > Modal (C5) > Solution (C6) > Solution Information

Object Name	Solution Information
State	Solved
Solution Information	
Solution Output	Solver Output
Newton-Raphson Residuals	0
Identify Element Violations	0
Update Interval	2.5 s
Display Points	All
FE Connection Visibility	
Activate Visibility	Yes
Display	All FE Connectors
Draw Connections Attached To	All Nodes

Line Color	Connection Type
Visible on Results	No
Line Thickness	Single
Display Type	Lines

TABLE

13

Model (C4) > Modal (C5) > Solution (C6) > Results

Object Name	Tota l	Tota l	Tota l	Tota l	Tota l	Tota l
	Deformatio n	Deformatio n 2	Deformatio n 3	Deformatio n 4	Deformatio n 5	Deformatio n 6
	Solved					
Scope						
Scoping Method	Geometry Selection					
Geomet ry	All Bodies					
Definition						

Type	Total Deformation					
Mode	1.	2.	3.	4.	5.	6.
Identifier						
Suppressed	No					
Results						
Minimum	0. m					
Maximum	13.8 86 m	13.8 39 m	13.8 84 m	13.8 91 m	17.1 78 m	13.7 65 m
Average	5.43 74 m	5.46 55 m	5.96 73 m	6.09 65 m	6.50 07 m	6.08 03 m
Minimum Occurs On	SYS-2\Solid					
Maximum Occurs On	SYS-2\Solid					

Information							
cy	Frequen	16.6	90.1	104.	292.	337.	545.
	8 Hz	36 Hz	42 Hz	07 Hz	24 Hz	74 Hz	

TABLE

14

Model (C4) > Modal (C5) > Solution (C6) > Total Deformation

Mode	Frequency [Hz]
1.	16.68
2.	90.136
3.	104.42
4.	292.07
5.	337.24
6.	545.74

TABLE

15

Model (C4) > Modal (C5) > Solution (C6) > Total Deformation 2

Mode	Frequency [Hz]
1.	16.68

2.	90.136
3.	104.42
4.	292.07
5.	337.24
6.	545.74

TABLE

16

Model (C4) > Modal (C5) > Solution (C6) > Total Deformation 3

Mode	Frequency [Hz]
1.	16.68
2.	90.136
3.	104.42
4.	292.07
5.	337.24
6.	545.74

TABLE

17

Model (C4) > Modal (C5) > Solution (C6) > Total Deformation 4

Mode	Frequency [Hz]
1.	16.68
2.	90.136
3.	104.42
4.	292.07
5.	337.24
6.	545.74

TABLE

18

Model (C4) > Modal (C5) > Solution (C6) > Total Deformation 5

Mode	Frequency [Hz]
1.	16.68
2.	90.136
3.	104.42
4.	292.07
5.	337.24

6.	545.74
----	--------

TABLE

19

Model (C4) > Modal (C5) > Solution (C6) > Total Deformation 6

Mode	Frequency [Hz]
1.	16.68
2.	90.136
3.	104.42
4.	292.07
5.	337.24
6.	545.74

Material Data

XZY PLA

TABLE

20

XZY PLA > Constants

Density	1186.3 kg m <sup>-3</sup>
---------	---------------------------

TABLE

21

XZY PLA > Color

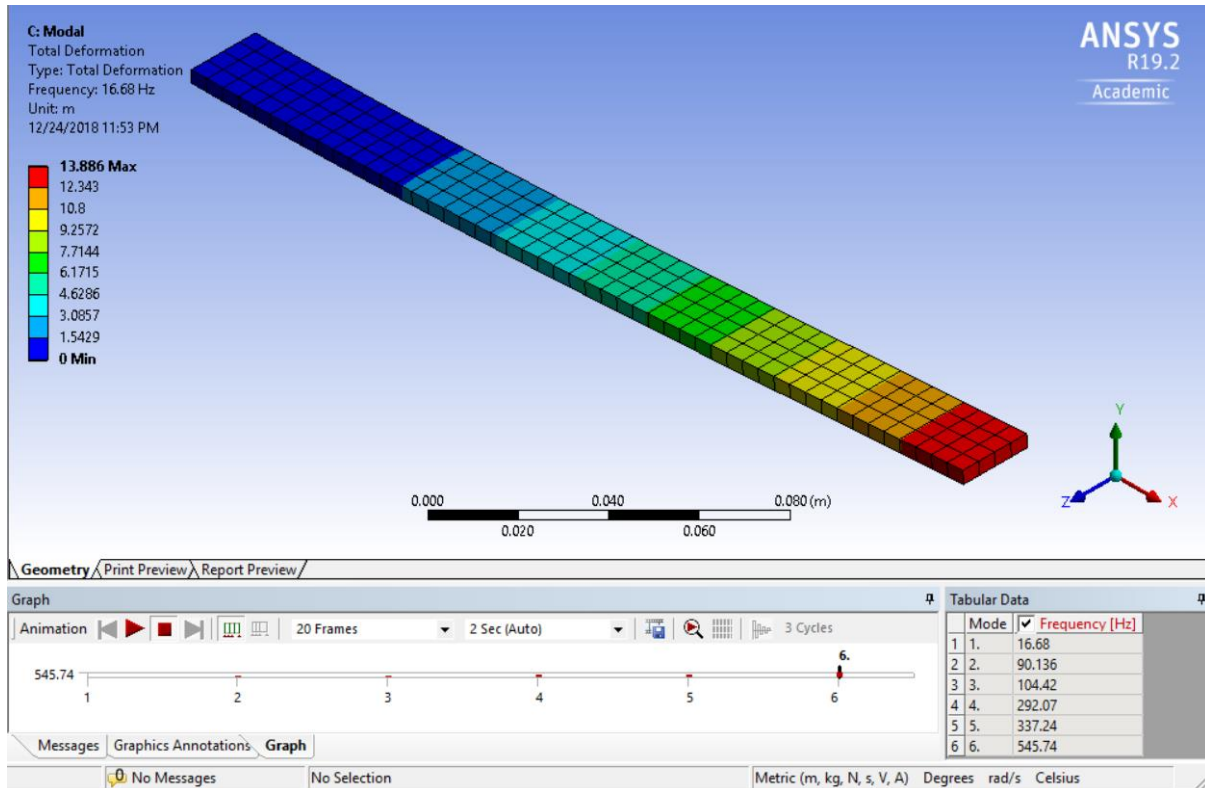
Red	Green	Blue
161	209	255

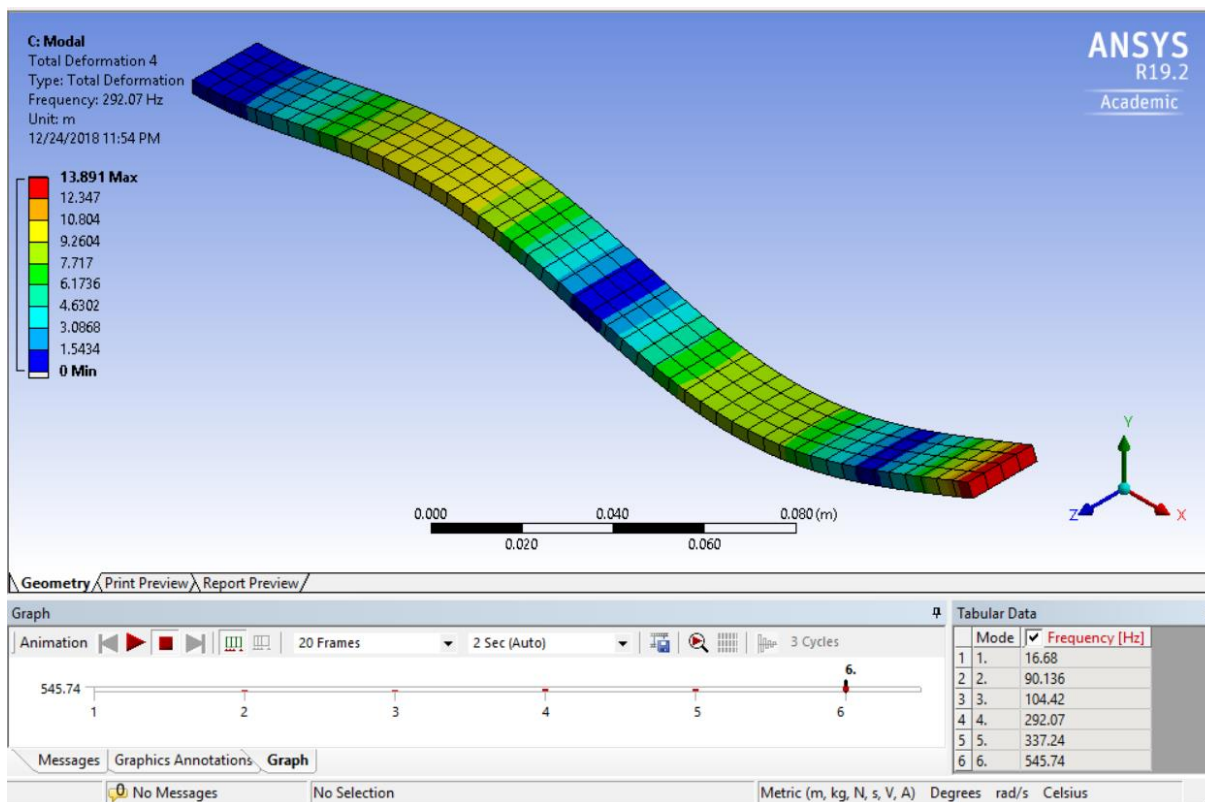
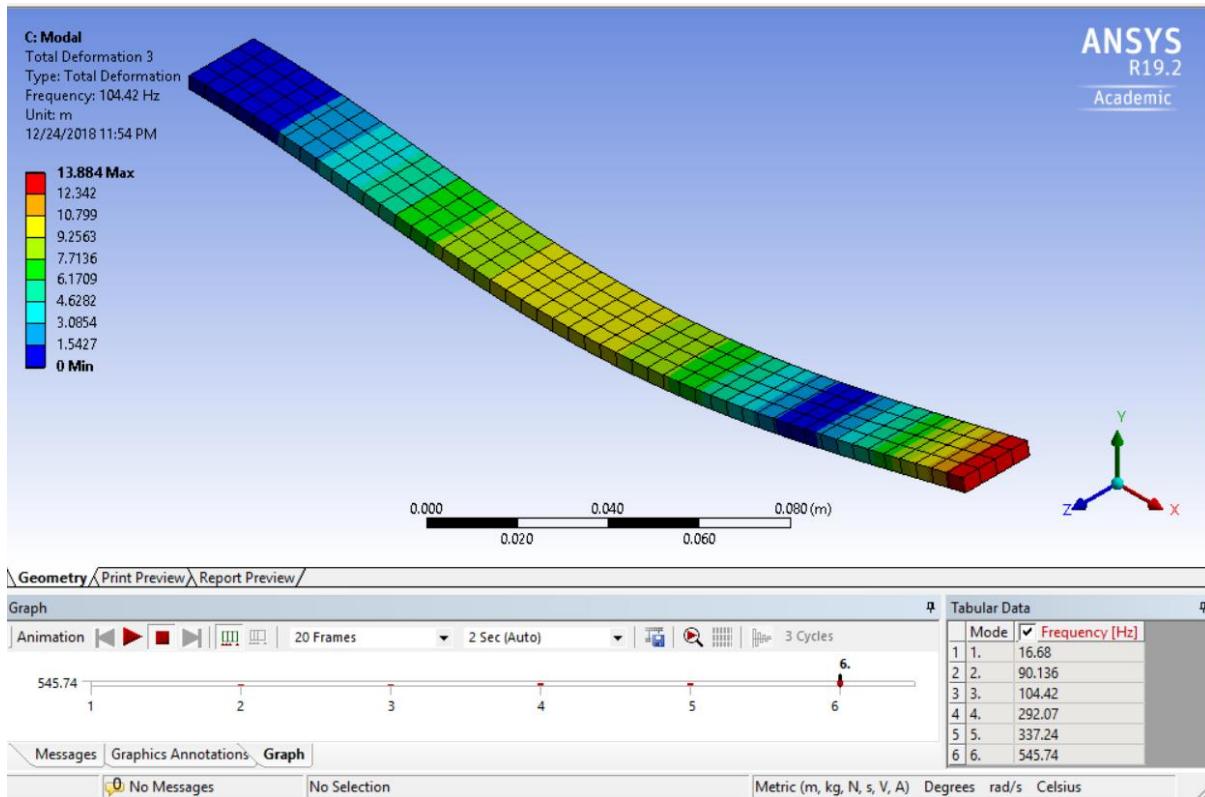
TABLE

22

XZY PLA > Orthotropic Elasticity

Young's Modulus in X direction Pa	Young's Modulus in Y direction Pa	Young's Modulus in Z direction Pa	Poisson's Ratio XY	Poisson's Ratio YZ	Poisson's Ratio XZ	Shear Modulus in XY Pa	Shear Modulus in YZ Pa	Shear Modulus in XZ Pa	Temperature C
3.15e+009	3.12e+009	2.92e+009	.35	.35	.35	1.159e+009	1.07e+009	1.029e+009	

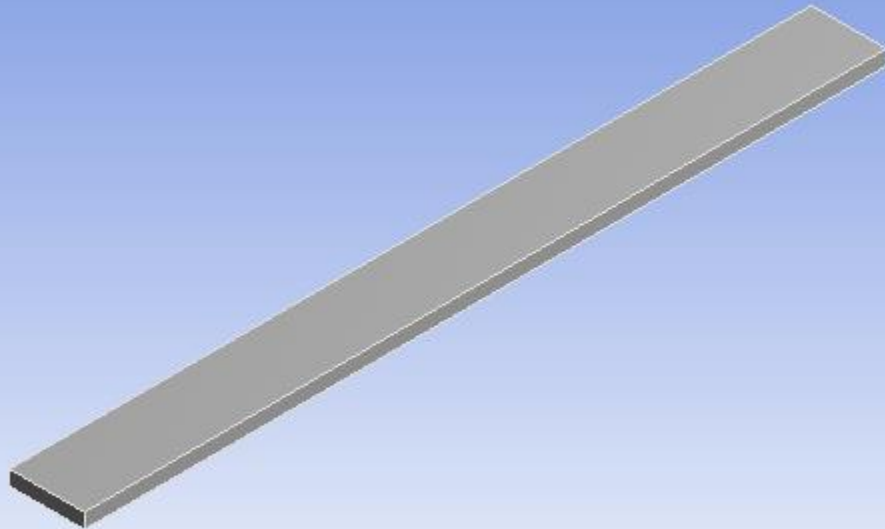






#### Appendix D3 Build orientation ZXY

First Saved	Monday, December 24, 2018
Last Saved	Tuesday, December 25, 2018
Product Version	19.2 Release
Save Project Before Solution	No
Save Project After Solution	No



## Contents

- [Units](#)
- [Model \(C4\)](#)
  - [Geometry](#)
    - [SYS-5\Solid](#)
  - [Materials](#)
    - [ZXY PLA](#)
    - [ZXY PLA 2](#)
  - [Coordinate Systems](#)
  - [Mesh](#)

- [Modal \(C5\)](#)
  - [Pre-Stress \(None\)](#)
  - [Analysis Settings](#)
  - [Fixed Support](#)
  - [Solution \(C6\)](#)
    - [Solution Information](#)
    - [Results](#)
- [Material Data](#)
  - [ZXY PLA](#)

Units

TABLE 1

Unit System	Metric (m, kg, N, s, V, A) Degrees rad/s Celsius
Angle	Degrees
Rotational Velocity	rad/s
Temperature	Celsius

Model (C4)

Geometry

TABLE

2

Model (C4) > Geometry

Object Name	Geometry
-------------	----------

State	Fully Defined
Definition	
Source	C:\Users\asus\AppData\Local\Temp\WB_DESKTOP-N3USIQU_asus_7184_2\unsaved_project_files\dp0\SYS-5\DM\SYS-5.scdoc
Type	SpaceClaim
Length Unit	Meters
Element Control	Program Controlled
Display Style	Body Color
Bounding Box	
Length X	2.009e-002 m
Length Y	4.e-003 m
Length Z	0.215 m
Properties	
Volume	1.7277e-005 m <sup>3</sup>

Mass	1.9917e-002 kg
Scale Factor Value	1.
Statistics	
Bodies	1
Active Bodies	1
Nodes	6181
Elements	1008
Mesh Metric	None
Update Options	
Assign Default Material	No
Basic Geometry Options	
Solid Bodies	Yes
Surface Bodies	Yes

Line Bodies	Yes
Parameters	Independent
Parameter Key	
Attributes	Yes
Attribute Key	
Named Selections	Yes
Named Selection Key	
Material Properties	Yes
Advanced Geometry Options	
Use Associativity	Yes
Coordinate Systems	Yes

Coordinate System Key	
Reader Mode Saves Updated File	No
Use Instances	Yes
Smart CAD Update	Yes
Compare Parts On Update	No
Analysis Type	3-D
Mixed Import Resolution	None
Clean Bodies On Import	No
Stitch Surfaces On Import	No

Decompose Disjoint Geometry	Yes
Enclosure and Symmetry Processing	Yes

TABLE

3

Model (C4) > Geometry > Parts

Object Name	SYS-5\Solid
State	Meshed
Graphics Properties	
Visible	Yes
Transparency	1
Definition	
Suppressed	No
Stiffness Behavior	Flexible
Coordinate System	Default Coordinate System
Reference Temperature	By Environment

Behavior	None
Material	
Assignment	ZXY PLA
Nonlinear Effects	Yes
Thermal Strain Effects	Yes
Bounding Box	
Length X	2.009e-002 m
Length Y	4.e-003 m
Length Z	0.215 m
Properties	
Volume	1.7277e-005 m <sup>3</sup>
Mass	1.9917e-002 kg
Centroid X	1.045e-003 m
Centroid Y	2.e-003 m
Centroid Z	0.1075 m

Moment of Inertia Ip1	7.675e-005 kg·m <sup>2</sup>
Moment of Inertia Ip2	7.7393e-005 kg·m <sup>2</sup>
Moment of Inertia Ip3	6.9646e-007 kg·m <sup>2</sup>
Statistics	
Nodes	6181
Elements	1008
Mesh Metric	None
CAD Attributes	
PartTolerance:	0.00000001
Color:143.175.143	

#### Coordinate Systems

TABLE

4

Model (C4) > Coordinate Systems > Coordinate System

Object Name	Global Coordinate System
State	Fully Defined

Definition	
Type	Cartesian
Coordinate System ID	0.
Origin	
Origin X	0. m
Origin Y	0. m
Origin Z	0. m
Directional Vectors	
X Axis Data	[ 1. 0. 0. ]
Y Axis Data	[ 0. 1. 0. ]
Z Axis Data	[ 0. 0. 1. ]

Mesh

TABLE

5

Model (C4) > Mesh

Object Name	Mesh
-------------	------

State	Solved
Display	
Display Style	Use Geometry Setting
Defaults	
Physics Preference	Mechanical
Element Order	Program Controlled
Element Size	3.e-003 m
Sizing	
Use Adaptive Sizing	Yes
Resolution	Default (2)
Mesh Defeaturing	Yes
Defeature Size	Default
Transition	Fast
Span Angle Center	Coarse
Initial Size Seed	Assembly

Bounding Box Diagonal	0.21597 m
Average Surface Area	1.7532e-003 m <sup>2</sup>
Minimum Edge Length	4.e-003 m
Quality	
Check Mesh Quality	Yes, Errors
Error Limits	Standard Mechanical
Target Quality	Default (0.050000)
Smoothing	Medium
Mesh Metric	None
Inflation	
Use Automatic Inflation	None
Inflation Option	Smooth Transition
Transition Ratio	0.272
Maximum Layers	5
Growth Rate	1.2

Inflation Algorithm	Pre
View Advanced Options	No
Advanced	
Number of CPUs for Parallel Part Meshing	Program Controlled
Straight Sided Elements	No
Number of Retries	Default (4)
Rigid Body Behavior	Dimensionally Reduced
Triangle Surface Mesher	Program Controlled
Topology Checking	Yes
Pinch Tolerance	Please Define
Generate Pinch on Refresh	No
Statistics	
Nodes	6181
Elements	1008

Modal (C5)

TABLE

6

Model (C4) &gt; Analysis

Object Name	Modal (C5)
State	Solved
Definition	
Physics Type	Structural
Analysis Type	Modal
Solver Target	Mechanical APDL
Options	
Environment Temperature	22. °C
Generate Input Only	No

TABLE

7

Model (C4) &gt; Modal (C5) &gt; Initial Condition

Object Name	Pre-Stress (None)
State	Fully Defined
Definition	

Pre-Stress Environment	None Available
------------------------	----------------

TABLE

8

Model (C4) > Modal (C5) > Analysis Settings

Object Name	Analysis Settings
State	Fully Defined
Options	
Max Modes to Find	6
Limit Search to Range	No
Solver Controls	
Damped	No
Solver Type	Program Controlled
Rotordynamics Controls	
Coriolis Effect	Off

Campbell Diagram	Off
Output Controls	
Stress	No
Strain	No
Nodal Forces	No
Calculate Reactions	No
General Miscellaneous	No
Analysis Data Management	
Solver Files Directory	C:\Users\asus\AppData\Local\Temp\WB_DESKTOP- N3USIQU_asus_7184_2\unsaved_project_files\dp0\SYS-6\MECH\
Future Analysis	None

Scratch Solver Files Directory	
Save MAPDL db	No
Contact Summary	Program Controlled
Delete Unneeded Files	Yes
Solver Units	Active System
Solver Unit System	mks

TABLE

9

Model (C4) > Modal (C5) > Loads

Object Name	Fixed Support
State	Fully Defined
Scope	

Scoping Method	Geometry Selection
Geometry	1 Face
Definition	
Type	Fixed Support
Suppressed	No

Solution (C6)

TABLE

10

Model (C4) > Modal (C5) > Solution

Object Name	Solution (C6)
State	Solved
Adaptive Mesh Refinement	
Max Refinement Loops	1.
Refinement Depth	2.
Information	
Status	Done

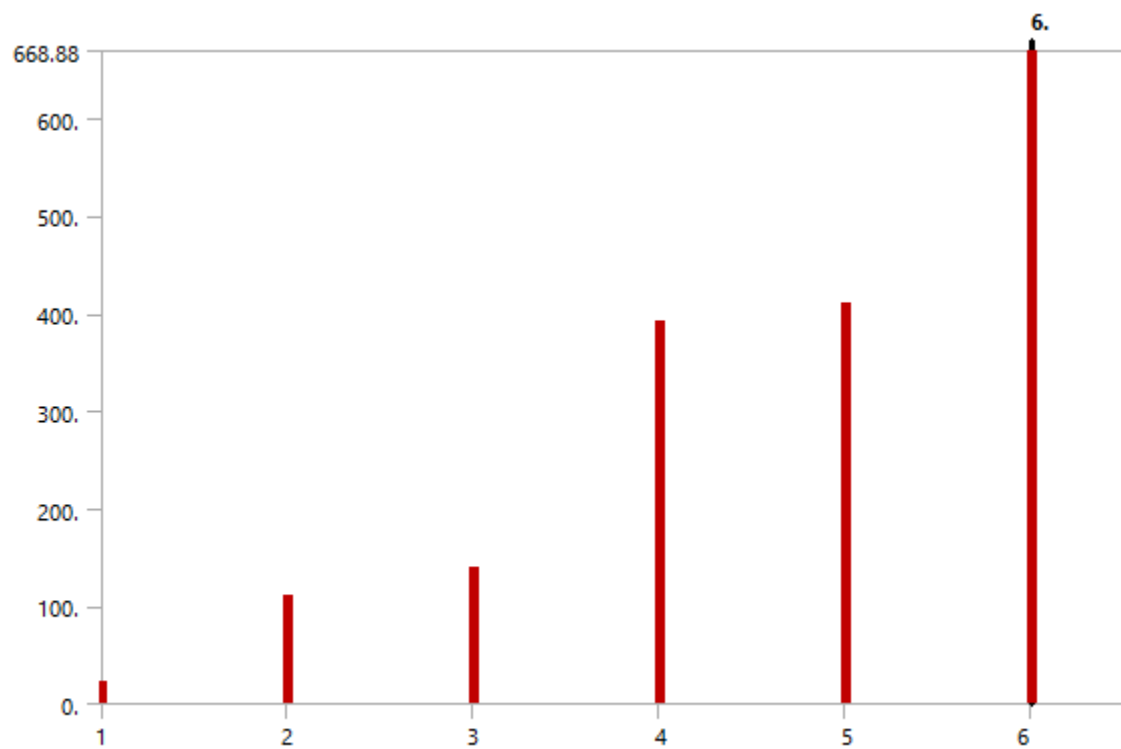
MAPDL Elapsed Time	3. s
MAPDL Memory Used	352. MB
MAPDL Result File Size	2. MB
Post Processing	
Beam Section Results	No

The following bar chart indicates the frequency at each calculated mode.

FIGURE

1

Model (C4) > Modal (C5) > Solution (C6)



TABLE

11

Model (C4) &gt; Modal (C5) &gt; Solution (C6)

Mode	Frequency [Hz]
1.	22.392
2.	111.2
3.	140.08
4.	391.4
5.	411.
6.	668.88

TABLE

12

Model (C4) &gt; Modal (C5) &gt; Solution (C6) &gt; Solution Information

Object Name	Solution Information
State	Solved
Solution Information	
Solution Output	Solver Output
Newton-Raphson Residuals	0

Identify Element Violations	0
Update Interval	2.5 s
Display Points	All
FE Connection Visibility	
Activate Visibility	Yes
Display	All FE Connectors
Draw Connections Attached To	All Nodes
Line Color	Connection Type
Visible on Results	No
Line Thickness	Single
Display Type	Lines

TABLE

13

Model (C4) > Modal (C5) > Solution (C6) > Results

Object	Tota	Tota	Tota	Tota	Tota	Tota
Name	1	1	1	1	1	1

	Deformation 1	Deformation 2	Deformation 3	Deformation 4	Deformation 5	Deformation 6
State	Solved					
Scope						
Scoping Method	Geometry Selection					
Geometry	All Bodies					
Definition						
Type	Total Deformation					
Mode	1.	2.	3.	4.	5.	6.
Identifier						
Suppressed	No					
Results						

Minimu m	0. m					
Maximu m	14.1 93 m	14.1 48 m	14.1 9 m	14.1 95 m	17.5 71 m	14.0 69 m
Average	5.55 64 m	5.58 46 m	6.09 91 m	6.22 83 m	6.23 42 m	6.21 98 m
Minimu m Occurs On	SYS-5\Solid					
Maximu m Occurs On	SYS-5\Solid					
Information						
Frequen cy	22.3 92 Hz	111. 2 Hz	140. 08 Hz	391. 4 Hz	411. Hz	668. 88 Hz

TABLE

14

Model (C4) > Modal (C5) > Solution (C6) > Total Deformation

Mode	Frequency [Hz]
1.	22.392

2.	111.2
3.	140.08
4.	391.4
5.	411.
6.	668.88

TABLE

15

Model (C4) > Modal (C5) > Solution (C6) > Total Deformation 2

Mode	Frequency [Hz]
1.	22.392
2.	111.2
3.	140.08
4.	391.4
5.	411.
6.	668.88

TABLE

16

Model (C4) > Modal (C5) > Solution (C6) > Total Deformation 3

Mode	Frequency [Hz]
1.	22.392
2.	111.2
3.	140.08
4.	391.4
5.	411.
6.	668.88

TABLE

17

Model (C4) > Modal (C5) > Solution (C6) > Total Deformation 4

Mode	Frequency [Hz]
1.	22.392
2.	111.2
3.	140.08
4.	391.4
5.	411.

6.	668.88
----	--------

TABLE

18

Model (C4) > Modal (C5) > Solution (C6) > Total Deformation 5

Mode	Frequency [Hz]
1.	22.392
2.	111.2
3.	140.08
4.	391.4
5.	411.
6.	668.88

TABLE

19

Model (C4) > Modal (C5) > Solution (C6) > Total Deformation 6

Mode	Frequency [Hz]
1.	22.392
2.	111.2
3.	140.08

4.	391.4
5.	411.
6.	668.88

Material Data

ZXY PLA

TABLE

20

ZXY PLA > Constants

Density	1152.8 kg m <sup>-3</sup>
---------	---------------------------

TABLE

21

ZXY PLA > Color

Red	Green	Blue
234	247	209

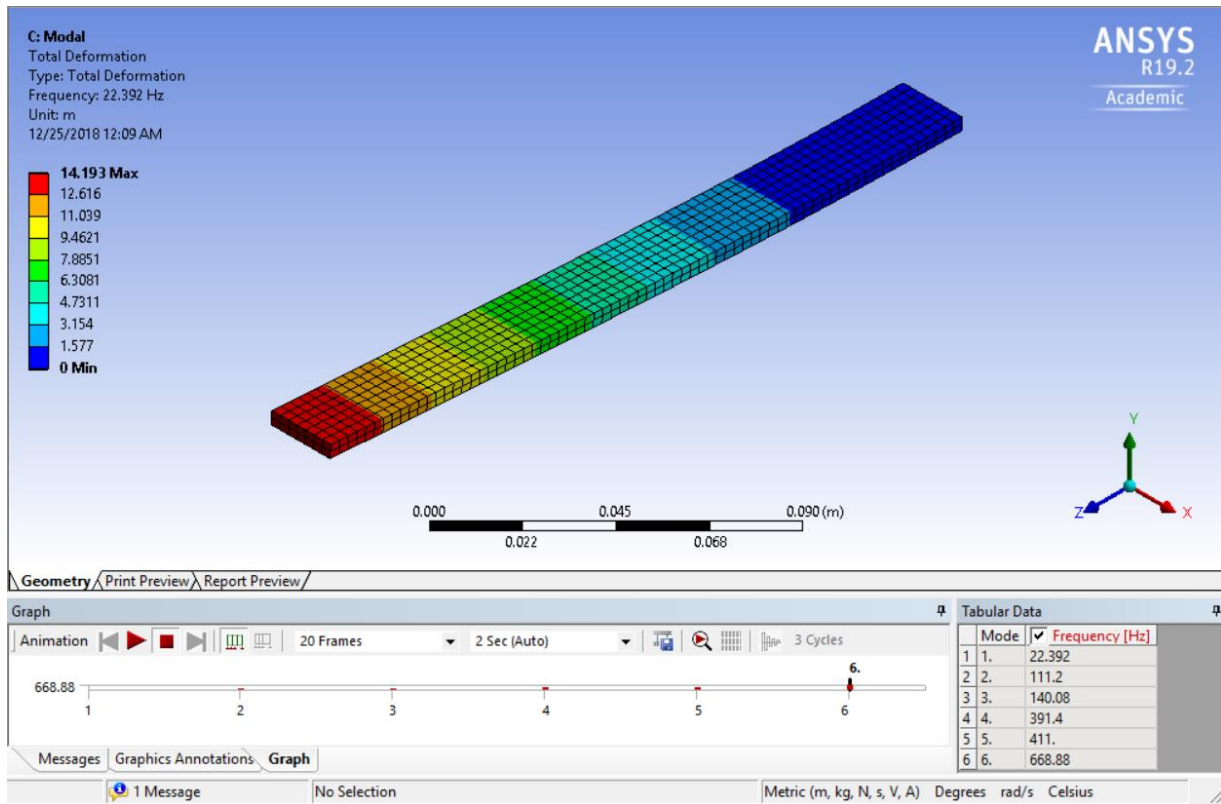
TABLE

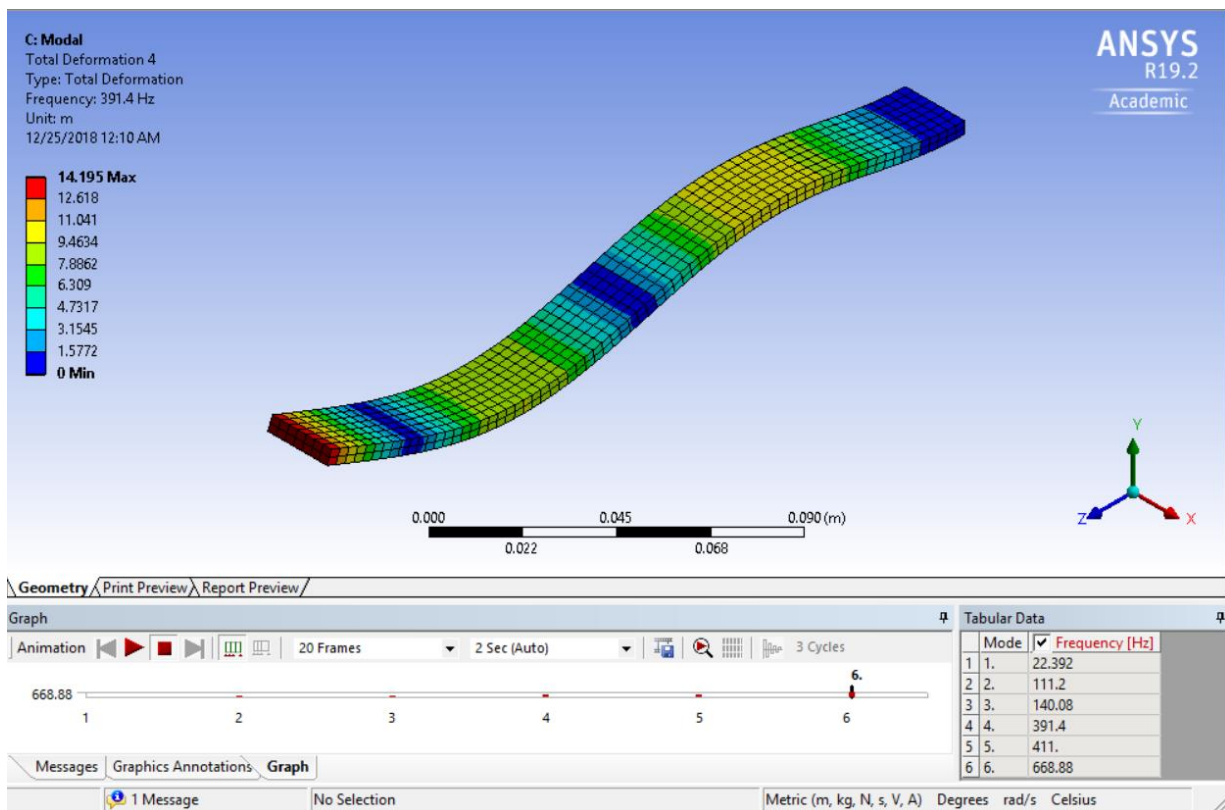
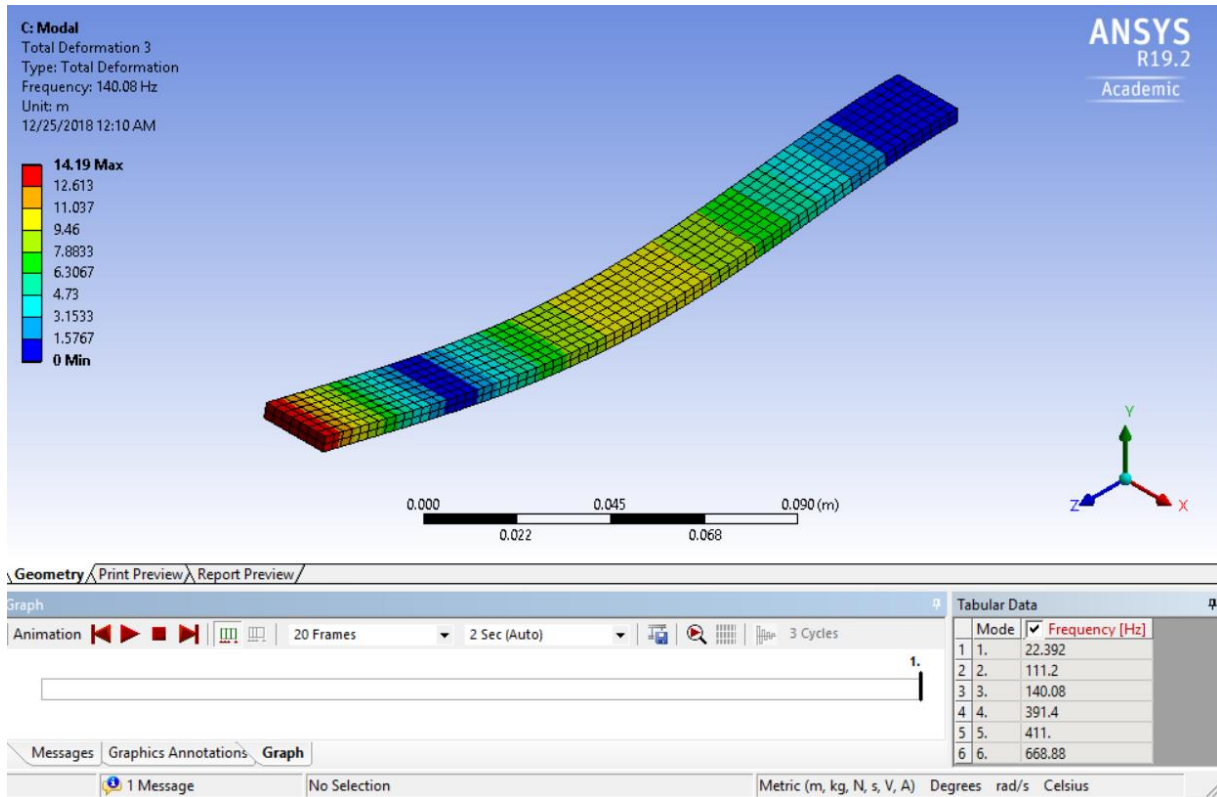
22

ZXY PLA > Orthotropic Elasticity

Y	Y	Y	F	F	F	S	S	S	T
Young's	Young's	Young's	Poisson's	Poisson's	Poisson's	Shear	Shear	Shear	Temperature
Modulus	Modulus	Modulus							in °C

s X direction n Pa	s Y direction n Pa	s Z direction n Pa	Ratio XY	Ratio YZ	Ratio XZ	Modulus XY Pa	Modulu s YZ Pa	Modulus XZ Pa	
3 .15e+00 9	3 .12e+00 9	2 .92e+00 9	0 .35	0 .35	0 .35	1 .159e+0 09	1 .07e+00 9	1 .029e+0 09	





## REFERENCES

- ASTM International . (2015). *ASTM E1876-15 Standard Test Method for Dynamic Young's Modulus, Shear Modulus, and Poisson's Ratio by Impulse Excitation of Vibration*. West Conshohocken, PA.: <https://doi-org.ezproxy.lib.ryerson.ca/10.1520/E1876-15>.
- ASTM International. (2017). *ASTM E756-05(2017) Standard Test Method for Measuring Vibration-Damping Properties of Materials*. West Conshohocken, PA : <https://doi-org.ezproxy.lib.ryerson.ca/10.1520/E0756-05R17>.
- CHO, C. (2007). Comparison of Three Methods for Determining Young's Modulus of Wood. . *Taiwan Journal for Science*, 297-306.
- Chong Liu. ( (2018)). "Optimization of shape control of a cantilever beam using dielectric elastomer actuators". . *AIP Advances* 8, 055015.
- D. Ridley-Ellis, M. L. ( 2018). "Impulse excitation measurement of small changes in elastic moduli and damping using R". *International Wood products Journal*, Vol. 9, No. 2, 74-79.
- Davide S. Paolino, H. G. (2017). "Damaged composite laminates: Assesment of residual Young's modulus through the Impulse Excitation Technique". . *Composites Part B* 128 , 76-8.
- Digilov., R. M. (2013). "Flexural Vibration Test of a Beam Elastically Restrained at One End: A New Approach for Young's Modulus Determination". . *Advances in Materials Science and Engineering* 329530.
- Ewen., J. R. (2007). "Dynamic Stiffness Formulation Using Timoshenko Theory for Free Vibration of Rotating Beams". . *AIAA DOI: 10.2514/6.*, 2277.

- Gang Wang, N. M. (n.d.). “Free in-plane vibration of rectangular plates”. . *19th AIAA Applied Aerodynamics Conference, Fluid Dynamics and Co-located Conferences*.
- Guan, C. ((2016) ). “Determining shear modulus of thin wood composite materials using a cantilever beam vibration method”. . *Building and Construction Materials*. 121 , 285-289.
- Haque., E. A. ( 2018, ). “Tensile properties, void contents, dispersion and fracture behaviour of 3D printed carbon nanofiber reinforced composites”. *Journal of Reinforced Plastics and Composites*, Vol. 37(6), 381–395.
- HEYLIGER, P. U. (2001). H. Anisotropic Elastic Constants: Measurement by Impact Resonance. . *Journal of Materials in Civil Engineering*, 356-363,.
- Jianlei Wang, H. X. ((2016) ). “A novel approach to improving mechanical properties of parts fabricated by fused deposition modeling”. . *Materials and Design* 105 , 152-159.
- John Ryan C. Dizon, A. H. ( (2018) ). “Mechanical characterization of 3D-printed polyers”. . *Additive Manufacturing* 20, 44-67.
- Juliana Breda Soares, J. F. ((2018) ). “Analysis of the influence of polylactic acid (PLA) colour on FDM 3D printing temperature and part finishing”. *Rapid Prototyping Journal* 24/8 , 1305-1316.
- Jun., Z. ((2013) ). “Theoretical Analysis and Experimental study of A Cantilever Beam-type Dynamic Vibration Absorber”. . *Applied Mechanics and Materials* Vol. 415 , 436-441.
- Lotfi Toubal, R. Z. (2018). “Moisture Effects on the Material Properties of a Jute/Epoxy Laminate: Impulse Excitation Technique Contribution”. *Journal of Natural Fibers* , Vol. 15, No. 1 , 39-52.

- M.F. Slim and A. Alhussein, A. B. (2017). "On the determination of of Young's modulus of thin films with impulse excitation technique". . *J. Mater. Res.*, Vol. 32, No.3, Feb 14, .
- Monti., A. ((2017) ). "Experimental and finite elements analysis of the vibration behavior of a bio-based composite sandwich beam". *Composites Part B* 110 , 466-475.
- N.B. Podymova, A. K. (2013). "Quantative evaluation of the effect of porosity on the local young's modulus of isotropic composites by using the laser optoacoustic method". . *Mechanics of Composite Materials*, Vol 49, No. 4.
- P Chiariotti, M. M. (2013). Diagnostic procedure on brake pad assembly based on Young's modulus estimation. *Measurement science and technology*, 24, 11.
- Prasob P.A., S. M. (2018 ). "Static and dynamic behavior of Jute/epoxy composites with ZnO and TiO<sub>2</sub> fillers at different temperature conditions". . *Polymer Testing* 69, 52-62.
- Ramesh., R. (2015). "*Study of free vibration characteristics of carbon epoxy based composite beams*".,
- S.M. Hashemi, M. R. (1987). "A Bernoulli-Euler Stiffness Matrix approach for vibrational analysis of spinning linearly tapered beams". *Canadian Acoustics* 24 (3),, 87.
- Shilpesh R. Rajpurohit, H. K. (2018). "Effect of process parameters on tensile strength of FDM printed PLA part". *Rapid Prototyping Journal*, Vol. 24 Issue: 8, 1317-1324 .
- Somen K. Bhudolia, P. P. ((2017) ). "Enhanced vibration damping and dynamic mechanical characteristics of composites with novel pseudo-thermoset matrix system". . *Composite Structures* 179 , 502-51.

- V.D. Sagias. ( (2018) ). “Mechanical properties of 3D printed polymer specimens”. . *Science Direct, Procedia Structural Integrity 10*, 85-90.
- Valerga., A. ((2017) ). “Preliminary study of PLA wire colour effects on geometric characteristics of parts manufactured by FDM”. *Procedia Manufacturing 13* , 924–931.
- Valerga., A. P. (2018). “Influence of PLA Filament Conditions on Characteristics of FDM Parts”. . *Materials · July 2018* .
- Walunj Prashant S, V. C. ((2015) ). “Investigation on modal parameters of rectangular cantilever beam using Experimental modal Analysis”. . *Materials Today: Proceedings 2*, 2121 – 2130.
- Wei Sun, Z. W. ((2018) ). “Inverse identification of the frequency-dependent mechanical parameters of viscoelastic materials based on the measured FRFs”. *Mechanical Systems and Signal Processing 98* , 816-833.
- Wenlei Song, Y. Z. ( (2017) ). “Mechanical parameters identification for laminated composites based on the impulse excitation technique”. . *Composite Structures 162*, 255-260.
- Wenzheng Wu, W. Y. (2017). “Influence of Layer Thickness, Raster Angle, Deformation Temperature and Recovery Temperature on the Shape-Memory Effect of 3D-Printed Polylactic Acid Samples”. *Material*, 10, 970;.
- Y. Song, Y. L.-Y. ( (2017) ). “Measurements of the mechanical response of unidirectional 3D-printed PLA”. . *Materials and Design 123*, 154-164.